Chapter III: ACCIDENTAL PHENOMENA AND CONSEQUENCES

Version 1.0 – June 2007

Table of content

3. ACCIDENTAL PHENOMENA AND CONSEQUENCES

3.1 ACCIDENTAL PHENOMENA

3.1.1 Release of Hydrogen

Contributing author	*Main contributions*	*Organisation*	*e-mail*
A.G. Venetsanos	Chapter coordinator	*NCSRD*	venets@ipta.demokritos.gr
P. Benard and A.G. Venetsanos	Subsonic and sonic jets	*UQTR, NCSRD*	Pierre.Benard@uqtr.ca
A.G Venetsanos and E. Papanikolaou	Two phase jets	*NCSRD*	
K. Verfondern	LH2 pool spreading and vaporisation	*FZJ*	k.verfondern@fz-juelich.de
K. Verfondern	Dispersion in the open atmosphere	FZJ	
E. Gallego	Dispersion in obstructed environment	UPM	eduardo.gallego@upm.es
J/M. Martin-Valdepeñas and M. A. Jimenez	Dispersion in confined environment	*UPM*	jmmv@csn.es
A.G. Venetsanos, K. Verfondern, P. Benard	*Numerical simulations*	*NCSRD, FZJ, UQTR*	
A.G. Venetsanos and P. Benard	*Knowledge gaps and recent progress*	*NCSRD*	

Contributing reviewer	Information reviewed	*Organisation*	*e.mail*
H. S. Ledin	Dispersion	HSL	stefan.ledin@hsl.gov.uk

3.1.1.1 Jets

Sonic and subsonic gaseous jets

Gaseous hydrogen releases through a hole or a conduct are produced as a result of a positive pressure difference between a container and its environment. The aperture is often modeled as a nozzle. Depending on the upstream pressure, a flow through a convergent nozzle to a lower downstream pressure can either be chocked (or sonic) or subsonic. The crossover pressure is a

function of the ratio of the constant volume to the constant pressure specific heat (Hanna and Strimaitis (1989).

The flow resulting from a subsonic release is basically an expanded jet. The concentration profile of hydrogen in this expanded jet is inversely proportional to the distance to the nozzle along the axis of the jet. At a given distance from the nozzle, the concentration profile of hydrogen in air is distributed according to a Gaussian function centered on the axis. The following formula has been suggested by Chen and Rodi (1980) for the axial concentration (vol) decay of variable density subsonic jets:

$$\frac{C(x)}{C_j} = K \frac{d_j}{x - x_0} \left(\frac{\rho_\alpha}{\rho_g} \right)^{1/2} \quad (1)$$

Where C(x) is the concentration (vol) at location x, C_j is the concentration at the outlet nozzle, d_j is the jet discharge diameter, ρ_α is the density of the ambient air, ρ_g the density of the gas at ambient conditions, x is the distance from the nozzle along the jet axis, x_0 is the virtual absicca of the hyperbolic decrease (usually neglected because it is of the order of magnitude as the real diameter) and K is a constant equal to 5.

For hydrogen, chocked releases occur when the upstream pressure is 1.9 times larger than downstream, otherwise the flow is subsonic. The flow rate of a chocked flow is only a function of the upstream pressure, whereas the flow rate of a subsonic release will depend on the difference between the upstream and downstream pressures. A release from a compressed gas storage system into the environment will therefore be chocked as long as the storage pressure remains larger than 1.89 bars.

A chocked release of hydrogen undergoes a pressure and a temperature drop at the exit of the nozzle. The pressure will drop until the exit pressure reaches the value of the downstream pressure. At that point, the release becomes subsonic and the exit pressure remains constant at the downstream value.

In the chocked regime, the gas velocity at the exit of the nozzle is exactly the sonic velocity of the gas. The flow rate can therefore be estimated from

$$\dot{m} = \rho A c \quad (2)$$

where ρ is the density of hydrogen at the exit of the nozzle, calculated using the local value of the temperature and the pressure. The flow rate will also be affected by the shape of the aperture, friction and the length of the conduit between the reservoir and the release point.

Because the exit density changes as a function of temperature and pressure, and because the sonic velocity is essentially proportional to the square root of the temperature, the flow rate will not remain constant but will vary as the upstream pressure drops (Fig. 3-1).

Figure 3-1 shows the effect of using real gas hydrogen properties compared to ideal gas. It is well known that at high storage pressures real hydrogen gas densities are lower than ideal gas densities. Table 1 compares real versus ideal hydrogen densities at temperature 288 K and pressures 200 and 700 bar, (values taken from the Encyclopedie des gaz). For given storage volume the real gas assumption results in less stored hydrogen mass and consequently less released mass in an accidental situation.

Table 3-1: Comparison between real and ideal gas properties

Pressure (bar)	*Real density (kg m^{-3})*	*Ideal density (kg m^{-3})*	*Relative error (%)*
200	*14.96*	*16.85*	*12.6*
700	*40.18*	*58.90*	*46.6*

The effect of real gas properties has been taken into account in the 1983 Stockholm hydrogen accident simulations by Venetsanos et al. (2003), where tables from Encyclopedie des gaz were used to obtain the hydrogen density. Real gas properties calculations based on the Beattie–Bridgeman equation of state were reported by Mohamed and Paraschivoiu (2005), who modeled a hydrogen release from a high pressure chamber. Real gas properties using the Abel-Nobel equation of state were considered by Cheng at al. (2005)[i] who performed hydrogen release and dispersion calculations for a hydrogen release from a 400bar tank through a 6 mm PRD opening and found that the ideal gas law overestimates the hydrogen release rates by up to 35% during the first 25 seconds after the release. Based on these findings these authors recommended a real gas equation of state to be used for high pressure PRD releases.

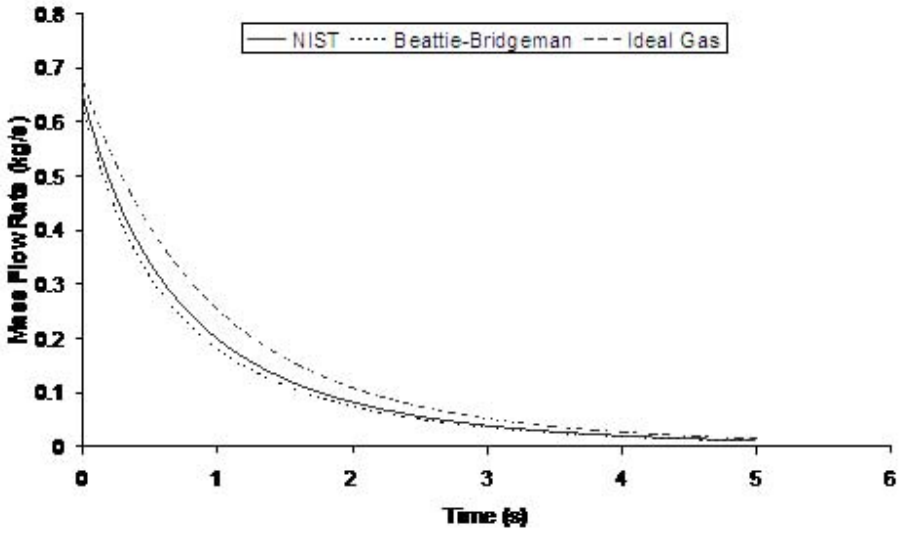

Figure 3-1 Mass flow rate as a function of time from a 6 mm aperture of a 345 bar compressed gas 27.3 litre cylinder (calculated using the NIST[ii], the Bettie-Bridgeman and the ideal gas equations of state based on Mohamed and Paraschivoiu (2005).

A chocked jet (Fig. 3-2) can be basically divided into an under-expanded region, where the flow becomes supersonic, forming a cone-like structure (the Mach cone) (Fig. 3-3); and an expanded region, which behaves similarly to an expanded subsonic jet. The under-expanded region is characterized by a complex shock wave pattern, involving bow and oblique shocks (Figures 3 and 4).

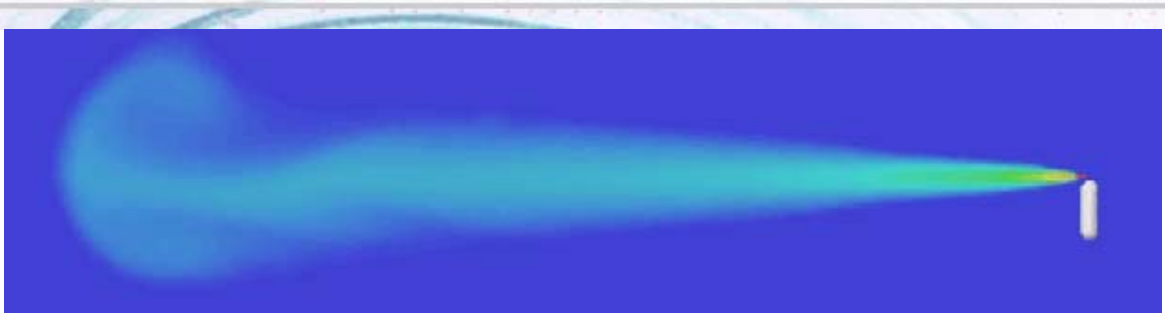

Figure 3-2 Chocked release from a 150 litre 700 bar reservoir (Source B. Angers et al.).

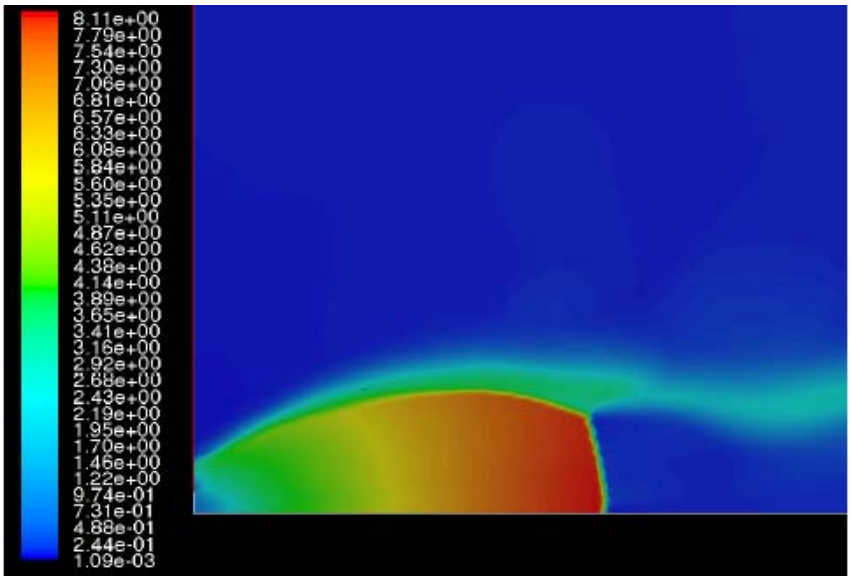

Figure 3-3 Under-expanded chocked release of hydrogen (the Mach number is calculated with respect to air).

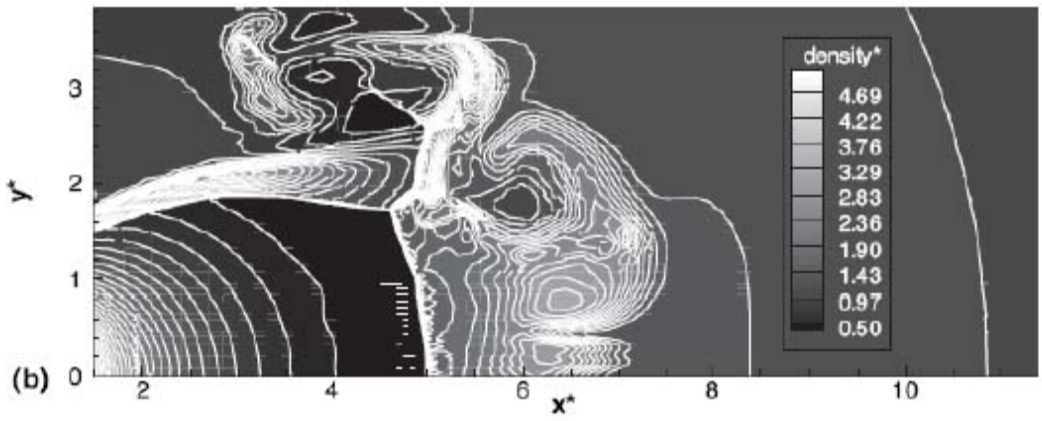

Figure 3-4 Normalized density contours as a function of position (hydrogen jet in hydrogen atmosphere; source: Pedro, Peneau, Oshkai & Djilali (2006)

As for subsonic releases, the concentration profile of hydrogen in the expanded region is inversely proportional to the distance to the nozzle along the axis of the jet and is distributed according to a Gaussian function at a fixed distance from the nozzle. The axial concentration decay can be calculated using the formula for variable density subsonic jets (Eq. 1), where the discharge diameter is replaced by the effective diameter, which is representatve of the jet diameter at the start of the subsonic region, i.e. after the Mach cone.

$$\frac{C(x)}{C_j} = K \frac{d_{eff}}{x - x_0} \left(\frac{\rho_\alpha}{\rho_g} \right)^{1/2} \tag{3}$$

For the determination of the effective diameter various approaches have been proposed, such as Birch et al. (1984), Ewan and Moodie (1986) and Birch at al. (1987). In this latest approach, the effective diameter and corresponding effective velocity is calculated by applying the conservation of mass and momentum, between the outlet and a position beyond the Mach cone where pressure first becomes equal to the ambient, assuming no entrainment of ambient air.

$$d_{eff} = \left(\frac{\rho_j u_j}{\rho_g u_{eff}} \right)^{1/2} d_j \tag{4}$$

Where ρ_j and u_j are the density and the velocity of the jet at the outlet (respectively), u_{eff} is the effective velocity, d_j the diameter of the outlet. The effective velocity is calculated using the following expression:

$$u_{eff} = u_j + \frac{p_j - p_\alpha}{\rho_j u_j} \tag{5}$$

where p_j is the pressure of the jet at the outlet and p_α is the ambient pressure.

Regarding the constant K entering Eq.3, different values have been reported in the literature. An average value of 4.9 is mentioned by Birch 1984. An average value of 5.4 was reported in Birch 1987. This approach (Birch 1984, 1987; Houf & Schefer 2005) has been validated experimentally for vertical chocked releases for pressures below 70 bars for natural gas and hydrogen.

A lower value K = 3.7 was reported by Ruffin et al. (1996) who investigated experimentaly the concentration field of horizontal supercritical jets of methane and hydrogen for 40 bars storage pressure and with orifice diameters in the range from 25 to 150 mm. Ruffin et al. used the Birch 1984 approach in defining the effective diameter. Furthermore, Chaineaux (2006) referring to the experiments in Chaineaux (1999) reported a value of 2.25 for 200 bar hydrogen release from a 0.5 mm hole and a value of .2.89 for 700bar hydrogen release from a 0.35mm hole.

Other experiments supporting the decay law of Eq. 3 are the experiments by Chitose et al., 2006[iii] who have measured the concentration profile of a hydrogen release from a 40 MPa storage unit. They observed that as a function of distance, the concentration profile of leaks with diameters ranging from 0.25 to 2 mm was inversely proportional to the distance to the nozzle and that all data points fell on a simple inverse power scaling law as a function of the normalized distance. Based on the experimental work, they obtained flammable concentration extents of 2.6 m, 6.6 m and 13.4 m for leak diameters of 0.2, 0.5 and 1.0 mm respectively. An

experiment to measure the concentration profile of a horizontal release using a 10 mm diameter leak through a broken pipe from a 40 MPa storage unit showed that the extent of the 4% (vol) concentration envelope reached a distance of about 18 meters, 3 seconds after release.

Flammable release extents can approximately be calculated using Eq. 3. The maximum extent of a time-dependent release will not be estimated using the initial storage pressure, but using a later value (see Houf and Schefer, 2005). Predicted flammable release extents are shown in Fig. 3-6 below. The axial distance to the lower flammability limit of 4% (vol) for hydrogen varies from 2 to 53 m for leak diameters ranging from 0.25 mm to 6.35 mm if the storage pressure is 1035 bars.

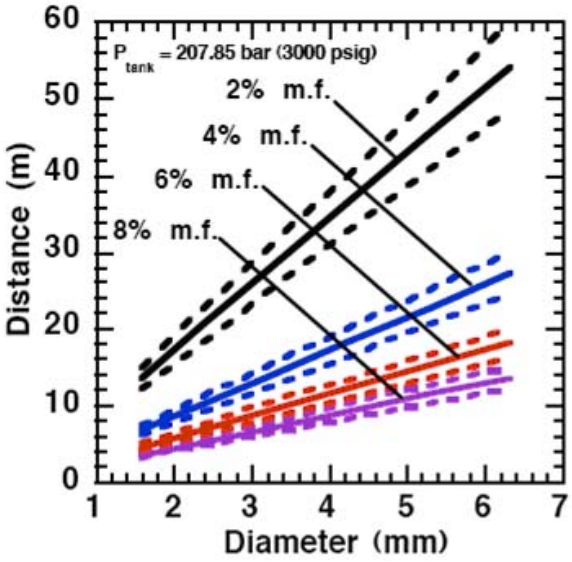

Figure 3-5 Distances to concentrations of 2.0%, 4.0%, 6.0%, and 8.0% mole fraction on the centreline of a jet release from a 207.85 bars tank for various leak diameter obtained using the Sandia/Birch approach. The dashed lines indicate upper and lower bounds with ±10% uncertainty in the value of the constant K. (from Houf and Shefer, (2006))

Two phase jets

The phenomena associated with two phase jet dispersion are reviewed by Bricard and Friedel (1998). Within a short distance just downstream from the outlet, the flow can experience drastic changes which must be considered for subsequent dispersion calculations. The physical phenomena taking place in this region comprise (i) flashing if the liquid is sufficiently superheated, (ii) gas expansion when the flow is choked and (iii) liquid fragmentation. The corresponding quantities to be determined as initial conditions for subsequent dispersion calculations are the flash fraction, the jet mean temperature, velocity and diameter, and the droplet size.

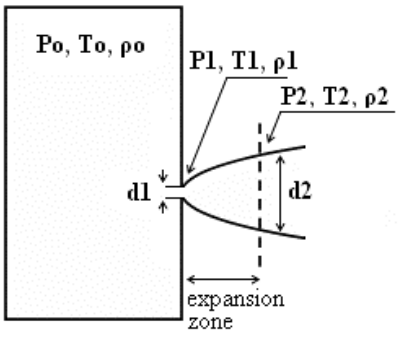

Figure 3-6 Model of a two-phase flashing jet

Flashing occurs when the liquid is sufficiently superheated at the outlet with respect to atmospheric conditions and corresponds to the violent boiling of the jet. The vapour mass fraction after flashing is most often determined in the models by assuming isenthalpic depressurization of the mixture between the outlet (position 1 in Figure 3-6) and the plane downstream over which thermodynamic equilibrium at ambient pressure is attained (position 2 in Figure 3-6):

$$x_2 = \frac{\int_1^2 C_{pf} dT}{H_{fg}} \tag{6}$$

Where H_{fg} is the latent heat of vaporization and C_{pf} is the liquid specific heat.

When the flow is choked at the outlet, the gas phase expands to ambient pressure within a downstream distance of about two orifice diameters. This causes a strong acceleration of the two-phase mixture and usually an increase of the jet diameter. In the models, the velocity and diameter of the jet at the end of the expansion zone are given by the momentum and mass balance, respectively, integrated over a control volume extending from the outlet (position 1) to the plane where atmospheric pressure is first reached (position 2). It is assumed that no air is entrained in this region. The approach is similar to the one described above for choked gaseous hydrogen jets. The corresponding equations according to Fauske and Epstein (1988) are:

$$d_2 = d_1 \left(\frac{\rho_1 u_1}{\rho_2 u_2} \right)^{1/2}, \; u_2 = u_1 + \frac{P_1 - P_2}{\rho_1 u_1} \tag{7}$$

Liquid fragmentation (or atomization) is caused by two main physical mechanisms: flashing and aerodynamic atomization. With flashing atomization, the fragmentation results from the violent boiling and bursting of bubbles in the superheated liquid, whereas aerodynamic atomization is the result of instabilities at the liquid surface. The determination of the initial droplet size (position 2) is a required initial condition, if the subsequent dispersion models account for fluiddynamic and thermodynamic non-equilibrium phenomena, like rainout and/or droplet evaporation. In the case of aerodynamic fragmentation, the maximum stable drop size is usually given by a critical Weber number, which represents the ratio of inertia over surface tension forces:

$$We_{\max} = \frac{\Delta U^2 \rho_g d_{\max}}{\sigma} \tag{8}$$

Where σ is the surface tension of the liquid, ρ_g is the gas density, $d_{\max}$ is maximum stable droplet diameter and ΔU the mean relative velocity between both phases. A range of values are used for the maximum Weber number, see Bricard an Friedel (1998) with 12 being the most common value.

In the previous discussion the mass flow rate and outlet conditions (position 1) were assumed known. Hanna and Strimaitis (1989) have reviewed various approaches for calculating the release mass flow rate for liquid and two-phase flow releases. Detailed information on the subject can be found in chapter 15 of Lees (1996), in chapter 9 of Etchells and Wilday (1998) as well as in the older review of critical two phase flow models by D'Auria and Vigni (1980)

If the liquid in the reservoir is at saturated conditions, and if equilibrium flow conditions are established (i.e. for outflow pipe lengths > 0.1 m) then the two-phase choked mass flux (kg s^{-1} m^{-2}) can be calculated following Fauske and Epstein (1988):

$$G = \frac{H_{fg}}{v_g - v_f}\left(\frac{1}{C_{pf}T}\right)^{1/2} \tag{9}$$

Where H_{fg} is the latent heat of vaporization, C_{pf} is the liquid specific heat, T is the saturation temperature which is function of the storage pressure p, v_g, v_f are the saturated vapour and liquid specific volumes. This equation applies only if the vapor mass fraction after depressurization to atmospheric pressure (position 2) obeys the following criterion:

$$x_2 < \frac{p\left(v_g - v_f\right)\left(C_{pf}T\right)}{H_{fg}^2} \tag{10}$$

Figure 3-7 shows the equilibrium choked mass flux calculated using Eq. (10) for an LH2 release as function of the storage pressure.

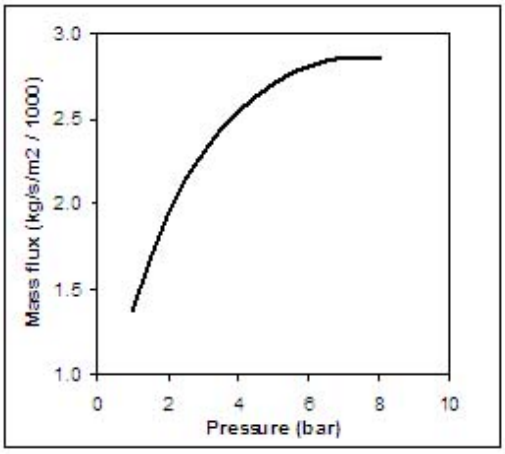

Figure3-7 Mass flux calculated using Eq. (4) for an LH2 release, as function of the storage pressure

3.1.1.2 LH2 Pool spreading and vaporisation

Liquefied gases are characterized by a boiling point well below the ambient temperature. If released from a pressure vessel, the pressure relief from system to atmospheric pressure results in spontaneous (flash) vaporization of a certain fraction of the liquid. Depending on leak location and thermodynamic state of the cryogen (pressure expelling the cryogen through the leak is equal to the saturation vapour pressure), a two-phase flow will develop, significantly reducing the mass released. It is connected with the formation of aerosols, which vaporize in the air without touching the ground. Conditions and configuration of the source determine features of the evolving vapour cloud such as cloud composition, release height, initial plume distribution, time-dependent dimensions, or energy balance. The phenomena that may occur after a cryogen release into the environment are shown in Fig. 3-8.

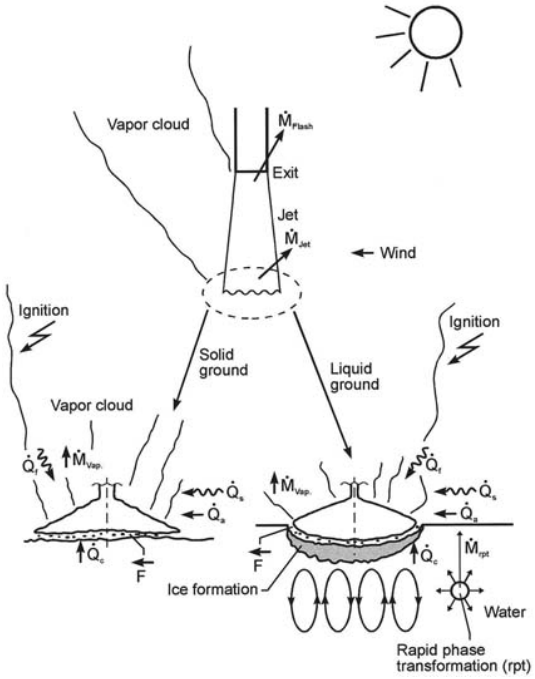

Fig. 3-8: Physical phenomena occurring upon the release of a cryogenic liquid

LH2 Vaporization

The release as a liquefied gas usually results in the accumulation and formation of a liquid pool on the ground, which expands, depending on the volume spilled and the release rate, radially away from the releasing point, and which also immediately starts to vaporize. The equilibrium state of the pool is determined by the heat input from the outside like from the ground, the ambient atmosphere (wind, insolation from the sun), and in case of a burning pool, radiation heat from the flame. The respective shares of heat input from outside into the pool are depending on the cryogen considered. Most dominant heat source is heat transport from the ground. This is particularly true for LH2, where a neglection of all other heat sources would result in an estimated error of 10-20%. For a burning pool, also the radiation heat from the flame provides a significant contribution. This is particularly true for a burning LNG pool due to its much larger emissivity resulting from soot formation (Dienhart 1995).

Upon contact with the ground, the cryogen will in a short initial phase slide on a vapor cushion (film boiling) due to the large temperature difference between liquid and ground. The vaporization rate is comparatively low and if the ground is initially water, no ice will be formed. With increasing coverage of the surface, the difference in temperatures is decreasing until – at the Leidenfrost point – the vapour film collapses resulting in enhanced heat transfer via direct contact (nucleate boiling). On water, there is the chance of ice formation which, however, depending on the amount of mass released, will be hindered due to the violent boiling of the cryogen, particularly if the momentum with which the cryogen hits the water surface is large. Unlike lab-scale testing (confined), ice formation was not often observed in field trials (unconfined).

The vaporization behaviour is principally different for liquid and solid grounds. On liquid grounds, the vaporization rate remains approximately constant due to natural convection processes initiated in the liquid resulting in an (almost) constant, large temperature difference between surface and cryogen indicating stable film boiling. On solid grounds, the vaporization rate decreases due to cooling of the ground. The heat flux into the pool can be approximated as being proportional to $t^{-1/2}$. The vaporization time is significantly reduced, if moisture is present in the ground due to a change of the ice/water properties and the liberation of the solidification enthalpy during ice formation representing an additional heat source in the ground.

LH2 Pool Spreading

Above a certain amount of cryogen released, a pool on the ground is formed, whose diameter and thickness is increasing with time until reaching an equilibrium state. After termination of the release phase, the pool is decaying from its boundaries and breaking up in floe-like islands, when the thickness becomes lower than a certain minimum which is determined by the surface tension of the cryogen (in the range of 1 to 2 mm). The development of a hydraulic gradient results in a decreasing thickness towards the outside.

The spreading of a cryogenic pool is influenced by the type of ground, solid or liquid, and by the release mode, instantaneous or continuous. In an instantaneous release, the release time is theoretically zero (or release rate is infinite), but practically short compared to the vaporization time. Spreading on a water surface penetrates the water to a certain degree, thus reducing the effective height responsible for the spreading and also requiring additional displacement energy at the leading edge of the pool below the water surface. The reduction factor is given by the density ratio of both liquids telling that only 7% of the LH2 will be below the water surface level compared to, e.g., more than 40% of LNG or even 81% of LN2.

During the initial release phase, the surface area of the pool is growing, which implies an enhanced vaporization rate. Eventually a state is reached which is characterized by the incoming mass to equal the vaporized mass. This equilibrium state, however, does not necessarily mean a constant surface. For a solid ground, the cooling results in a decrease of the heat input which, for a constant spill rate, will lead to a gradually increasing pool size. In contrast, for a water surface, pool area and vaporization rate are maximal and remain principally constant as was concluded from lab-scale testing despite ice formation. A cutoff of the mass input finally results in a breakup of the pool from the central release point creating an inner pool front. The ring-shaped pool then recedes from both sides, although still in a forward movement, until it has completely died away.

A special effect was identified for a continuous release particularly on a water surface. The equilibrium state is not being reached in a gradually increasing pool size. Just prior to reaching the equilibrium state, the pool is sometimes rather forming a detaching annular-shaped region,

propagates outwards ahead of the main pool (Brandeis 1983). This phenomenon, for which there is hardly experimental evidence because of its short lifetime, can be explained by the fact that in the first seconds more of the high-momentum liquid is released than can vaporize from the actual pool surface; it becomes thicker like a shock wave at its leading edge while displacing the ground liquid. It results in a stretching of the pool behind the leading edge and thus a very small thickness, until the leading edge wavelet eventually separates. Realistically the ring pool will most likely soon break up in smaller single pools drifting away as has been often observed in release tests. Whether the ring pool indeed separates or only shortly enlarges the main pool radius, is depending on the cryogen properties of density and vaporization enthalpy and on the source rate.

Also so-called rapid phase transitions (RPT) could be observed for a water surface. RPTs are physical ("thermal") vapor explosions resulting from a spontaneous and violent phase change of the fragmented liquid gas at such a high rate that shock waves may be formed. Although the energy release is small compared with a chemical explosion, it was observed for LNG that RPT with observed overpressures of up to 5 kPa were able to cause some damage to test facilities.

Experimental Work

Most experimental work with cryogenic liquefied gaseous fuels began in the 1970s concentrating mainly on LNG and LPG with the goal to investigate accidental spill scenarios during maritime transportation. A respective experimental program for liquid hydrogen was conducted on a much smaller scale, initially by those who considered and handled LH2 as a fuel for rockets and space ships. Main focus was on the combustion behavior of the LH2 and the atmospheric dispersion of the evolving vapor cloud after an LH2 spill. Only little work was concentrating on the cryogenic pool itself, whereby vaporization and spreading never were examined simultaneously.

The NASA LH2 trials in 1980 (Chirivella 1986) were initiated, when trying to analyze the scenario of a bursting of the 3000 m^3 of LH2 containing storage tank at the Kennedy Space Center at Cape Canaveral and study the propagation of a large-scale hydrogen gas cloud in the open atmosphere. The spill experiments consisted of a series of seven trials, in five of which a volume of 5.7 m^3 of LH2 was released near-ground over a period of 35-85 s. Pool spreading on a "compacted sand" ground was not a major objective, therefore scanty data from test 6 only are available. From the thermocouples deployed at 1, 2, and 3 m distance from the spill point, only the inner two were found to have come into contact with the cold liquid, thus indicating a maximum pool radius not exceeding 3 m.

In 1994, the first (and only up to now) spill tests with LH2, where pool spreading was investigated in further detail, were conducted in Germany. In four of these tests, the Research Center Juelich (FZJ) studied in more detail the pool behavior by measuring the LH2 pool radius in two directions as a function of time (Dienhart 1995). The release of LH2 was made both on a water surface and on a solid ground. Thermocouples were adjusted shortly above the surface of the ground serving as indicator for presence of the spreading cryogen.

The two spill tests on water using a 3.5m diameter swimming pool were performed over a time period of 62 s each at an estimated rate of 5 l/s of LH2, a value which is already corrected by the flash-vaporized fraction of at least 30%. After contact of the LH2 with the water surface, a closed pool was formed, clearly visible and hardly covered by the white cloud of condensed water vapor. The "equilibrium" pool radius did not remain constant, but moved forward and backward within the range of 0.4 to 0.6 m away from the center. This pulsation-like behavior, which was also observed by the NASA experimenters in their tests, is probably caused by the irregular efflux due to the violent bubbling of the liquid and release-induced turbulences. Single small floes of ice escaped the pool front and moved outwards. After cutting off the source, a

massive ice layer was identified where the pool was boiling. In the two tests on a solid ground given by a 2 x 2 m^2 aluminum sheet, the LH2 release rate was (corrected) 6 l/s over 62 s each. The pool front was also observed to pulsate showing a maximum radius in the range between 0.3 and 0.5 m. Pieces of the cryogenic pool were observed to move even beyond the edge of the sheet. Not always all thermocouples within the pool range had permanent contact to the cold liquid indicating non-symmetrical spreading or ice floes which passed the indicator.

Computer Modelling

Parallel to all experimental work on cryogenic pool behavior, calculation models have been developed for simulation purposes. At the very beginning, purely empirical relationships were derived to correlate the spilled volume/mass with pool size and vaporization time. Such equations, however, were according to their nature strongly case-dependent. A more physical approach is given in mechanistic models, where the pool is assumed to be of cylindrical shape with initial conditions for height and diameter, and where the conservation equations for mass and energy are applied (e.g., Fay 1978 and Briscoe 1980]. Gravitation is the driving force for the spreading of the pool transforming all potential energy into kinetic energy. Drawbacks of these models are given in that the calculation is terminated when the minimum thickness is reached, that only the leading edge of the pool is considered, and that a receding pool cannot be simulated.

State-of-the-art modeling applies the so-called shallow-layer equations, a set of non-linear differential equations based on the conservation laws of mass and momentum, which allows the description of the transient behavior of the cryogenic pool and its vaporization. Several phases are being distinguished depending on the acting forces dominating the spreading:

1. gravitational flow determined by the inertia of the cryogen and characterized by a hydraulic gradient at the front edge;
2. gravitational viscous flow after pool height and spreading velocity have decreased making sheer forces at the boundary dominant;
3. equilibrium between surface tension and viscous forces with gravitation being negligible.

During spreading, the pool passes all three phases, whereby its velocity is steadily decreasing. For cryogens, these models need to be modified with respect to the consideration of a continuously decreasing volume due to vaporization. Also film boiling has the effect of reducing sheer forces at the boundary layer.

Based on these principles, the UKAEA code GASP (Gas Accumulation over Spreading Pools) has been created by Webber (Webber 1991) as a further development of the Brandeis model (Brandeis 1983). It was tested mainly against LNG and also slowly evaporating pools, but not for liquid hydrogen. Brewer also tried to establish a shallow-layer model to simulate LH2 pool spreading, however, was unsuccessful due to severe numerical instabilities except for two predictive calculations for LH2 aircraft accident scenarios with reasonable results (Brewer 1981).

At FZJ, the state-of-the-art calculation model, LAUV, has been developed, which allows the description of the transient behavior of the cryogenic pool and its vaporization (Dienhart 1995). It addresses the relevant physical phenomena in both instantaneous and continuous (at a constant or transient rate) type releases onto either solid or liquid ground. A system of non-linear differential equations that allows for description of pool height and velocity as a function of time and location is given by the so-called “shallow-layer” equations based on the conservation of mass and momentum. Heat conduction from the ground is deemed the dominant heat source for vaporizing the cryogen, determined by solving the one-dimensional or optionally

two-dimensional Fourier equation. Other heat fluxes are neglected. The friction force is chosen considering distinct contributions from laminar and from turbulent flux. Furthermore, the LAUV model includes the possibility to simulate moisture in a solid ground connected with a change of material properties when water turns to ice. For a water ground, LAUV contains, as an option, a finite-differences submodel to simulate ice layer formation and growth on the surface. Assumptions are a plane ice layer neglecting a convective flow in the water, the development of waves, and a pool acceleration due to buoyancy of the ice layer.

The code was validated against cryogen (LNG, LH2) spill tests from the literature and against own experiments. LN2 release experiments were conducted on the KIWI test facility at the Research Center Juelich, which was used for a systematic study of phenomena during cryogenic pool spreading on a water surface. The leading edge of the LN2 pool is usually well reproduced. There is, however, a higher uncertainty with respect to the trailing edge whose precise identification was usually disturbed by waves developed on the water surface and the breakup of the pool into single ice islands when reaching a certain minimum thickness.

The post-calculations of LH2 pool spreading during the BAM spill test series have also shown a good agreement between the computer simulations and the experimental data (see Fig. 9) (Dienhart 1995).

The post-calculations of LH2 pool spreading during the BAM spill test series have also shown a good agreement between the computer simulations and the experimental data (see Fig. 9) (Dienhart 1995).

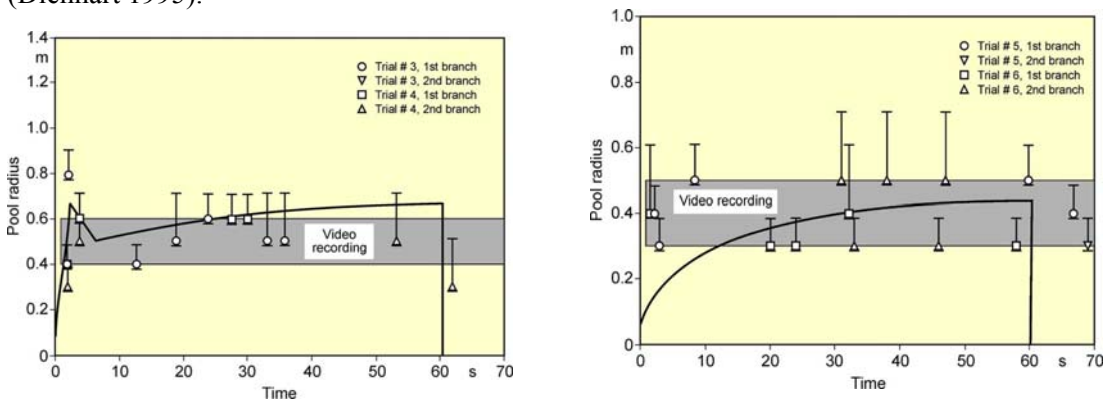

Figure 3-9: Comparison of LH2 pool measurements with respective LAUV calculations for a continuous release over 62 s at 5 l/s on water (left) and at 6 l/s on an Al sheet (right)

During the tests on water, the pool front appears at the beginning to have shortly propagated beyond the steady state presumably indicating the phenomenon of a (nearly) detaching pool ring typical for continuous releases. The radius was then calculated to slowly increase due to the gradual temperature decrease of the ice layer formed on the water surface. Equilibrium is reached approximately after 10 s into the test, until at time 62.9, i.e., about a second after termination of the spillage, the pool has completely vaporized. Despite the given uncertainties, the calculated curve for the maximum pool radius is still well within the measurement range. The ice layer thickness could not be measured during or after the test; according to the calculation, it has grown to 7 mm at the center with the longest contact to the cryogen. The spill tests on the aluminum ground (right-hand side) conducted with a somewhat higher release rate is also characterized by a steadily increasing pool radius. The fact that the attained pool size here is smaller than on the water surface is due to the rapid cooling of the ground leading soon

to the nucleate boiling regime and enhanced vaporization, whereas in the case of water, a longer film boiling phase on the ice layer does not allow for a high heat flux into the pool. This effect was well reproduced by the LAUV calculation.

3.1.2 Dispersion of Hydrogen

3.1.2.1 Dispersion in the Open Atmosphere

Many different accident situations are conceivable, which can give rise to the inadvertent emission of a flammable substance and which have great influence on the evolution of a vapor cloud. It can be released as a liquid or a gas or a two-phase mixture. The component, from which the substance is released, may be a tank, a pump, a valve, pipe work or other equipment. The orifice, through which it is leaking, can vary over different shapes and sizes. The leaking fluid can flow into different geometries. And finally it is the thermodynamic conditions of the fluid, which determine its release behaviour. Four major categories for the release of liquid or gaseous hydrogen can be identified:

1. small-scale, moderate hydrogen release from permeation or boil-off;
2. vaporization of a liquid hydrogen pool on a solid or liquid surface;
3. two-phase jet release of hydrogen after opening a system under pressure; and
4. rapid escape of hydrogen to all sides after the catastrophic failure of a pressure

Phenomena

The generation of a gas cloud in the atmosphere is principally caused by forces resulting from the internal energy of the gas and/or from energy inside the system, from which the gas has escaped, or from a relative excess energy in the environment. Those opposed are dissipative forces, among which atmospheric turbulence is the most important one.

In case there is no early ignition, the vapour cloud shape is further determined by density differences, atmospheric conditions, and topography. Several phases of a gas cloud formation can be distinguished: In the early phase, the gas cloud is still unmixed and usually heavier than the ambient air. Its spreading is influenced by gravitational force resulting in a near-ground, flat cloud. The following phase is characterized by a gradual entrainment of air from outside into the gas cloud enlarging its volume, thus lowering gas concentration, and changing its temperature. In the final phase, due to atmospheric dispersion, density differences between cloud and ambient air will be leveled out, where concentrations eventually fall below flammability limits. Thus density of the gas mixture vapor cloud varies with time.

The turbulence structure of the atmosphere is composed of large-scale turbulence described by the large-scale wind field, and of isotropic turbulence, which is a rapid variable superimposed to the medium wind field. The latter is generated due to the fact that “roughness elements” extracts kinetic energy from the medium wind field, which is transferred to turbulence energy. It is this energy and of particular importance the small eddies, which finally determine the spreading of the gas cloud; the larger eddies are responsible for its meandering. Further factors influencing the turbulence structure within a gas cloud, apart from the atmospheric turbulence of the wind and temperature field inside the turbulent boundary layer (5 mm < z < 1500 m), are:

1. velocity gradient (sheer force between wind field and gas cloud);
2. current created by buoyancy forces;
3. heat transfer from ground into cold gas (thermally induced turbulence); and

4. rapid expansion from vaporization of cryogens.

Fluctuations in the concentration as a consequence of the atmospheric turbulence are typically in the order of a factor of 10 above the statistical average.

The spreading of a gas cloud in the atmosphere is strongly influenced by the wind conditions which change with height. Vertical wind profiles can be determined as a function of the so-called stability categories depending on the temperature conditions. As an example, Pasquill suggested the categories A, B, C for unstable, D for neutral, E, F for stable conditions, (Pasquill, 1961). The spreading mechanism of a gas in the atmosphere is mainly by mixing with the ambient air. The boundary layer between gas and air governs momentum and mass exchange, which is much stronger than molecular diffusion. Horizontal dispersion perpendicular to wind direction is about the same for all stability categories; it is different for vertical dispersion. Under stable conditions, vertical exchange is small leading to a long-stretched downwind gas cloud. In contrast, a temperature decrease with height, which is stronger than the adiabatic gradient (-0.98 K/100 m), results in an effective turbulent diffusion and rapid exchange. This is particularly true for a hydrogen gas cloud, which behaves in a neutral atmosphere as if it were in an unstable condition. Worst-case scenario would be the existence of a large hydrogen gas cloud generated with minimal internal turbulence, on a cold, humid day with high wind velocity and strong atmospheric stability.

The jet release of a liquefied cryogen under pressure is connected with the formation of aerosols. The two (or three)-phase mixture developed exhibits an inhomogeneous concentration distribution. There will be a rapid vaporization, which may create locally high H_2 concentrations. It was observed that the larger the liquid fraction of the two-phase jet, the larger was the evolving flammable vapor cloud (Kneebone 1974) Another effect observed for vertical jet-like gas releases under certain conditions is a bifurcation of the plume into two differently rotating vortices. After a short acceleration phase, a double vortex is developing which eventually splits up. This effect may reduce the height of the gas cloud and lead to a stronger horizontal spreading (Zhang 1993).

With respect to just vaporized LH_2, the lifetime as a heavier-than-air cloud (1.3 kg/m^3) is relatively short. It needs only a temperature increase of the hydrogen gas from 20 K to 22 K to reach the same density of the ambient air (1.18 kg/m^3). This short time span of negative buoyancy is slightly prolonged by the admixed heavier air, before the buoyancy becomes positive and enhances with further temperature increase. Unlike pool vaporization leading to only weak vapor cloud formation, instantaneous release of LH_2 or high release rates usually result in intensive turbulences with violent cloud formation and mixing with the ambient air. If LH_2 is released onto water, rapid phase transitions occur, which are connected with very high vaporization rates. The exiting vaporized gas also carries water droplets into the atmosphere increasing the density of the vapor cloud and thus influencing its spreading characteristics.

The spreading behaviour of a large gas cloud is different from a small one meaning that the effects in a small cloud cannot necessarily be applied to a large one. For small releases, the dynamics of the atmosphere are dominant and mainly covering gravitational effects due to the rapid dilution. For large amounts released, the evolving gas cloud can influence itself, the atmospheric wind conditions changing wind and diffusion profiles in the atmosphere. This so-called “vapor blanket” effect could be observed particularly at low wind velocities, where the atmospheric wind field was lifted by the gas cloud and the wind velocity inside the cloud dropped to practically zero.

The near-ground release of cryogenic hydrogen resulting in a stable stratification has, in the initial phase, a damping influence on the isotropic turbulence in the boundary layer to the ambient air, thus leading to a stabilization of the buffer layer (so-called cold sink effect). For small wind speeds, additional effects such as further heating of the gas cloud due to energy

supply from diffusion, convection, or absorption of solar radiation, as well as radiation from the ground will play a certain role, since they reduce gas density and enhance positive buoyancy.

A still deep-cold hydrogen gas cloud exhibits a reduced heat and mass exchange on the top due to the stable stratification. A stronger mixing will take place from the bottom side after the liftoff of the cloud resulting from buoyancy and heating from the ground. The dilution is slightly delayed because of the somewhat higher heat capacity of hydrogen compared to air. In case of a conversion of para to ortho hydrogen, a heat consuming effect (708.8 kJ/kg), reduces the positive buoyancy. This process, however, is short compared to dispersion.

Another effect determining a cold hydrogen cloud behaviour is the condensation and solidification, respectively, of moisture which is always present in the atmosphere. The phase change is connected with the liberation of heat. Therefore density is decreased and thus buoyancy is enhanced. The higher the moisture content in the atmosphere, the sooner is the phase of gravitation-induced spreading of the vapour cloud terminated. The effect of condensation also results in a visible cloud, where at its contour lines, the temperature has just gone below the dew point. For high moisture contents, the flammable part of the cloud is inside the visible cloud. For a low moisture content, flammable portions can also be encountered outside the visible cloud. The visible and flammable boundaries coincide at conditions for an ambient temperature of around 270-300 K and humidity levels of 50-57 %.

According to the “model of adiabatic mixing” of ambient air and hydrogen gas, assuming there is no net heat loss or gain for the mixture, there is a direct correlation between mixture temperature and hydrogen concentration, if air temperature and pressure and relative humidity be known. This means on the other hand that thermocouples could be used as hydrogen detectors. The model was found to be in good agreement with measured concentrations. Taking the conditions of the NASA LH_2 spill trials as an example, the cloud boundaries were assessed of having had a hydrogen concentration of around 8-9 %.

The topography has also a strong influence on the atmospheric wind field and thus on the spreading of the gas cloud. Obstacles such as buildings or other barriers increase the degree of turbulence such that the atmospheric stability categories and their empirical basis are loosing their meaning locally. This situation requires the application of pure transport equations which may become very complex due to the generation of vortices or channeling effects (Perdikaris 1993). A gas cloud intersecting a building will be deflected upwards reducing the near-ground concentration in comparison to unobstructed dispersion. On the other hand, if the source is near the building in upwind direction, a vortex is created with a downwards directed velocity component, which may increase the near-ground concentration. This effect, however, may be more important for heavy gases than for the lighter gases.

Experimental Activities

The first hydrogen release experiments conducted with LH_2 date back to the late 1950s (Cassut 1960, Zabetakis 1961). They included, however, only little information on concentrations and were basically limited to visual recordings. The experimental series with LH_2 release conducted by A.D.Little were dedicated to the observation of the dispersion behavior showing that still cold hydrogen gas does not rise immediately upwards, but has the tendency to also spread horizontally. The initial column-like cloud shape later transforms into a hemispherical shape. Measurements of the translucence reveal large variations in the concentrations indicating incomplete mixing. The continuous release at a rate of 2 l/s over 16 min and of 16 l/s over 1 min and for wind speeds between 1.8-7.6 m/s, the developing visible vapor cloud had an extension of up to 200 m before fading away. Gusty winds had the effect of splitting up the gas cloud.

The first and up to now most relevant test series to study hydrogen dispersion behaviour was conducted by NASA in 1980 with the near-ground release of LH_2. In five tests, a volume of 5.7

m^3 was released over a period of 35-85 s; in two more tests the released volumes were 2.8 m^3 in 18 s and 3.2 m^3 in 120 s, respectively (Witcofski 1984, Chirivella 1986). Eight times the concentration was measured at a total of 27 positions. Temperature measurements were also indicators for H_2 concentration. These trials have shown that the H_2 vapour cloud can drift for up to several hundred m, particularly if the ground is able to sufficiently cool. The tests also demonstrated that the vaporization rate of LH_2 is strongly dependent on the type of release, much more so than that of other cryogens.

In 1994, the German Bundesanstalt fur Materialforschung und Prüfung (BAM) conducted LH_2 release experiments with the main goal to demonstrate the safety characteristic of a rapidly decaying hydrogen vapour cloud in the open atmosphere in contrast to the behaviour of vaporizing LPG. Six LH_2 spill tests were conducted with amounts released of 0.5-1 m^3 (total 260 kg) at rates of around 0.6-0.8 kg/s. The tests were also to show the influence of adjacent buildings on the dispersion behaviour (Schmidtchen 1994, Dienhart 1995).

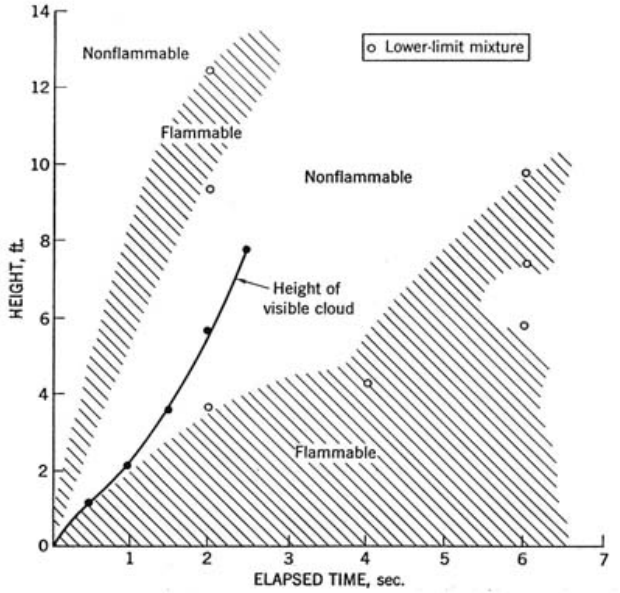

Figure 3-10: Shape of H2-air vapour cloud, from (Zabetakis 1961)

3.1.2.2 Dispersion in Obstructed Environment

When studying the hydrogen dispersion in obstructed environment it should be taken into account that the dispersing cloud behaviour completely differs for the cases of gaseous and liquefied hydrogen spills. Actually, hydrogen disperses as a heavier-than-air gas when escapes to the atmosphere from the liquid state and is characterized by horizontal movement and relatively long dilution times, whereas in gaseous form hydrogen is a buoyant gas. In this sense some of the results presented for the dispersion of other flashing liquids could be applicable to the hydrogen dispersion. For example Chan (1992) performed calculations for the numerical simulations of LNG vapour dispersion from a fenced storage area, and found that vapour fence can significantly reduce the downwind distance and hazardous area of the flammable vapour clouds. However, a vapour fence could also prolong the cloud persistence time in the source area, thus increasing the potential for ignition and combustion within the vapour fence and the

area nearby. Also Sklavounos and Rigas (2004) performed a validation of turbulence models in heavy gas dispersion over obstacles, which could also be applied for the earlier stages of the spill.

In the presence of buildings or other obstacles, the wind direction is also expected to play an important role for the cloud dispersion, due to the shielding effects of these obstacles.

The obstacle effect is twofold, in one way it inhibits gas convection, but on the other hand creates turbulence, thereby increasing gas dilution, extending the flammable region, and even accelerating the flame. Hydrogen may cause a series of accidental events (jet fire, flash fire, detonation, fireball, confined vapor cloud explosion), depending on the time of ignition and the space confinement. Unless an immediate ignition occurs, it becomes evident that dispersion calculation is required, in order to determine the lower flammable limit zones in the greater area of hydrogen facilities and hence preventing, via appropriate measures, flash fires and confined vapor cloud explosions corresponding to delayed ignition, see for example the work of Rigas and Sklavounos (2005).

Though accidents related to storage and use of hydrogen will certainly occur, there is not much data available in the literature about what happens when liquid hydrogen is accidentally released near the ground between buildings of a residential area. Only few numerical codes used for dispersion estimation can be applied to hydrogen, which means that further developmental work is necessary in this field.

Statharas et al. (2000) describe the modelling of liquid hydrogen release experiments using the ADREA-HF 3-D time dependent finite volume code for cloud dispersion and compare with experiments performed by Batelle Ingenieurtechnik for BAM as part of the Euro-Quebec-Hydro-Hydrogen-Pilot-Project (EQHHPP). They mainly deal with LH_2 near ground releases between buildings. The simulations illustrated the complex behaviour of LH_2 dispersion in presence of buildings, characterized by complicated wind patterns, plume back flow near the source, dense gas behaviour at near range and significant buoyant behaviour at the far range. The simulations showed the strong effect of ground heating in the LH_2 dispersion, as can be observed comparing Figs 3-11 and 3-12. The model also revealed major features of the dispersion that had to do with the ‘‘dense’’ behaviour of the cold hydrogen and the buoyant behaviour of the ‘‘warming-up’’ gas as well as the interaction of the building and the release wake.

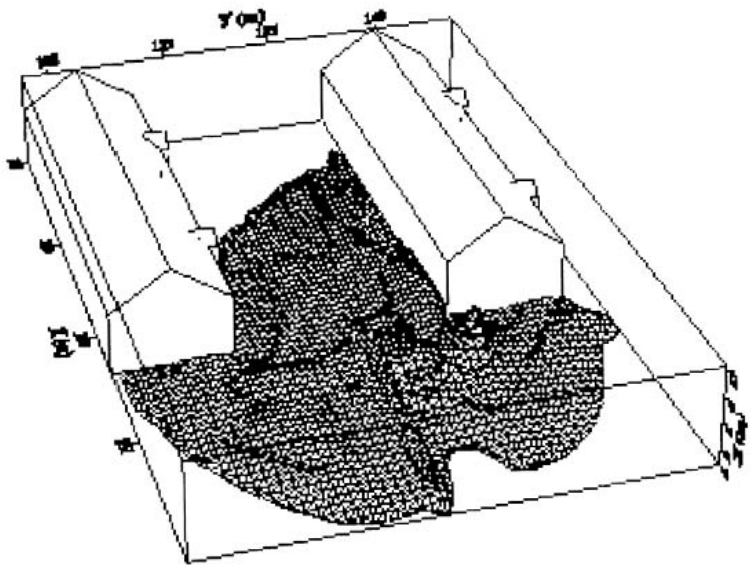

Figure 3-11 Predicted 4% isosurface at t = 100 s, without ground heating effects (Statharas et al., 2000).

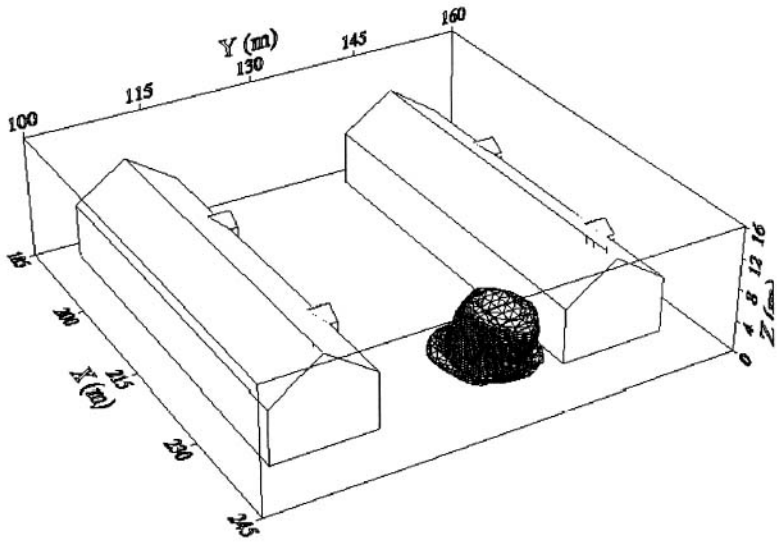

Figure 3-12: The predicted 4% isosurface at t = 100 s, with ground heat effects (Statharas et al., 2000).

Schmidt et al. (1999) performed a numerical simulation of hydrogen gas releases between buildings. Gas cloud shape and size were predicted using the Computational Fluid Dynamics code FLUENT 3. The modelling was made as close as possible to the pattern of the liquid hydrogen release experiments performed by BAM in the framework of the EQHHPP. Four main results were found:

- The release of hydrogen at high velocities (up to the critical velocity) results in a much more hazardous situation than a release at low exit velocities. At high velocities, high concentrations of H2 near the ground and a considerable enlargement of the range where explosive mixtures occur, have to be expected (Figs 3-13 and 3-14).

The approach of the hydrogen cloud to walls or other obstacles influences the pattern of the concentration field. Parts of the objects which obstruct the cloud dispersion cause a dilatation of the regions with explosive mixtures.

Strong wind and low release velocities lead to an enhancement of the upward drifting of the hydrogen cloud. This minimizes the risk of the occurrence of explosive mixtures near the ground.

The range of average concentrations of hydrogen produced by a gas release in a vertical direction starts to widen at relatively low heights. This results in an enlargement of the range with explosive mixtures.

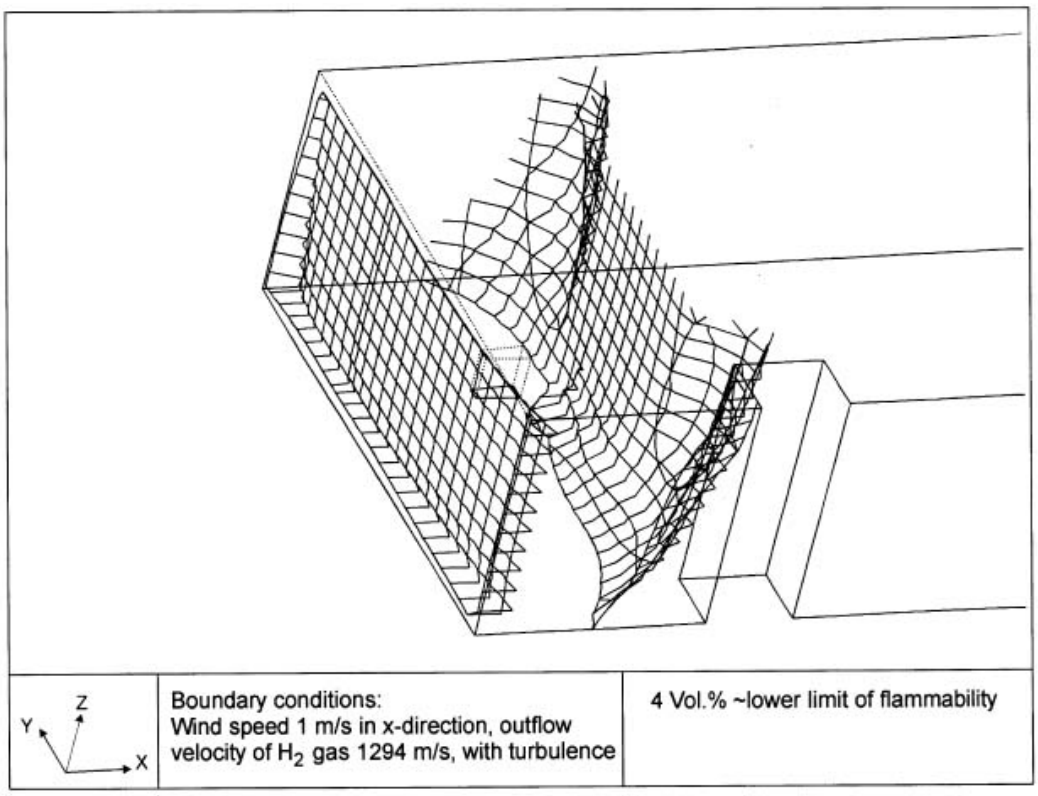

Figure 3-13: Fast release in z direction, 4 . % iso-surface (Schmidt et al., 1999).

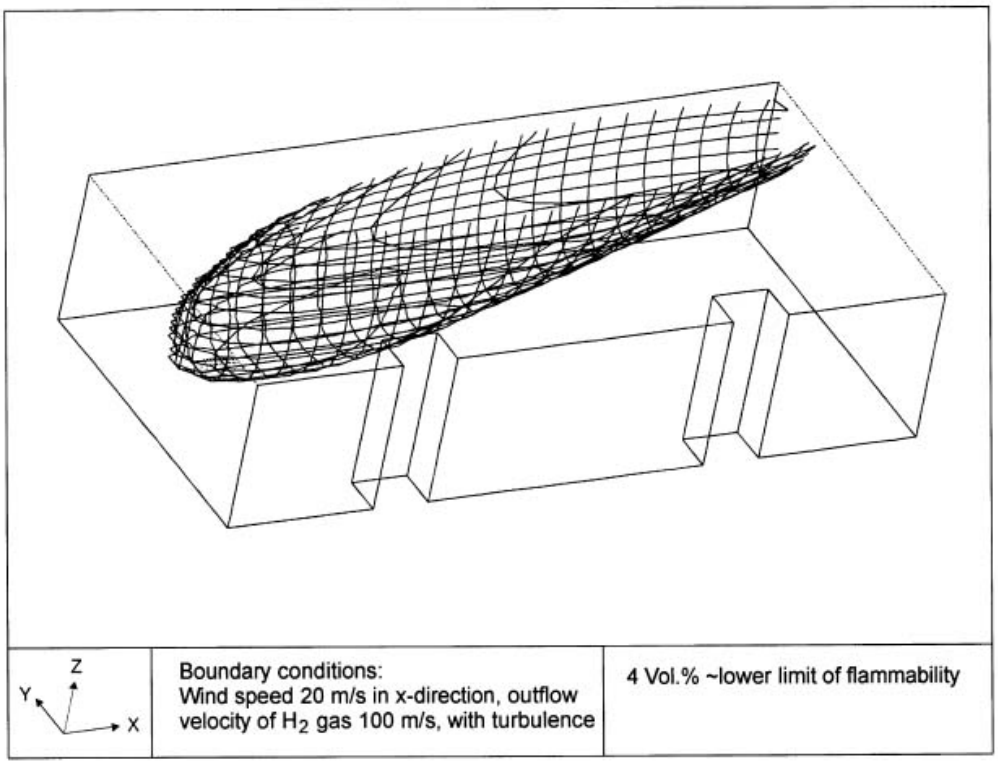

Figure 3-14: Slow release in z direction, 4 . % iso-surface (Schmidt et al., 1999).

Venetsanos et al. (2003) performed a study of the source, dispersion and combustion modelling of an accidental release of hydrogen in an urban environment. The paper illustrates an application of CFD methods to the simulation of an actual hydrogen explosion. Results from the dispersion calculations together with the official accident report were used to identify a possible ignition source and estimate the time at which ignition could have occurred, see Fig. 3-15. The combustion simulation shows that an initially slow(laminar) flame, that accelerates due to the turbulence generated by the geometrical obstacles in the vicinity (primarily the pressure tanks). Since the hydrogen cloud is very concentrated, with a large region with more than 15% hydrogen by volume, there is ample scope for flame acceleration. However, the general geometrical configuration is rather open, and beyond the bundles of pressure tanks there are few obstacles. This will tend to restrain the acceleration of the flame and prevent the flame from accelerating to very high speeds as seen in the simulations. These results are to a large extent compatible with the reported accident consequences, both in terms of near-field damage to building walls and persons, and in terms of far-field damage to windows. Their results demonstrate that hydrogen explosions in practically unconfined geometries will not necessarily result in fast deflagration or detonation events, even when the hydrogen concentration is in the range where such events could occur in more confined situations.

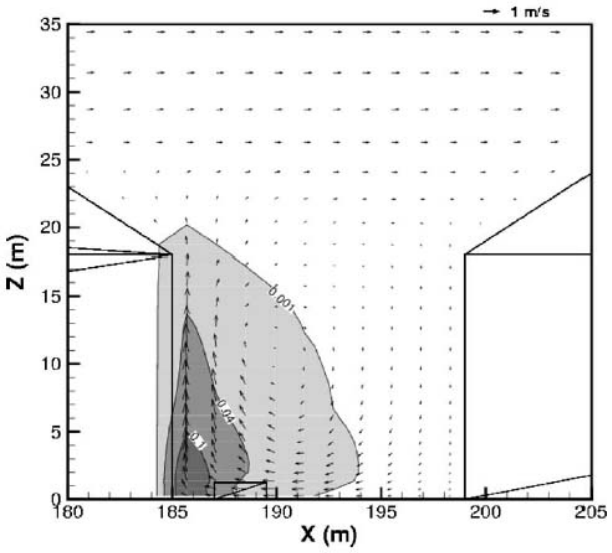

Figure 3-15: Predicted velocity and volume concentration field on a vertical cross-canyon plane at 9 m downwind from the source and time 10 s after start of the release (Venetsanos et al., 2003)

3.1.2.3 Dispersion in Confined Environment

Hydrogen Behaviour

The accidental release of hydrogen in confined environment differs from the open atmosphere and semi-confined cases in the fact that the leakage is located in a room. Then, the released hydrogen gets mixed with the room atmosphere, building up there or dispersing outwards through venting holes.

Depending on the storage system, hydrogen leaks as liquid or gaseous phase. For leaks involving LH_2, vaporization of cold hydrogen vapour towards the atmosphere may provide a warning sign because moisture condenses and forms a fog. This vaporization process usually occurs rapidly, forming a flammable mixture. On the other hand, for GH2 leaks, gas diffuses rapidly within the air.

The hydrogen gas released or vaporised will disperse through the environment by both diffusive and buoyant forces. Being more diffusive and more buoyant than gasoline, methane, and propane, hydrogen tends to disperse more rapidly. For low-momentum, gaseous hydrogen leaks, buoyancy affects gas motion more significantly than diffusivity. For high-momentum leaks, which are more likely in high-pressure systems, buoyancy effects are less significant, and the direction of the release will determine the gas motion; on the other hand, a jet is established, which reduces its inertia while it mixes.

Conversely, saturated hydrogen is heavier than air at those temperatures existing after evaporation. However, it quickly becomes lighter than air, making the cloud positively buoyant. At the end, localized air streams due to ventilation will also affect gas movement. Therefore, in all cases, a light gas cloud is developed near to the leak. It is rich in hydrogen, which is less dense than air in the room. This density difference induces a vertical buoyant force, making the hydrogen-rich cloud rise up and the heavier atmosphere air drop down. A region which is richer in hydrogen is developed and a buoyant plume is established. This plume mixes with the surrounding atmosphere but in a non-homogeneous way. When the plume impinges the top of the enclosure, it spreads throughout the ceiling and stagnates there. Depending on the release

location and the geometrical aspect ratio (slenderness) of the building, the inertia forces would be able to drive the atmosphere to either well-mixed or stratified conditions.

In the medium and long-term, other mixing phenomena could appear and change the atmosphere conditions. Other releases of hydrogen could push the hydrogen-rich cloud downwards favouring homogeneous conditions. Heat transfer (mainly by convection) between room atmosphere and walls could induce secondary circulation loops, thereby enhancing the mixing processes.

All of these phenomena yield the final distribution of hydrogen within the confined environment: well-mixed, stratified, locally accumulated, etc. Moreover, the presence of some systems could change these conditions, normally helping the mixing process. They are: venting systems, connections to other rooms, fan coolers, sprays, rupture disks, etc. In order to deal with accident events, some mitigation systems have been developed as dilution systems (by injection of inert gas), igniters (which burn flammable mixtures) and recombiners (which oxidise hydrogen in a controlled way) etc. Valuable devices are the Passive Autocatalytic Recombiners (PAR), which reduce the hydrogen mass by inducing the reaction with oxygen at low hydrogen concentrations, using palladium or platinum as catalysts.

In summary, six stages of a release in a confined environment can be identified: (1) leakage; (2) jet; (3) buoyant plume; (4) homogeneous/stratified dispersion; (5) convective and venting phenomena; and (6) mitigation systems (if any).

The phenomena related to leakages and jets have been analysed in the chapter on “release of hydrogen”, considering the phase of the hydrogen release (liquid or gas), the structures developed (spills, jets and so on), the sonic or subsonic condition at the hole and other related phenomena.

After them, the hydrogen-rich cloud losses its inertia and buoyant forces become dominant. Usually, this cloud is less dense than the surrounding air and then the force is directed upwards. When the hydrogen released is very cold, buoyant forces could point downwards. However, the heat and mass transfers during the mixing process reduce the mixture density and invert the buoyant force direction. The fluid structure established is a plume, where two regions are distinguished: forced plumes and buoyant plumes. At the forced plume both forces (inertia and buoyancy) are of similar magnitude and separate pure inertia region (jet) apart from the pure buoyant region (plume).

The buoyancy to inertia ratio is expressed by the densimetric Froude number

$$Fr = \frac{\rho_0 {U_0}^2}{(\rho_\infty - \rho_0) g d_0}, \qquad (11)$$

where U_0, ρ_0 and d_0 are the fluid velocity, the fluid density and the diameter at the break point, respectively, g is the gravity acceleration and ρ_∞ is the bulk density. Using this dimensionless number, Gebhart et al. (1988) recommend the following expressions (Table 3-1) for the three regions of a vertical upward structure. The x-direction is along the centreline of the structure, u_c, ρ_c and c_c the fluid velocity, the fluid density, and concentration at the centreline. Notice that velocity (u) and concentration (c) profiles at any transversal plane are expressed by Gaussian functions.

When the structure shape is very different from an upward vertical one, these regions need to be established by numerical simulations (see 3.1.2.4 below).

Table 3-2 Recommended expressions for the three regions of a vertical upward structure (from Gebhart et al. 1988).

REGIONS	*INERTIA*	*INTERMEDIUM*	**BUOYANCY**
STRUCTURE	JET	FORCED PLUME (OR BUOYANT JET)	BUOYANT PLUME
BOUNDS	$Fr^{-1/4}\left(\frac{\rho_0}{\rho_\infty}\right)^{-1/4}\left(\frac{x}{d_0}\right) < 0.5$	$0.5 \le Fr^{-1/4}\left(\frac{\rho_0}{\rho_\infty}\right)^{-1/4}\left(\frac{x}{d_0}\right) \le 5$	$5 < Fr^{-1/4}\left(\frac{\rho_0}{\rho_\infty}\right)^{-1/4}\left(\frac{x}{d_0}\right)$
$\frac{u_c}{U_0}$	$6.2\left(\frac{\rho_0}{\rho_\infty}\right)^{-1/2}\left(\frac{x}{d_0}\right)^{-1}$	$7.26Fr^{-0.05}\left(\frac{\rho_0}{\rho_\infty}\right)^{9/20}\left(\frac{x}{d_0}\right)^{-1}$	$3.5Fr^{-1/3}\left(\frac{\rho_0}{\rho_\infty}\right)^{-1/3}\left(\frac{x}{d_0}\right)^{-1/5}$
$\frac{(\rho_\infty - \rho_c)}{(\rho_\infty - \rho_0)}$	$5\left(\frac{\rho_0}{\rho_\infty}\right)^{-1/2}\left(\frac{x}{d_0}\right)^{-1}$	$0.44Fr^{1/16}\left(\frac{\rho_0}{\rho_\infty}\right)^{-7/16}\left(\frac{x}{d_0}\right)^{-5/4}$	$9.35Fr^{1/6}\left(\frac{\rho_0}{\rho_\infty}\right)^{-1/3}\left(\frac{x}{d_0}\right)^{-5/3}$
$\frac{c_c}{C_0}$	$6.34\left(\frac{x}{d_0}\right)^{-1}$	--	$12.16Fr^{1/3}\left(\frac{\rho_0}{\rho_\infty}\right)^{1/3}\left(\frac{x}{d_0}\right)^{-5/3}$
$\frac{u}{u_c}$	$\exp\left[-92\left(\frac{r}{x}\right)^2\right]$	--	$\exp\left[-90\left(\frac{r}{x}\right)^2\right]$
$\frac{c}{c_c}$	$\exp\left[-52\left(\frac{r}{x}\right)^2\right]$	--	$\exp\left[-80\left(\frac{r}{x}\right)^2\right]$

Molecular vs. Turbulent Mixing

The relative importance of advection and diffusion in the distribution or mixing of a chemical species like hydrogen may be derived through non-dimensioning the general advection-diffusion equation of transport. This dominance is a function of flow velocity u, species diffusivity *D* and time *t*, and may be expressed in terms of the non-dimensional Péclet number:

$$Pe = \frac{D}{u^2 t} = \frac{D}{uL}, \qquad (12)$$

where *D* is the diffusion coefficient, *u* is the velocity, *t* is time and *L* is a characteristic length scale. Diffusion is the dominant mechanism when Pe>>1 and transport by advection dominates for Pe<<1. It is important to note that, whenever large times, t, or characteristic lengthscale, L = ut, are considered, the advection transport would always dominate. The Péclet number expresses the ratio between the characteristic times of advection and diffusion. The length travelled by a particle is proportional to t for advection and to $t^{1/2}$ for diffusion.

Characteristic length and time scales for advection and diffusion transport may be expressed by

$$L_{advection} = ut \quad (13)$$

$$t_{advection} = \frac{L}{u} \quad (14)$$

$$L_{diffusion} = \sqrt{Dt} \quad (Eq. 15)$$

$$t_{diffusion} = \frac{L^2}{D} \quad (Eq. 16)$$

These expressions are useful as rules of thumb.

Potential for Accumulation Depending on Leaking

When the jet or buoyant plume is established within the enclosure, the medium-term atmosphere conditions would be either well-mixed or inhomogeneous. The relevant phenomena are: (1) local accumulation on dead-end regions; (2) stratification-homogenisation in ceilings; (3) homogenisation by convective motions; (4) venting phenomena; and (5) mitigation systems.

Local accumulation usually happens in regions near the release point or in the way of circulation loops. There are regions in the enclosure with dead-end enclosures, badly-vented or ceiling, which make difficult the ascending dispersive motions.

Stratification-homogenisation in ceilings is a more complex phenomenon. The stratification consists on forming stable layers of fluid which do not mix each other, because of the lack of atmosphere gradients apart from jets, plumes or boundary layers. When stratification happens the fluid is not stagnated, but the motion does not allow mixing between separate layers.

The mixing patterns established in the enclosure are induced by jets, plumes and convective heat transfer. These phenomena induce moments in the fluid, which produce the competition between two forces: inertia and buoyancy. When the inertia forces are dominant, the enclosure atmosphere will get mixed. When buoyancy is prevailing the stratification remains, and in this case the vertical gradient is established as a balance of (Woodcock et al., 2001): (1) thermo-hydrodynamic stability (by temperature gradients); (2) horizontal fluxes (by air entrainment); (3) ceiling plumes (by Rayleigh-Bénard convective motions).

The thermo-hydrodynamic stability is characterised by the Richardson number, Ri,

$$Ri_{e,H} = \frac{(\rho_\infty - \rho_0)gH}{\rho_\infty u_e^{\,2}} \quad (17)$$

and the Reynolds number

$$\mathrm{Re}_{e,H} = \frac{\rho_\infty u_e H}{\mu_0} \quad (18)$$

where H the enclosure height, u_e the entrainment velocity and μ_0 the dynamic viscosity at the break point. When Richardson number is greater than unity and greater than the inverse of the Reynolds number, buoyancy forces dominate inertia forces and the density gradients at the horizontal direction are negligible. From this condition, Peterson (1994)[iv] established criteria for stratification in a confined environment (bounded at the upper part, but open in transversal directions to avoid accumulation).

In the case of a round jet, stratification occurs when the following criterion is satisfied:

$$\left(\frac{H}{d_0}\right) Fr^{-1/6} \left(1+\frac{d_0}{0.2\sqrt{2}H}\right)^{2/3} >> 1 \qquad (19),$$

as demonstrated by Lee et al. (1974)[v] and Jain and Balasubramanian (1978) (Fig.3-16).

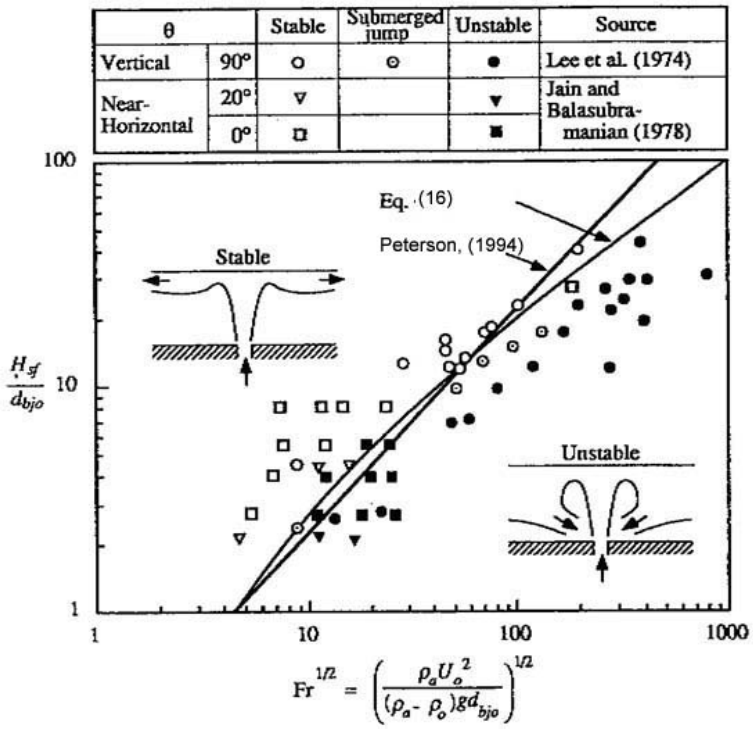

Figure 3-16 Stratification criteria for round jets (Peterson, 1994)

In case of a round buoyant plume, the criterion is the following

$$\frac{4.17}{0.35}\left(\frac{H}{d_0}\right)^{5/3} Fr^{-1/6} >> 1 \qquad (20)$$

These criteria are not conditions sufficient to quantify the buoyancy gradients. It is necessary to analyse other effects in order to establish mixing or stratified conditions in enclosures: horizontal fluxes and ceiling plumes. The Rayleigh number, Ra, which is defined as

$$Ra_H = \frac{g(\rho_\infty - \rho_w)H^3}{\rho_\infty \nu^2}\Pr, \qquad (21)$$

is used in this case to determinate these conditions. When the Rayleigh number is greater than 109, the turbulent fluxes generate density gradients which reduce the stability of the stratified layers, and initiates mixing patterns (Woodcock et al., 2001).

Finally, the location of the release point could reduce established inhomogeneous conditions in a closed room, by the fact that the inertia forces are not enough to impulse the hydrogen below the release point. Then hydrogen will accumulate at the upper part of the room and the mixing process will be led by slower phenomena: molecular diffusion or convective heat. Some experiments as NUPEC M-8-1 (CSNI, 1999[vi]) and Shebeko et al. (1988) have illustrated this phenomenon.

Influence of Natural Ventilation of Structures

In general, the accidental release of hydrogen in confined environments will be affected by ventilation streams coming from other rooms or from the atmosphere. As a general safety rule: "Any structure containing hydrogen system components shall be adequately ventilated when hydrogen is in the system" (NASA, 1997). The amount of ventilation required will vary in each case depending on the total supply of hydrogen, the rate of generation, and the venting arrangement from the process or hydrogen system. The goal of any hydrogen ventilation system is to keep the concentration below the lower flammability limit (4% at normal conditions).

Ventilation systems use vents, ducts, heat exchangers, fans and other components. They are based on the principles of natural or forced convection as described above in this chapter. Under most common conditions, hydrogen has a density lighter than air and tends to rise upwards when in contact with air. On the other hand, the air temperature affects the ventilation behaviour: warmer air is less dense than cooler air, and therefore warm air tends to push upwards when in contact with cooler air.

The use of a fan, as a forced ventilation system, has to supply approximately 25 times the volume of hydrogen to maintain a safe concentration of hydrogen. The reliability of this system depends on the eventual event of a mechanical or electrical failure.

In order to avoid these reliability problems, passive systems are usually established on hydrogen applications in enclosures. A typical configuration is based on using high and low vents on walls. Under most common conditions, hydrogen has a lighter density than air and tends to rise upward when in contact with air. Moreover, warmer air is less dense than cooler air, and so warm air tends to push upwards when in contact with cooler air. In general, a ventilation system is driven more by air temperature differences than by hydrogen concentration, and can be affected by the difference of temperature between the enclosure and the external environment.

On a cool day, when the inside temperature is hotter than outside, the lighter warm air mixed with the lighter hydrogen in the enclosure will rise together out the high vent, drawing fresh cool air in through the low vent. Both the temperature of the warm air and the presence of hydrogen will drive the ventilation rate. Under these conditions, the hydrogen amount in the enclosure will decrease. On a warm day, the direction of air flowing through the vents can reverse. When this happens, warm air trying to enter the top vent pushes back the hydrogen trying to rise out the same vent, causing the hydrogen to stagnate and build up inside the enclosure. On this condition the hydrogen is trapped within the enclosure and the molecular diffusion is the only mechanism to mix the hydrogen. Therefore, the explosive conditions could be not avoided.

Other systems use tubes as a small chimney that catches the hydrogen at some elevation. The use of these tubes in combination with low or high vents, being set at the same height on the

wall, prevents some of the unwanted thermal convection described above. However, the combination of these systems has to be studied in detail, considering the effect of the external conditions in order to avoid failures in the ventilation behaviour under certain circumstances.

Experimental Tests

Tests most representative of hydrogen behaviour within enclosures are the following:

- The Russian tests by Shebeko et al., (1988): hydrogen distribution experiments for a subsonic release of hydrogen in a closed vessel.

- GEXCON, NH and STATOIL (GEXCON, 2003) performed hydrogen dispersion experiments in a confined compartmented space.

- CEA has performed slow release helium dispersion tests in their MISTRA facility, Caron-Charles and Blumenfeld (2001), also Blumenfeld and Caron-Charles.

- Tests in the gallery facility of INERIS

A valuable knowledge and experimental database has been compiled in the field of nuclear fission safety through an extensive program of tests for hydrogen distribution and mixing within confined geometries, with the aim to develop and validate numerical tools for modelling hydrogen relases and mixing processes. Geometrical conditions are typical of nuclear reactor containments (large and multi-compartment), and test conditions are very nuclear-specific (high contents of steam, no venting). As an example they are worth mentioning the tests performed in the HDR and BMC facilities in Germany or the NUPEC one in Japan (CSNI, 1999), as well as those planned or performed at the ThAI (Kanzleiter, 2005) and PANDA (Auban, 2006) facilities.

3.1.2.4 Numerical Simulations

The object of dispersion modeling of hydrogen releases is the calculation of the concentration distribution of hydrogen in their vicinity. From this distribution, envelopes of constant concentrations encompassing higher concentration levels can be determined, from which clearance distances to limit the consequences resulting form accidental ignition. The shape of these envelopes can be complex, and will depend on the emission problem, which determines the nature of the flow and its rate of release, the obstacle configurations and the environmental conditions. Computer fluid dynamics simulations are thus often used to perform such calculations, as they can take into account in principle any level of details.

Calculation Models for the Simulation of Atmospheric Dispersion of Gas Clouds

There are several classes of calculation models to simulate the atmospheric dispersion of gas clouds:

1. Gaussian model
2. Jet model
3. Box or slab model
4. Particle simulation model
5. k-ε model representing CFD models
6. Large Eddy Simulation

The Gaussian plume model is the classical approach for the simulation of the spreading of neutral (sufficiently diluted) gases incl. pollutants or radioactivity. It is a simple model describing the concentration profile as a solution of the diffusion/advection differential equation with empirical coefficients depending on the atmospheric conditions. This model, however, is inappropriate for treating the buoyant behavior of light or heavy gases.

Dispersion models are often accompanied by a jet release model to calculate the dispersion of a released gas with significant momentum flux, which is the dominant parameter for jets. The jet can be classified into two main zones, a region of adjustment from storage conditions to atmospheric pressure and a region of "conventional" jet dispersion at ambient conditions. If storage conditions are pressurized, the initial zone of adjustment will possibly include flashing for a liquid or choked two-phase jet. The conventional dispersion region begins with a so-called region of flow establishment, in which similarity profiles for the concentration and axial velocity evolve; following this the jet evolves with self-similar profiles. The main features distinguishing the various jet models are the treatment of the air entrainment and the choice of the similarity profile (e.g., top-hat, Gaussian).

The macro or two-zones mixture model developed by BASF (Giesbrecht 1980) regards the bursting of a pressure vessel, where the high exit velocity results in a fully turbulent propagation of the vessel contents. Two zones are distinguished: a core zone of the vapor cloud where (cold) liquid droplets are still existing, and a boundary zone. In the core zone, ideal mixture with spatially constant and temporally decreasing concentration is assumed, while in the boundary zone, a spatially constant and temporally decreasing turbulent diffusion coefficient is assumed.

In box or slab models, the released gas cloud is assumed to be of cylindrical shape. The processes of advection (transport by the mean wind field), air entrainment, and gravitational spreading are implemented in empirical correlations which were derived from experiments. Box models were basically developed to simulate heavier-than-air vapor clouds with averaged temperature and concentration. In extended versions, vertical profiles of temperature and concentration can be assumed. Acknowledged box models are the US code DEGADIS (Havens 1990) or the British code HEGADAS (McFarlane 1990).

Particle simulation models are based on the stochastic nature of the movement of particles in the atmospheric wind field. In a simulation, numerous (typically 5000-15,000) particles are being emitted and their trajectories traced making a statistical analysis of the velocity fluctuations. The turbulent velocity is considered to undergo changes only after a certain time defined as the Lagrange correlation time. The distribution of the particles in a given calculation grid is then a measure for the concentration distribution. An improvement of the model is given by assuming a so-called Markov process for a particle meaning that the fluctuation part is further subdivided into a component representing the capability of remembering, and a random component. The velocity at time t is then composed of a fraction proportional to the "old" velocity at time t-dt and a remainder produced in a random number generator. One representative particle simulation model is the German code LASAT (Martens 1991).

State-of-the-art modeling of the transient behavior of gases with either positive or negative buoyancy in the atmosphere is provided by Computer Fluid Dynamics (CFD) models, which simulate complex flow processes by solving the Navier-Stokes equations in an Eulerian 3D (or 2D) calculation grid structure. This approach comprises the conservation equations of mass, momentum, and energy. Apart from being (in most cases) immensely time-consuming, these models require a detailed input of initial and boundary conditions.

In the two-equation k-ε turbulence model, special partial differential equations are solved to describe the transport of turbulence as well as its generation and dissipation. Of all the approaches, the k-ε model offers the highest relative independence of empirical relations. It

appears to be the only one to allow a proper simulation of hydrogen dispersion, because it meets the requirements of describing effects such as turbulence energy in the gas cloud, interaction with the atmospheric wind field, the characteristic positive buoyancy, transient sources with initial momentum, and last but not least, gas flow in a complex geometry (buildings, terrain). The k-ε modelling and many of its variations have been implemented in a number of computer codes distinguished by the choice of the numerical solution method, which was found to have a significant effect on the calculation procedure.

Large Eddy Simulation (LES) is a technique that is rapidly finding widespread use. It is a computer intensive approach, where the large eddies are treated explicitly, while the smaller eddies are modelled using a so-called sub-grid scale model. Development of sub-grid scale models is a very active field. The sub-grid scale model introduces a constant, C_s, which is not a constant, Pope (2004). Pope (2004) also showed that it would not be possible to obtain a grid independent solution, as the value for C_s needed to be adjusted as the mesh was refined. LES also requires care when setting up the model and specifying the initial flow field, including velocity and concentration fluctuations.

Simulation of Hydrogen Dispersion in the Atmosphere

Only a few efforts have been made in the past to simulate the dispersion of hydrogen gas mostly due to the poor experimental data base available. Early efforts were made in the late 1970s by the Los Alamos National Laboratories on a box model for hydrogen taking into account heat transport from the ground into the cloud (Edeskuty 1980), and then applying the Gaussian model of neutral and buoyant dispersion as part of the WHAZAN software package (Stewart 1990).

The NASA has developed the code AFGASDM applicable to LH_2 and other aviation fuels. The model is something between a Gaussian model and an Eulerian grid model solving the conservation equations following a gas "parcel" released as a puff until it has diluted below the flammability limits. Effects of air entrainment and phase changes are also taken into account (Brewer 1981).

The k-ε atmospheric dispersion model POLLUT was developed at the TU Munich to describe hot gas plumes escaping from stacks of power plants. The code was used in a DLR study (Eichert 1992) to investigate hydrogen dispersion from accidental release of LH_2 from vehicle tanks both in open terrain and in a road tunnel.

The computer code CHAMPAGNE of Mitsubishi Heavy Industries is a multi-phase, multi-component thermodynamics model originally dedicated to the assessment of severe accident in fast breeder nuclear reactors. It has been modified to also treat the formation and propagation of hydrogen vapor clouds. CHAMPAGNE was successfully applied to the NASA LH_2 spill tests from 1980 (Chitose 1996).

Simulation of hydrogen dispersion in semi-confined environments

A subsonic horizontal hydrogen jet experiment and subsequent CFD simulation was reported by Swain (2004) (Figure 3-17 and Table 3-3). Hydrogen was released at 25 scf/min through a 1 cm diameter orifice. The predicted concentrations showed good agreement with measurements.

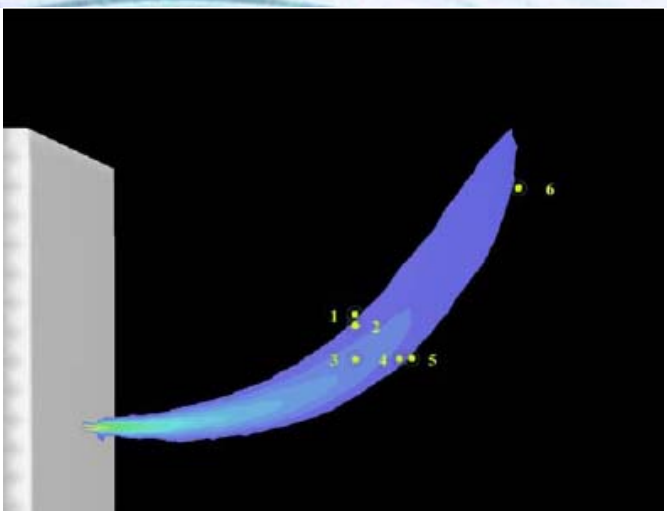

Figure 3-17 Concentration contour of a 25 scf/min release. The numbers show locations where the concentration of hydrogen was measured experimentally

Table 3-3

Sensor position	Experimental H2 concentration (%)	Simulation H2 concentration (%)	Deviation (%)
1	5.0-5.9	5.04	-8.13
2	5.6-7.0	6.96	10.48
3	9.4-10.8	13.99	38.50
4	8.1-9.4	8.25	-5.70
5	5.6-6.6	5.29	-13
6	3.5-4.6	5.37	32.60

The BAM 5 and 6 LH2 dispersion experiments in the presence of buildings (Marinescu-Pasoi and Sturm 1994) were simulated by (Statharas 2000) using the ADREA-HF code. The source was modeled using a series of two phase flow jets. Liquid phase evaporation during the dispersion was taken into account using the homogeneous equilibrium model. The calculations were performed using a one-equation turbulence model. Reasonable agreement with measured concentrations was reported when ground heating was taken into account.

The Battelle k-ε model BASSIM originally designed for hydrogen combustion in nuclear containments has been applied to predicting the BAM LH_2 release trials in 1994, providing reasonable qualitative results for 3D effects of hydrogen dispersion behavior (Rastogi 1994).

The 1983 Stockholm (Sweden) hydrogen accident was simulated by (Venetsanos et al. 2003) using the ADREA-HF code for dispersion and the REACFLOW code for the combustion. An integral tool was applied to simulate the release of 4 kg of hydrogen from a network of 18 interconnected cylinders of 15 l volume each containing hydrogen at 200 bar.

Figure 3-18: Simulation of the 1983 Stockholm hydrogen accident (Venetsanos et al., 2003), Left: Modelled site and lorry carrying 4 kg of hydrogen in 18x50 l, 200 bar bottles (red circle), Right: Predicted lower flammability hydrogen-air cloud at time 10 seconds after start of release

Simulation of hydrogen dispersion in confined environments

The use of hydrogen applications (especially automotive) in confined environments like private garages, public parking, maintenance shops, electrolyzers, compressor buildings, tunnels, etc. requires detailed evaluation of the risk related to potential hydrogen leaks and if necessary identification of measures to be taken in order to avoid buildup of flammable/explosive hydrogen atmospheres. In this respect the CFD methodology has been widely used as shown in the review below, since it is generally able to realistically account for the various geometrical configurations and complex release conditions.

Hydrogen leaks inside a residential garage compared against gasoline, natural gas and propane leaks in the same environment were simulated by Swain (1998) using the FLUENT code. Calculations were based on the GEOMET garage geometry (2.52 x 6.59 x 2.74 m) with a single vent placed in the center of one wall of an otherwise sealed garage. The leak rates for fuels other than hydrogen were adjusted for equal size holes and equal energy flow rates in the fuel lines considering both laminar and turbulent flow where applicable. The results of the simulations show that for the lower leakage rate (1000 l/hr) and typical garage air exchange (2.92 ACH representing natural ventilation), hydrogen and methane did not create dangerous conditions while propane and gasoline did produce dangerous conditions in similar accident scenario. For the larger fuel leakage rate (7200 l/hr) and minimal air exchange rate (0.2 ACH) all four fuels produced very large combustible clouds after 2 hours of leakage. However, the energy content of the combustible clouds was different, with hydrogen being at most % that of the other fuels. Both natural gas and hydrogen filled the entire garage with a flammable mixture after two hours, while propane and gasoline filled just over half of the garage volume with a flammable mixture. At the higher air exchange rate (2.92 ACH), the hydrogen still filled the garage with a flammable mixture, which reached about 6.6 % hydrogen concentration after two hours.

Hydrogen dispersion experiments in a half-scaled hallway and subsequent CFD validation using the FLUENT code were performed by Swain (1999). The hallway geometry dimensions are 2.9 × 0.74 × 1.22 m. Hydrogen leaked at a rate of 2 SCFM (0.94 lt/s) from the floor at the left end. At the right end of the hallway, there were a roof vent and a lower door vent for the gas ventilation. Four sensors were used to record the local hydrogen concentration variations with time. Predicted hydrogen concentrations time series were found in good agreement with the experimental data. The same experiments were simulated by Agranat et al. (2004), using the PHOENICS code. Predicted results were found similar to the ones obtained using the FLUENT code with maximum concentration differences between the two models of about 20 %.

Boil-off from the cryogenic hydrogen tank of a car in a private garage was simulated by Breitung et al. (2001) using the GASFLOW code to calculate the temporal and spatial distribution of hydrogen and criteria to evaluate the flame acceleration and detonation potential. Boil-off was assumed occurring at a rate of 170 g day^{-1} and the boil-off release to occur intermittently in five pulses per day of 100 or 10 s time period each, which gave 0.34 or 3.4 g s^{-1} respectively.

The facility modifications and associated incremental costs that may be necessary to safely accommodate hydrogen fuel cell vehicles (HFCVs) in four support facility case studies: 1) commercial multi-story above-ground parking, 2) commercial multi-story below-ground parking, 3) residential two vehicle garages and 4) commercial maintenance/repair/service station were evaluated by the California Fuel Cell Partnership (CaFCP, 2004). For each case study, a baseline building design was developed incorporating functional requirements and applicable conventional building codes. CFD modelling (FLUENT) was used to analyze a limited set of H2 leak scenarios inside the four types of facilities. The study was based on parking a 5-passenger sedan with compressed H2 gas reservoir carrying capacity of 6 kg at 10,000 psi (689.5 bar) pressure. The HFCV was designed to comply with SAE J2578 and J2579 standards for H2 and fuel cells, which include provisions for safety systems onboard the vehicle. Such assumed mechanisms include the implementation of a hydrogen detector in each wheel well. Each detector was designed to signal a shut down and isolation H2 procedure upon detecting 1% H2. Another assumed mechanism includes the use of an on-board computer that is capable of shutting down H2 flow upon detecting a larger than 20 CFM leak (9.4 lt s^{-1}) when the vehicle is dormant. In addition the HFCV was equipped with a valve that isolates H2 in the tank upon engine (fuel cell) shut down. This assumed isolation mechanism was designed to monitor and test for leaks upon vehicle shut down and prior to start up by the on-board computer. In the study most of the modelling scenarios were based on a 20 CFM leak from beneath the vehicle. This leak rate corresponded to a fuel cell power output of about 50 kW. For the considered hydrogen release scenarios it was found that:

For the considered residential garage layout no modifications to the baseline structures would appear to be necessary for vehicles equipped with safety systems that detect hydrogen leaks according to the chosen scenarios. CFD modelling of one configuration showed that a 1% hydrogen concentration would reach the wheel well within 28 seconds where detectors could initiate a shut off of the fuel supply. Since not all vehicles will be equipped with hydrogen detectors, or be configured like the chosen vehicle design, additional modelling provided data on the time for a 5% hydrogen concentration to accumulate at the garage ceiling. This information may be used by carmakers to develop strategies to limit the amount of time that the vehicle operates at zero speed before shutting off the fuel supply.

For the considered below and above ground parking facilities no modifications to the baseline structures were recommended. Existing ventilation in the below ground structure would dilute a 20-CFM hydrogen leak so that a flammable mixture would only exist in close proximity to the vehicle. Similarly, natural ventilation would dilute hydrogen leaks for the above ground parking facility.

For the considered maintenance facility no modifications to the baseline structures were recommended. The high rates of ventilation would dilute the assumed 20-CFM leak and result in a flammable mixture only in close proximity to the vehicle. The potential for flammable mixtures forming at the ceiling of the facility was also assessed. The time required for a hydrogen leak to result in 20% of the LFL at the ceiling was determined for different vehicle leak rates. Options for improving the ventilation in the building are presented in the report.

Helium dispersion experiments in a private garage (dimensions: 6.42 x 3.71 x 2.81 m) including a mockup of a car and performed by Swain (1998) were simulated by Papanikolaou and

Venetsanos (2005) using the ADREA-HF code and the standard k-ε model. Helium was released below the car at a flow rate of 7200 l/hr. The predicted results were found generally in acceptable agreement with the experiment. For the case with the lowest vent size the vertical concentration gradient was found underestimated compared to the experiment. This was attributed to the turbulence model overestimating mixing under the given low flow conditions.

Tunnel accidents with an LH2 powered vehicle were simulated by Breitung et al. (2000). The investigated scenarios assume damage of the LH2 system, release of gaseous hydrogen, mixing with air, ignition and finally combustion. Calculations showed that gaseous hydrogen rises to the tunnel ceiling forming a strongly stratified mixture. Shape, size, inner structure and temperature of the evolving H2-air cloud were calculated. Using new developed criteria, the time and space regions with potential for fast combustion modes were identified. For the given hydrogen sources the combustion regime is governed by the ignition time. For late ignition a slow and incomplete combustion of the partly premixed H2-air cloud along the tunnel ceiling was predicted. For early ignition a standing diffusion flame develops with dimensions and heat fluxes determined by the hydrogen release rate. Temperature, oxygen and flow velocity fields during the combustion were computed. In both cases only minor pressures were generated. The highest damage potential appeared to exist for intermediate ignition times.

Simulations of hydrogen releases from LH2 and CGH2 private vehicles (cars) in a naturally ventilated tunnel were reported by Wilkening et al. (2000). The work was performed within the framework of the EIHP project. The ADREA-HF code was used for the dispersion calculations. The REACFLOW code was used for the combustion calculations. Two LH2 release scenarios were considered. A flow restrictor installed and a two-phase release of 8.3 g/s was assumed in the first scenario. A shut-off valve activated 5 seconds after the release and a gaseous release of 60 g/s was considered in the second. For the CGH2 scenario sonic release from a 200 bar storage tank was assumed. The reported overpressure results indicated that for the scenarios considered there is no major difference in using liquid hydrogen or compressed hydrogen fuel.

Simulations of hydrogen releases from CGH2 commercial vehicles (busses) in city environment, tunnel environment and maintenance garage environment were performed during the EIHP2 project, using the ADREA-HF code for dispersion and the REACFLOW code for combustion. Three different storage pressures were considered for the CGH2 releases 200, 350 and 700 bar. Comparative simulations were performed for a 200bar CNG bus.

Catastrophic hydrogen releases inside the Alpha H2BPS (H2 Backup Power System by Stewart Energy) generator room were simulated by Agranat et al. (2004) under real industrial working scenarios and real geometry, using the PHOENICS code and the LVEL turbulence model. Two scenarios were considered in the simulations: a vertical fast release from a high-pressure line and a horizontal fast release from a medium-pressure line. The CFD simulations showed that the two installed sensors are capable of detecting 10 % LFL cloud (0.41%) separately at 8.8 and 9.7 seconds for the high-pressure vertical leak, but only one sensor which is closer to the leak orifice can detect the same concentration cloud within 20 seconds for the medium-pressure horizontal release. The numerical simulation confirmed that the current sensor installation can promptly report the potential catastrophic hydrogen leak under the above scenarios. However, the fact that 10 % LFL hydrogen cloud cannot reach one sensor during the horizontal release indicates that the sensor location can be further optimized and more sensors are required for the systems.

The method for determination of maximum ventilation described in the standard IEC EN 60079-10 was validated by Nilsen et al. (2004) for a small hydrogen production (by water electrolysis) unit located inside two different enclosure geometries, using the FLACS code for dispersion and the PHAST code for release. It was found that the model suggested in standard IEC EN 60079-10 is not a conservative approach when deciding the ventilation capacity large enough to keep flammable gas clouds at a negligible size and therefore must be used with care.

High pressure hydrogen release experiments inside the storage room of a full scale model of a hydrogen refueling station were reported by Tanaka et al.. Storage pressure was 40 MPa while nozzle diameters in the range 0.8-8 mm. The storage room with dimensions 6x5x4 m included 35 cylinders of 250 l capacity each. Ventilation openings of 1m height existed on all 4 sidewalls and where either 50 % or 100 % open. The time history of the average hydrogen concentration in the room was modelled using a simple gas accumulation model [Cleaver et al. 1994][vii] and compared against the experimental data. It was found that the model is able to predict well the experimental concentrations in the experiments involving more slowly varying pressure (lower nozzle diameters), but tends to overpredict the concentrations for the higher nozzle diameter.

CFD simultions of hydrogen dispersion in tunnels was performed by (Mukai et al. 2005), using the STAR-CD code and standard k-ε model. The amount of hydrogen leaked was 60 m^3 (approximately 5.08 kg), which corresponds to the amount necessary for future fuel cell vehicles to achieve their desired running distance. The study considered the typical longitudinal and lateral areas of tunnels, the underground ventilation facilities and the electrostatic dust collectors.

3.1.3 Knowledge Gaps and Recent Progress

Simulations of hydrogen dispersion using the CFD methodology have increasingly grown in number during the last 10 years and are expected to grow even more in the near future. Prediction of the time and space distribution of the flammable hydrogen clouds evolving after accidental hydrogen leaks of various types in widely different environments is the main output necessary for subsequent risk assessment estimation of the various hydrogen applications. In this process, simulations have been performed using different CFD codes (commercial or research tools) and different modelling strategies (turbulence models, source treatment, discretization options, etc.).

To ensure the quality and trust in industrial CFD applications best practice guidelines have been developed in the past either of a general character like (ERCOFTAC 2000) or more related to particular applications like (HSL 2003). No CFD guidelines specific to hydrogen dispersion applications have been proposed.

Taking the above in consideration a significant effort has been concentrated within the European Network of Excellence HYSAFE with aim to perform a systematic evaluation of the various CFD approaches (codes and models) in predicting hydrogen dispersion, based on a series of benchmark exercise problems, using existing and new state of the art experimental data.

The results of the first such hydrogen dispersion benchmark exercise (SBEP-V1) were reported by (Gallego et al. 2005). The experiment simulated was that of (Shebeko et al. 1988), who investigated the dispersion of hydrogen in an hermetically closed cylinder (20 m^3 volume) by measuring axial hydrogen concentrations (6 locations) at times from 2 to 250 minutes following an initial 60 s vertical subsonic jet release at a rate of 4.5 l/s from a 10mm nozzle. Large variations in predictions were monitored during this first benchmark (as expected), which could be attributed to variations in turbulence models, boundary conditions as well as discretization options.

The aim of the second hydrogen dispersion benchmark exercise (SBEP-V3) was three fold a) to further investigate on the ability of the models to predict the long term stratification/diffusion problem in a confined space, b) to test the ability of models to predict the concentration field of a vertical subsonic hydrogen jet release and c) to attempt to minimize or justify large variations

between model predictions. Recently performed hydrogen dispersion experiments by INERIS at their gallery facility (garage like enclosure with dimensions 7.2 x 3.8 x 2.9 m) were used for this benchmark. The release was vertical upwards at a rate of 1 g/s from an orifice of 20 mm diameter and lasted for a period of 240 s. The total simulation time was 5400 s. The benchmark took part in two phases a blind pre-test phase and a post–test one.

Further benchmarks focus on testing the ability to predict free choked hydrogen flows, obstacle effects on hydrogen dispersion within confined spaces as well as hydrogen dispersion from LH_2 releases.

Computer fluid dynamics simulations of choked flows are difficult to tackle due to the presence of the shock waves. The simulations may require, for commercial solvers, resolving the Mach cone and the shock wave patterns to some degree of details. Since the extent of the flammability envelopes resulting from chocked releases from apertures of about 1 cm may reach 10 to 100 m depending on the storage pressure, length scales of up to five orders of magnitude must be covered by the mesh. In addition, convergence will usually be problematic.

The difficulties faced by direct CFD simulations of choked releases may be alleviated by using effective diameter approaches. The applicability of effective diameter approaches to horizontal releases of hydrogen should be investigated further, particularly for the large hydrogen releases resulting from high pressure flows, where the effects of buoyancy on the shape of the release remain an issue.

For choked hydrogen releases the fact that the molar concentration is proportional to the inverse distance has been observed experimentally, but given that significantly different proportionality constants have been reported, a systematic investigation both experimental and computational is still required to cover a wider range of storage pressures and orifice diameters.

Regarding obstacle effects on hydrogen dispersion it should be mentioned that steady-state flow rates can lead to unsteady behaviour of the dispersion pattern in some cases, particularly when impingement flows or external flows (over a surface) are considered, due to significant vortex shedding. Such situations may require a statistical definition of the constant (flammable) concentration envelope, based on the probability distribution of finding a given concentration of hydrogen at a specific location at a given time.

The two most commonly used turbulence models, k-ε and k-ω models, have a number of known limitations, i.e. relating to modelling of highly buoyant flows and flows exhibiting high anisotropy. A Large Eddy Simulation technique is in theory better suited to such flow situations, but is currently too computer intensive for routine calculations of large number of scenarios. This is especially the case of long (in real-time) simulations.

Finally as far as LH2 release and dispersion are concerned it seems that more experimental information is needed to trigger further physical understanding and model development/improvement. From the past experience it seems that these proposed tests should focus on better control over the experimental conditions (less uncertainty).

3.1.4 References and Sources

Hanna S.R., and Strimaitis D., Workbook on Test Cases for Vapor Cloud Source Dispersion Models, American Institute of Chemical Engineers, New York, pp. 122

Chen C.J. and Rodi W. (1980), Vertical Turbulent Buoyant Jets – A review of Experimental Data, HMT-4 Pergamon

Encyclopedie des gaz. (1976) L'Air Liquide, Division Scientifique, Amsterdam: Elsevier

Venetsanos, A.G., Huld, T., Adams, P., and Bartzis, J.G. (2003) Source, dispersion and combustion modelling of an accidental release of hydrogen in an urban environment, J. Hazard. Materials A105, 1-25.

Mohamed K., Paraschivoiu M. (2005) Real gas simulation of hydrogen release from a high-pressure chamber, Int. J. Hydrogen Energy 30, 903–912

Cheng Z., Agranat V.M., Tchouvelev A.V., Houf W. and Zhubrin S.V. (2005) PRD hydrogen release and dispersion, a comparison of CFD results obtained from using ideal and real gas law properties, Proceedings First International Conference on Hydrogen Safety, 8-10 September, Pisa, Italy.

Lemmon, E.W., A.P. Peskin, M.O. McLinden, and D.G. Friend, (2000) NIST Thermodynamic and transport properties of pure fluids (NIST 12), Version 5.0, National Institute of Standards and Technology, Gaithersburg, MD

Angers B., Hourri A., Bénard P., Tessier P. and Perrin J. (2006), Simulations of hydrogen releases from high pressure storage systems, WHEC 16, 13-16 June, 2006 Lyon France

Birch, A.D., Brown, D.R., Dodson, M.G., and Swaffield, F., (1984) The Structure and Concentration Decay of high Pressure Jets of Natural Gas, Combustion Science and Technology 36, 249-261

Ewan B.C.R. and Moodie K., (1986) Structure and velocity measurements in under-expanded jets, Combustion Science and Technology 45, 275-288

Birch, A.D., Hughes, D.J., and Swaffield, F., (1987) Velocity Decay of High Pressure Jets, Combustion Science and Technology 52, 161-171.

Houf, W., Schefer, R., (2005) Predicting Radiative Heat Fluxes and Flammability Envelopes from Unintended Releases of Hydrogen, Presented at 16th Annual Hydrogen Conference and Hydrogen Expo USA, March 29 – April 1, Washington, D.C.,

Ruffin E., Mouilleau Y. and Chaineaux J., (1996) Large scale characterization of the concentration field of supercritical jets of hydrogen and methane, J. Loss Prevention Process Ind. 9, pp. 279-284

Chaineaux J., (2006) Contribution to WP 12 (and WP 3): EXPLOJET, a tool for the determination of hazardous zones dimensions, HySafe project presentation, InsHyde meeting,

Chaineaux J., (1999) Leak of Hydrogen from a pressurized vessel-Measurement of the resulting concentration field, EIHP Workshop on dissemination of goals, preliminary results and validation of the methodology, Bruxelles, pp.156-161

Chitose K. et al., (2006) Research on fundamental properties of hydrogen, IEA/Task 19 Meeting, Vancouver, Canada

Houf, W., Schefer, R., (2006) Predicting Radiative Heat Fluxes and Flammability Envelopes from Unintended Releases of Hydrogen, to be published in the International Journal of Hydrogen Energy

Bricard P., Friedel L., (1998) Two-phase jet dispersion, J. Hazard. Mater. 59, (287-310).

Lees F.P., (1996) Loss Prevention in the Process Industries. Hazard Identification, assessment and Control, Vol. 1, Second Edition, Reed Educational and Professional Publishing Ltd.,

Etchells J. and Wilday J. (1998) Workbook for chemical reactor relief system sizing, Health and Safety Executive (HSE) books, pp. 237,

D'Auria F., Vigni P., (1980) Two-phase critical flow models. A technical addendum to the CSNI state of the art report on critical flow modelling, Universita degli Studi di Pisa, Istituto di Impianti Nucleari,

Fauske, H.K., Epstein, M., (1988) Source term considerations in connection with chemical accidents and vapour cloud modelling, J. Loss Prev. Process Ind., Vol. 1, pp. 75-83

Dienhart B., (1995) Ausbreitung und Verdampfung von flüssigem Wasserstoff auf Wasser und festem Untergrund, Research Center Juelich Report No. Juel-3155

Brandeis J., Ermak D.L., (1983) Numerical Simulation of Liquefied Fuel Spills: I. Instantaneous Release into a Confined Area, Int. J. Numerical Methods in Fluids, 3, 1983, pp. 333-345; II. Instantaneous and Continuous LNG Spills on an Unconfined Water Surface, Int. J. Numerical Methods in Fluids, 3, pp. 347-361.

Chirivella J.E., Witcofski R.D., (1986) Experimental Results from Fast 1500-Gallon LH2 Spills, Am. Inst. Chem. Eng. Symp. Ser., 82, No. 251, pp. 120-140.

Fay J.A., (1978) A Preliminary Analysis of the Effect of Spill Size on the Level of Hazard from LNG Spills on Land and Water, US Department of Energy Report No. DOE/EV-0002,

Briscoe F., Shaw P., (1980) Spread and Evaporation of Liquid, Progr. Energy Com. Sci. 6, pp. 127-140.

Webber D.M., (1991) Source Terms, J. Loss Prevention in the Process Industries, 4, pp. 5-15.

Brewer G.D., et.al., (1981) Assessment of Crash Fire Hazard of LH2-Fueled Aircraft, NASA Lewis Research Center Final Report No. NASA-CR-165525,

Kneebone A., (1974) Prew L.R., Shipboard Jettison Tests of LNG onto the Sea. Proc. 4th Int. Conf. On LNG, Algiers, Algeria, Session V, Paper 5.

Zhang X., Ghoniem A.F., (1993) A Computational Model fort he Rise and Dispersion of Wind-Blown, Buoyancy-Driven Plumes, I. Neutrally Stratified Atmosphere. Atmospheric Environment 27A, 2295-2311

Perdikaris G.A., (1993) Dreidimensionale Ausbreitung von Abgasen aus Muellverbrennungsanlagen und Deponien – Einfluss von Bebauung, Gelaendestruktur, Witterung und Freisetzungshoehe. Technical University of Munich

Cassut L.H., Maddocks F.E., Sawyer W.A., (1960) A Study of the Hazards in the Storage and Handling of Liquid Hydrogen. Adv. Cryo. Eng. 5, 55-61

Zabetakis M.G., Furno A.L., Martindill G.H., (1961) Explosion Hazards of Liquid Hydrogen. Adv. Cryo. Eng. 6, 185-194.

Witcofski R.D., Chirivella J.E., (1984) Experimental and Analytical Analyses of the Mechanisms Governing the Dispersion of Flammable Clouds Formed by Liquid Hydrogen Spills. Int. J. Hydrogen Energy 9, 425-435.

Schmidtchen U., Marinescu-Pasoi L., (1994) Dispersion of Hydrogen and Propane Gas Clouds in Residential Areas. Proc. 10th World Hydrogen Energy Conference, Cocoa Beach, USA, 255-268.

Chan, S.T. (1992) Numerical simulations of LNG vapor dispersion from a fenced storage area. Journal of Hazardous Materials, Volume 30, Issue 2 , pp.195-224

Sklavounos, S., and Rigas, F. (2004) Validation of turbulence models in heavy gas dispersion over obstacles. Journal of Hazardous Materials, Volume 108, Issues 1-2, pp.9-20.

Rigas, F., and Sklavounos, S. (2005) Evaluation of hazards associated with hydrogen storage facilities International Journal of Hydrogen Energy. 30, pp.1501-1510

Statharas, J.C., Venetsanos, A.G., Bartzis, J.G., Wurtz, J., and Schmidtchen, U. (2000) Analysis of data from spilling experiments performed with liquid hydrogen. Journal of Hazardous Materials, Volume 77, Issues 1-3, pp.57-75

Schmidt, D., Krause, U., and Schmidtchen, U. (1999) Numerical simulation of hydrogen gas releases between buildings. International Journal of Hydrogen Energy, Volume 24, Issue 5, pp.479-488

Gebhart B, Jaluria Y, Mahajan RL, Sammakia B, (1988) Buoyancy-Induced Flows and Transport, Hemisphere, New York

Woodcock J, Peterson PF, Spencer DR, (2001) Quantifiying the Effects of Break Source Flow Rates on AP600 Containment Stratification". Nuclear Technology, Vol. 134, pp. 37-48,

Peterson PF, (1994) Scaling and Analysis of Mixing in Large Stratified Volumes", International Journal of Heat and Mass Transfer, Vol. 37, Suppl. 1, pp. 97-106, Elsevier Science

Lee J.H., Jirka G.H., Harleman D.R.F., (1974) Stability and Mixing of a Vertical Round Buoyant Jet in Shallow Water", MIT, Ralph M Parson Laboratory for Water Resources and Hydrodynamics, Tech. Rep. no. 195

Jain SC, Balasubramanian V, (1978) Horizontal Buoyant Jets in Quiescent Sallow Water. J. Environ. Engng. Div., Proc. ASCE, Vol. 104, EE4

CSNI, (1999) State of Art Report on Containment Thermahydraulics and Hydrogen Distribution, OECD Nuclear Energy Agency, Nuclear Safety, NEA/CSNI/R(99) 16

Shebeko, Y.N., Keller, V.D., Yeremenko, O.Y., Smolin, I.M., Serkin, M.A., Korolchenko A.Y., (1988) Regularities of formation and combustion of local hydrogen-air mixtures in a large volume, Chemical Industry, 21, pp. 24(728)-27(731) (in Russian)

NASA, (1997) Safety Standard for Hydrogen and Hydrogen Systems: Guidelines for Hydrogen System Design, Materials Selection, Operations, Storage, and Transportation, NSS 1740.16

GexCon (2003) 03-F46201-rev00 report (confidential)

Caron-Charles M, and Blumenfeld L, (2001) The MISTRA experiment for Field Containment Code Validation: First Results" 9th Int. Conf. on Nuclear Engineering, ICONE-9, Nice

Blumenfeld L, (1991)Caron-Charles M, "Jet et panache d'hélium" CEA Saclay, Gif sur Yvette

Kanzleiter T, Fischer K, Häfner W, (2005) THAI multi-compartment containment experiments with atmosphere stratification. NURETH-11, Avignon

Auban, O., Zboray, R., Paladino, D., (2006) Investigation of Large-Scale Gas Mixing and Stratification Phenomena related to LWR Containment Studies in the PANDA Facility, submitted to Nuclear Engineering and Design

Giesbrecht H., et.al., (1980) Analyse der potentiellen Explosionswirkung von kurzzeitig in die Atmosphaere freigesetzten Brenngasmengen, Teil 1: Gesetze der Wolkenausbreitung und -deflagration aus Berstversuchen and Metallbehaeltern. Chem.-Ing.-Tech. 52, 114-122

Havens J.A., Spicer T., (1990) LNG Vapor Dispersion Prediction with the DEGADIS Dense Gas Dispersion Model, Topical Report, University of Arkansas in Fayetteville, USA

McFarlane K., et.al., (1990) Development and Validation of Atmospheric Dispersion for Ideal Gases and Hydrogen-Fluoride, Part I: Technical Reference Manual, Shell Research Ltd., Thornton Research Center

Martens R., Massmeyer K., (1991) Untersuchungen zur Verifizierung von komplexen Modellen zur Beschreibung des Schadstofftransports in der Atmosphaere, Report GRS-A-1844, Gesellschaft fuer Reaktorsicherheit, Garching, Germany

Edeskuty F.J., et.al., (1980) Hydrogen Safety and Environmental Control Assessment, Report LA-8225-PR, Los Alamos Scientific Laboratory, USA

Stewart W.F., Dewart J.M., Edeskuty, F.J., (1990) Safe Venting of Hydrogen. Proc. 8th World Hydrogen Energy Conference. Honolulu, USA 1209-1218

Eichert H., et.al., (1992) Gefaehrdungspotential bei einem verstaerkten Wasserstoffeinsatz, Deutsche Forschungsanstalt fuer Luft- und Raumfahrt (DLR), Stuttgart, Germany

Chitose K., Ogawa Y., Morii T., (1994) Analysis of a Large-Scale Liquid Hydrogen Spill experiment Using the Multi-Phase Hydrodynamics Analysis Code (Champagne). Proc. 11th World Hydrogen Energy Conference. Stuttgart, Germany 2203-2211

Swain, M., (2004) Codes and standards analysis, 2004 annual program review meeting of the hydrogen, fuel cells & infrastructure program of the US Department of Energy

Marinescu-Pasoi L., Sturm, B. (1994) Messung der Ausbreitung einer Wasserstoff- und Propangaswolke in bebautem Gelände and Gasspezifische Ausbreitungsversuche", Battelle Ingenieurtechnik GmbH, Reports R-68.202 and R-68.264

Rastogi A.K., Marinescu-Pasoi L., (1994) Numerical Simulation of Hydrogen Dispersion in Residential Areas. Proc. 10th World Hydrogen Energy Conference. Cocoa Beach, USA 245-254

Swain M.R., Schriber J.A. and Swain M.N., (1998) "Addendum to Hydrogen Vehicle Safety Report: Residential Garage Safety Assessment. Phase-1: Risks in Indoor vehicle storage", Prepared for Directed Technologies Inc., pp 118

GEOMET final report IE-2647 (1993) Hydrogen Emissions from EV Batteries Undergoing Charging in Residential Garages", prepared for Electric Power Research Institute, Palo Alto, CA, by GEOMET Technologies, Inc., October 22

Swain M.R., Grilliot E.S. and Swain M.N., (1999) "Experimental verification of a hydrogen risk assessment method", Chemical Health & Safety, pp 28-32

Agranat V., Cheng Z. and Tchouvelev A., (2004), "CFD Modeling of Hydrogen Releases and Dispersion in Hydrogen Energy Station", Proceeding of WHEC-15, Yokohama

Breitung W., Necker G., Kaup B., Veser A., (2001) Numerical Simulation of hydrogen release in a private garage", Proceedings of the 4th international symposium on Hydrogen power - theoretical and engineering solutions, HYPOTHESIS IV. Vol. 1-3, 542 pages, Stralsund (Germany)

CaFCP Technical report (2004) 'Support facilities for hydrogen fuelled vehicles-Conceptual design and cost analysis study', Prepared for California Fuel Cell Partnership by Parsons and Brinckerhoff in association with TIAX and University of Miami

Swain M.R., Grilliot E.S. and Swain M.N., (1998b) "Addendum to Hydrogen Vehicle Safety Report: Residential Garage Safety Assessment. Phase-2: Risks in Indoor vehicle storage", Prepared for Directed Technologies Inc., pp 35

Papanikolaou E.A. and Venetsanos A.G. (2005) CFD modelling for helium releases in a private garage without forced ventilation", Proceedings of the first international Conference on Hydrogen Safety, Pisa

Breitung W., Bielert U., Necker G., Veser A., Wetzel F.J., Pehr K., (2000) Numerical Simulation And Safety Evaluation Of Tunnel Accidents With A Hydrogen Powered Vehicle, Proceedings of the 13th World Hydrogen Energy Conference, Beijing

Wilkening H., Venetsanos A.G., Huld T., Bartzis J.G., (2000) Safety Assessment of Hydrogen as a fuel for vehicles by numerical simulation", paper presented at the Euro-Conference "New and Renewable Technologies for Sustainable Development", Madeira Island, Portugal

The European Integrated Hydrogen Project (EIHP and EIHP-2), www.eihp.org

Nilsen S., Hoiset S., Saeter O., Lunde E., Andersen H., (2004), "CFD simulations of accidental releases of hydrogen - decision basis for classification of hazardous zones in H2 production enclosures", Proceeding of Loss Prevention Symposium in Prague.

Tanaka T., Azuma T., Evans J.A., Cronin P.M., Johnson D.M., Cleaver R.P., (2005) Experimental study on hydrogen explosions in a full scale hydrogen filling station model, Proceedings First International Conference on Hydrogen Safety, Pisa

Cleaver R.P., Marshall M.R., Linden P.F., (1994) J. Hazard. Materials, 36, 209-226

Mukai S., Suzuki J., Mitsuishi H., Oyakawa K., Watanabe S., (2005) CFD simulation on diffusion of leaked hydrogen caused by vehicle accident in tunnels, Proceedings First International Conference on Hydrogen Safety, Pisa

Casey M., Wintergerste T., (2000) Best Practice Guidelines, ERCOFTAC Special interest group on "Quality and Trust in Industrial CFD", Version 1

Ivings M.J., Lea C.J., Ledin H.S., Outstanding Safety Questions concerning the analysis of ventilation and gas dispersion in gas turbine enclosures: Best Practice Guidelines for CFD, HSL report CM/03/12.

Gallego, E., Migoya, E., Martin-Valdepenas, J. M., Garcia, J., Crespo, A., Venetsanos, A., Papanikolaou, E., Kumar, S., Studer, E., Hansen, O. R., Dagba, Y., Jordan, T., Jahn, W., Oíste, S., Makarov, D., (2005) An Intercomparison Exercise on the Capabilities of CFD, International Conference on Hydrogen Safety, Pisa, Italy

Pasquill, F., (1961) The estimation of dispersion of windborne material, *Meteorology Magazine* 90 (1063):33-49

Pope, S. B., (2004) Ten questions concerning the large eddy simulation of turbulent flows, New Journal of Physics 6:35

3.1.5 Hydrogen Ignition

Contributing author	Main contributions	Organisation	e.mail
Stuart Hawksworth	Chapter coordinator	HSL	
Luc de Broisia	Static electricity	INERIS	
Andrzej Teodorczyk	Electrical spark Auto-ignition	WUT	ateod@itc.pw.edu.pl

Contributing reviewer	Information reviewed	Organisation	e.mail

3.1.5.1 Introduction

There are number of potential ignition sources for flammable mixtures of hydrogen with an oxidant, which include flames, electrical sparks, fused wires, incendiaries, hot surfaces, heating, rapid adiabatic compression, shock waves and catalytic materials. All of these processes heat a portion of the combustible mixture to a sufficiently high temperature such that adjacent un-combusted layers also react, producing a flame, which propagates through out the mixture.

Basic combustion properties

Technical report ISO/TR 15916 (2004) presents basic combustion properties of hydrogen in air mixtures. These are reproduced in the Table 3-4 below.

Table 3-4 Ignition and combustion properties for hydrogen-air mixtures at 25 °C and 101.3 kPa

Lower flammability limit (% vol.)	Lower detonation limit (%vol.)	Stoichiometric mixture (% vol.)	Upper detonation limit (% vol.)	Upper flammability limit (% vol.)	Minimum Ignition Energy (mJ)	Auto-ignition temperature (°C)
4.0	18.3	29.5	59.0	75.0	0.017	585

The flammability of hydrogen in air with nitrogen as a diluent is presented by Molnárné et al (2003), and flammability diagrams are presented at temperatures from 20°C to 400°C, and pressures from atmospheric to 100 bar. The flammability diagram for 20°C and atmospheric pressure is given in Fig. 3-19 below, reproduced from Molnárné et al (2003), with permission.

The limiting oxygen concentration at 20°C and atmospheric pressure can be read from Fig 3-19 as 20.4% air. Since air contains 21% oxygen, the limiting oxygen concentration is 0.204 x 21% = 4.3% oxygen. Raising the temperature widens the limits, but the lower limit has the greater ratio of change. The major change is to increase the upper limit, and decrease the limiting oxygen concentration (LOC). The diagram at 400°C and atmospheric pressure is as in Fig. 3-20. Note that the limiting oxygen concentration has fallen to 6.2% air, corresponding to a LOC of 1.3%, and the upper limit has risen from 75.6% to 87.6%. The lower explosive limit has fallen from 4.1 to 1.4%.

Similar effects are shown for increases in pressure, with the limits generally falling with pressure, and the limiting oxygen concentration rising. Tabulated data for the effect of temperature at atmospheric pressure is shown below in Table 3-5, and the effect of pressure at 20°C is shown below in Table 3-6 and Table 3-7.

Table 3-5 Effect of Temperature on Hydrogen Flammability - DIN 51649-1

Temperature °C	LEL % volume	UEL % volume	Limiting Air Concentration % volume	LOC % volume
20	4.1	75.6	20.4	4.3
100	3.4	77.6	19.1	4.0
200	2.9	81.3	15.0	3.2
300	2.0	83.9	10.9	2.3
400	1.4	87.6	6.2	1.3

Table 3-6 Effect of Pressure on Hydrogen Flammability - 2.7 dm3 Bomb

Pressure bar	LEL % volume	UEL % volume	Limiting Air Concentration % volume	LOC % volume
1	4.3	78.5	21.5	4.5
10	4.9	72.4	27.6	5.8
100	5.8	74.1	25.9	5.4

Table 3-7 Effect of Pressure on Hydrogen Flammability - prEN 1839-B

Pressure bar	LEL % volume	UEL % volume	LOC % volume
1	4.0	95.2	4.5
10	5.0	94.2	5.8
100	5.7	94.9	5.1

Note that there are small discrepancies between the Tables for 20°C and 1 bar. This is because the limit determinations were carried out using different methods. The preferred method is that of EN 1839-B.

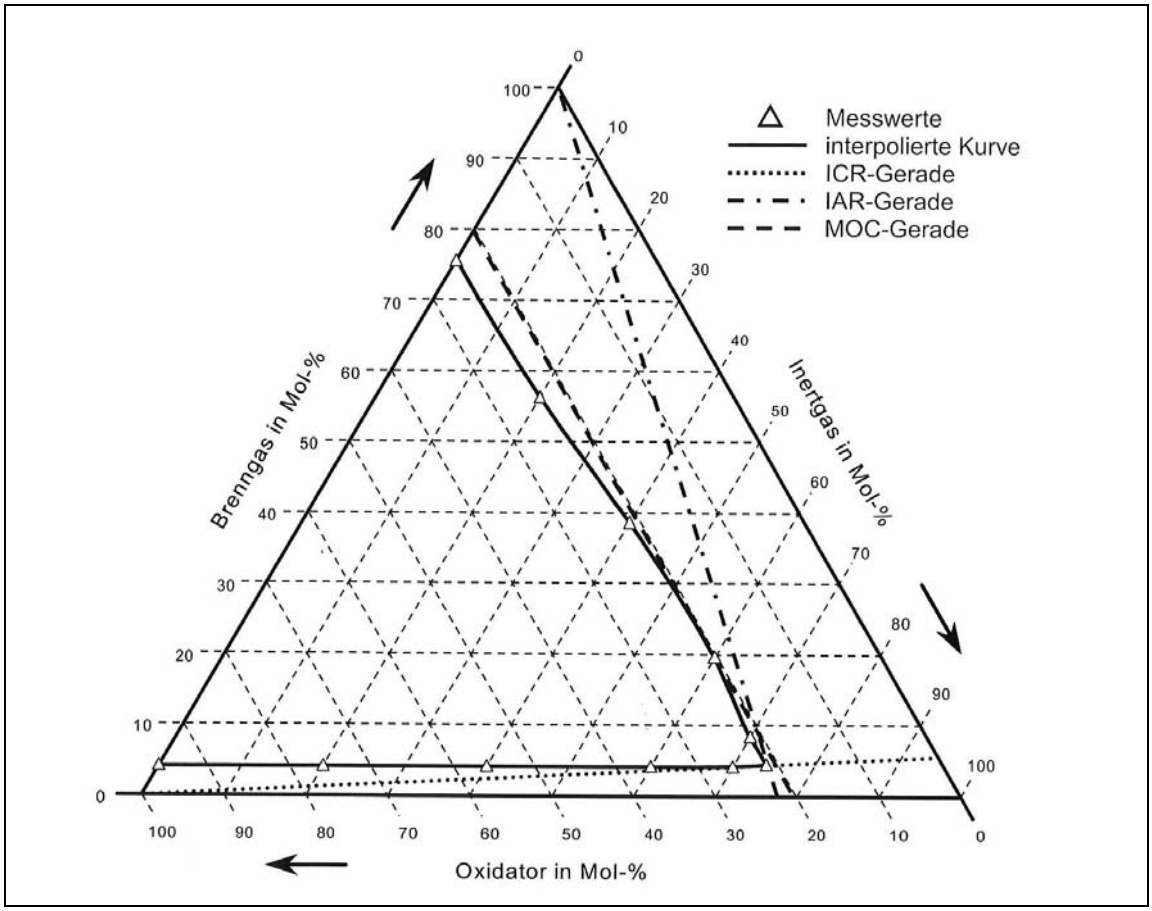

Fig 3-19- Flammability Diagram for Hydrogen/Air/Nitrogen at 20℃ and 1 bar

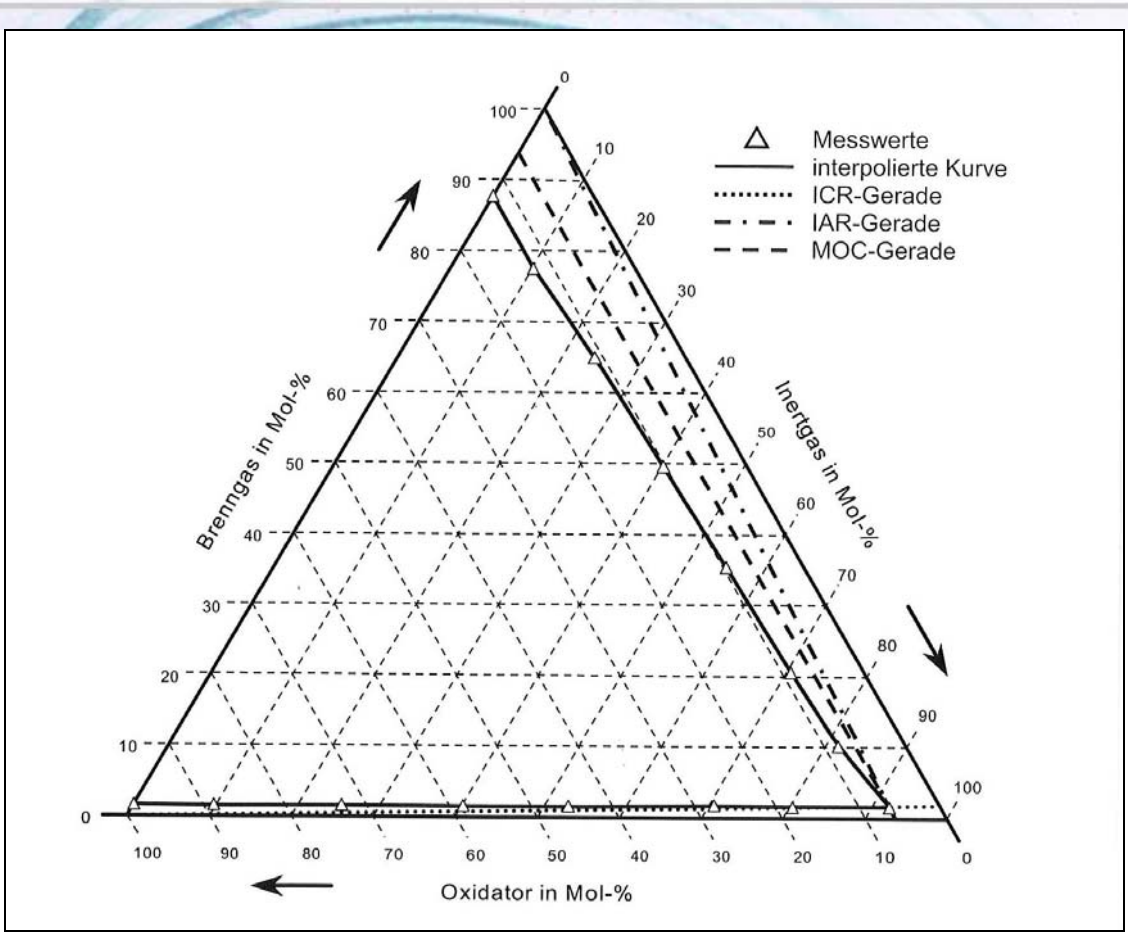

Fig. 3-20 Flammability Diagram for Hydrogen/Air/Nitrogen at 400°C and 1 bar

For hydrogen, the minimum ignition energy is low at 0.017 mJ for mixtures with air (ISO, 2004), and even lower at 0.0012 mJ for mixtures with oxygen (Kuchta, 1986). Hydrogen has a such a low minimum ignition energy that it is often difficult to determine the exact mechanism and cause of an ignition when it occurs. In some incidents where hydrogen has been involved in an explosion or fire, it has not been certain as to the source of ignition and the mechanism of the release. Some incidents have had obvious ignition sources such as flames or grinding sparks, but other incidents had releases of hydrogen where all obvious sources of ignition had been excluded, and self ignition had been blamed. The propensity of hydrogen to ignite in this fashion for no apparent reason has been reported several times previously, by Reider (1965), Lees, (1991), Anon (1922), and Fenning and Cotton (1930). In these incidents, no specific cause for ignition was identified. Several mechanisms have been suggested, of which two are worthy of note for discussion. The first mechanism is that of the reverse Joule-Thomson effect exhibited by hydrogen, and the second, the so-called "diffusion ignition" mechanism.

References and sources

Reider, Roy, (1965) An Unconfined, Large-Volume Hydrogen-Air Explosion, Pyrodynamics, **2**, 249-261.

Lees, F.P., (1991), in *Loss Prevention in the Process Industries*, Vol 3, Butterworth Heinemann Ltd., Oxford - Case History A77, at Ilford, Essex, Appendix 1 page 48; Case History A126, at Richmond, California, Appendix 1 page 62; Case History B33, at an unreported location, Appendix 1 page 72.

Anon, (1922), Spontaneous Ignition of Escaping Hydrogen, Engineering, **113**, April 21, page 502.

Fenning, R.W., & Cotton, F.T., (1930), Two Unexpected Hydrogen-Air Explosions, Engineering, **130**, August 22, page 252.

Kuchta, Joseph M., (1985), *Investigation of Fire and Explosion Accidents in the Chemical, Mining, and Fuel-Related Industries A Manual*, U.S. Bureau of Mines Bulletin 680.

ISO (2004), Basic considerations for the safety of hydrogen systems, ISO/TR15916: 2004

Molnárné, M., Schendler, T. and Schröder, V., (2003) *Sicherheitstechnische Kenngrößen, Band 2: Explosionsbereiche von Gasgemischen*, Wirtschaftsverlag NW, Bremerhaven, ISBN 3-89701-746-6

3.1.5.2 Static Electricity

The ignition hazards posed by static electricity require specific precautions to taken. A Technical Report by CENELEC (2003) does not specifically refer to hydrogen but does refer to the flammable gas Group IIC and the ignition hazards associated with static electricity. This report addresses the maximum areas of insulating materials that may become charged, and restricting the maximum area limits the maximum charge that can be transferred from the surface in the form of a brush discharge. Such a discharge does not have a specific energy, but the ignition properties can be compared to those of a spark discharge between two conductors. The comparison has been discussed by Gibson and Harper (1988), who proposed the term *incendivity* to compare the quantity of charge transferred with its capability to ignite a flammable mixture with a given minimum ignition energy. Further work by von Pidoll (2004) gives specific guidance on the maximum tolerable charge transfer to ensure freedom from ignition. However, he has correlated the charge transferred with minimum ignition energy and the gas groups defined by the IEC in their standard, but does not take account of the time and spatial characteristics of the discharge. The maximum tolerable charge transferred for hydrogen is given by the CENELEC (2003) as 10 nC. This is a very small quantity of charge, and hence hydrogen is extremely prone to ignition from electrostatic discharges from insulating or non-conductive materials.

When using non-conductive solid materials there are restrictions on the size of chargeable surfaces. The restriction on the size of chargeable surfaces depends on the ignitability of the gases and vapours and the classification of the hazardous area:

a) For sheet materials the area is defined by the exposed (chargeable) area;
b) For curved objects the area is the projection of the object giving the maximum area;
c) For long narrow materials, such as cable sheaths or pipes, the maximum size is defined by the transverse dimension.

The restrictions on areas are given in the tables 3-8 and 3-9.

Table 3-8 Restriction on chargeable surface depending on zones and gas categories

Zone	Maximum area, cm^2		
	Group IIA	Group IIB	Group IIC
0	50	25	4
1	100	100	20
2	No limit	No limit	No limit

Table 3-9 Restrictions on widths of narrow materials depending on zones and gas categories

Zone	Maximum area, cm^2		
	Group IIA	Group IIB	Group IIC
0	0.3	0.3	0.1
1	3.0	3.0	2.0
2	No limit	No limit	No limit

There have been several instances in the past where accidental hydrogen releases have ignited spontaneously. Whilst these have been investigated, no satisfactory explanation has been produced, but there have been suggestions that some form of electrostatic charging has been present, resulting in an ignition. In view of the very low ignition energy of hydrogen, such ignitions are a distinct possibility. Astbury and Hawksworth (2005) have undertaken a critical review of several incidents with their postulated mechanisms, and has concluded that there is a distinct possibility that releases which ignite spontaneously may be of an electrostatic origin.

Whilst electrostatics can be due to an obvious charging mechanism, such as the discharge from a sheet of insulating plastic as described above, ignition of hydrogen from electrostatics generated from or by the hydrogen itself is a far more difficult mechanism to define. Generally, there is no particular propensity for pure gases to become electrostatically charged, as described by CENELEC (2003). As reported by Astbury and Hawksworth (2005), work at the U.K. Health and Safety Laboratory on releasing high pressure (15 MN m^{-2}) hydrogen through various nozzles from 0.5 to 12 mm in diameter did not result in any spontaneous ignition at all. This would suggest that straightforward *pure* hydrogen does not in itself ignite.

However, there have been reports, particularly one by the periodical Engineering (Anon, 1930) reporting work undertaken by Nusselt in Germany, after a spontaneous ignition of hydrogen. Much of this work centred on the possibility of a catalytic effect from fine rust that was present. However, when hydrogen was released in the dark through a nozzle fitted with a funnel and a wire probe, corona discharges were seen, and on tapping the nozzle to disturb the rust, an ignition took place. Clearly under these circumstances the corona discharge was sufficient to ignite the released hydrogen. It is likely that the corona was started by the movement of the hydrogen generating an electrostatically charged dust cloud which was sufficient to produce an electrostatic field of a strength high enough to initiate a corona from the wire inserted into the funnel.

References and sources

CENELEC (2003), Electrostatics – Code of practice for the avoidance of hazards due to static electricity, PD CLC/TR 50404:2003.

Gibson, N. and Harper, D.J., (1988), Parameters for Assessing Electrostatic Risk from Non-Conductors - A Discussion, J. Electrostatics, **21**, 27-36.

von Pidoll, U. et al, (2004), Determining the Incendivity of Electrostatic Discharges without Explosive Gas Atmospheres, IEEE Trans. Ind. Applic., **40**, No.6, 1467-75.

IEC (1996), International Electrotechnical Commission Report IEC 60079-20:1996, *Electrical apparatus for explosive gas atmospheres – Part 20: Data for flammable gases and vapours, relating to the use of electrical apparatus*.

Astbury, G.R. and Hawksworth, S.J., (2005), Spontaneous Ignition of Hydrogen Leaks: A Review of Postulated Mechanisms, Proceedings of the International Conference on Hydrogen Safety, September 8th-10th, Congress Palace, Pisa, Italy.

Anon., (1922), Spontaneous Ignition of Hydrogen, *Engineering*, 113, April 21, p. 502.

3.1.5.3 Electric Spark

Electrical sparks are defined as discontinuous electrical discharges across a gap, in an otherwise complete electric circuit, between at least two electrodes occurring when the voltage exceeds the breakdown voltage. The characteristics of the discharge depend very much on the discharge circuit involving capacitors, resistors and inductors. In many technical applications, especially in spark ignition engines, optimized, standard ignition systems are used. Typically the systems are based on a capacitor to store the energy supplied by a high voltage generator, complemented by a circuit of low induction and resistance containing an electronic device triggering the spark for control and synchronization purposes. In Fig. 3-21 a schematic diagram of the voltage and current of ignition spark as a function of time is presented after Maly and Vogel (1978).

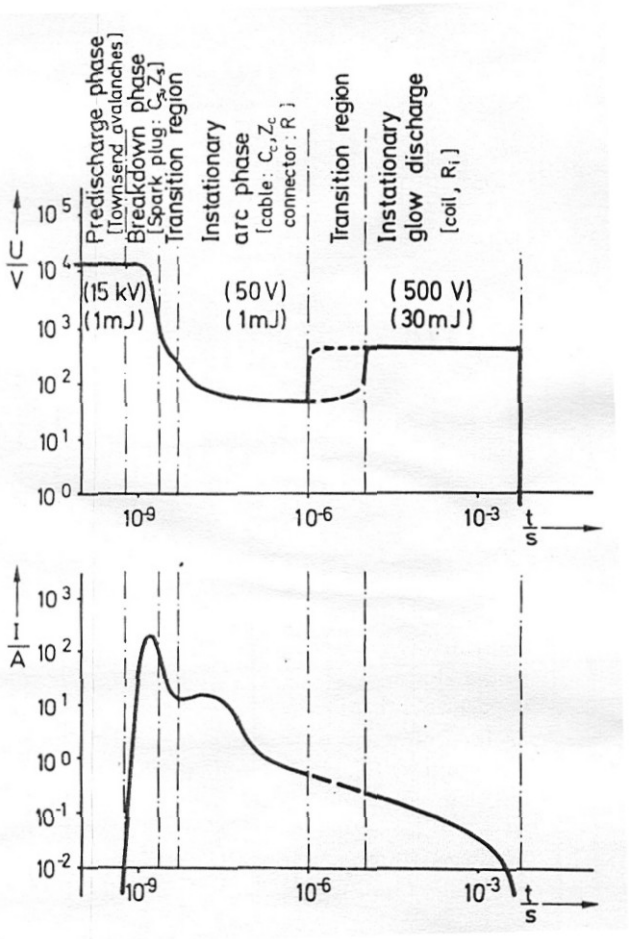

Fig. 3-21: Schematic diagrams of voltage and current of technical ignition systems as functions of discharge time. Typical values are given in parentheses, circuit parameters responsible for a discharge mode are indicated in brackets.

As it can be seen a typical electrical spark of a commercial ignition system can be divided in three phases. First a breakdown phase is initiated which creates in the gas a small diameter (~40 µm) conducting plasma channel between the two electrodes. The phase is very short (1-10 ns) and characterized by high voltages (~10 kV) and currents (~200 A). Temperatures in the plasma channel reach up to 60 000 K, the molecules are fully dissociated and ionized causing the pressure to jump to 200 bar creating an intense shock wave and expansion of the discharge zone. The high conductivity of the plasma reduces the voltage provided by the circuit and the arc phase is initiated. The arc voltage is low (<100 V) although the current may be as high as the electrical circuit permits (up to several kA). The maximum temperature in the discharge

zone drops to about 6000 K and ionization falls to a 1% level. The arc expands mainly due to conduction and diffusion producing bell shaped temperature and ionization profiles. Heat losses create appreciable cathode and anode voltage falls and the glow phase begins during which currents drop to a 200 mA level, the gas temperature is less than 3000 K and ionization less than 0,01%. The conversion efficiency of electrical to thermal energy of the gas decreases from the breakdown to the glow phase mostly due to the heat losses to the electrodes. To initiate a flame shortly after breakdown the chemical reaction must produce enough energy to overcome heat losses and the ignition kernel has to grow beyond a critical size for the flame to develop, typically must be two times larger than the laminar flame thickness. Obviously the electrodes, their separation, shapes and material play an important role in this process.

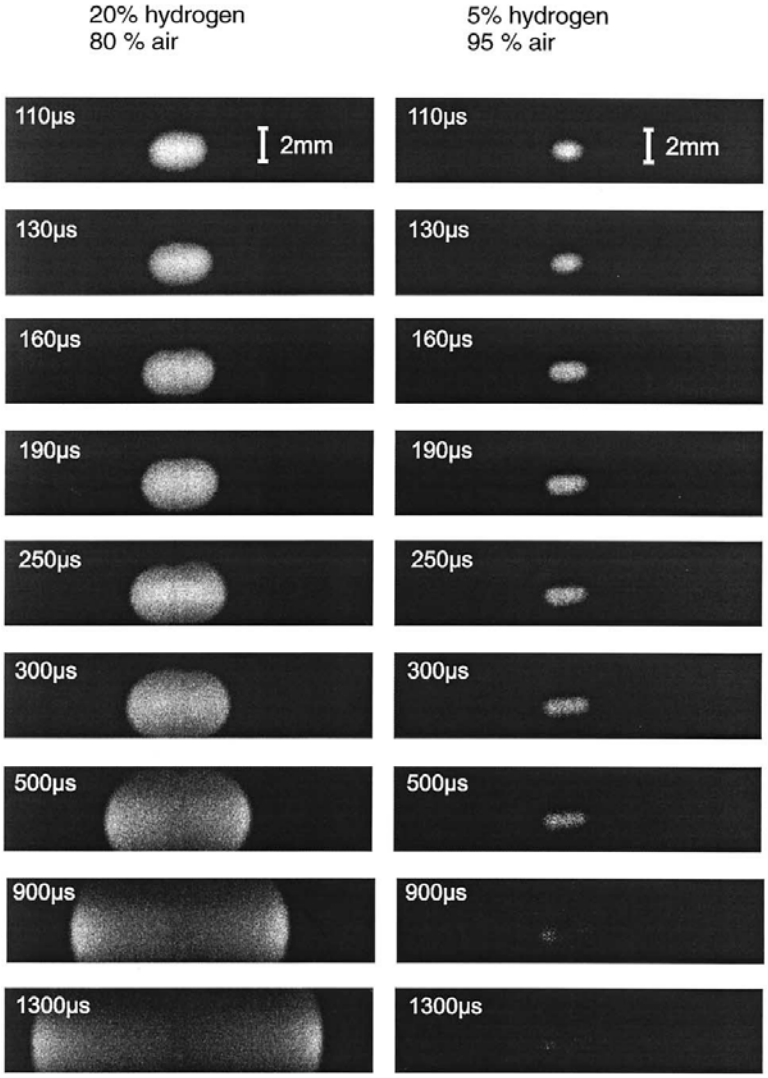

Fig. 3-22 Temporal evolution of a flame kernel visible as a relative OH concentration profiles recorded by PLIF for an ignitable and below the ignition limit mixture of hydrogen and air. Spark duration was 100 µs.

Spark ignition constitutes a very complex interplay between plasma kinetics, chemical kinetics, molecular transport processes and fluid dynamics. Experimental investigations of spark kernels and their transition to flame kernels are rendered difficult because of very short process times, extremely high core temperatures and large gradients in the refractive index. In general, only flame propagation subsequent to spark ignition can be studied by laser diagnostic methods. Therefore, internal structures of the plasma core remain mostly unknown. A complete

mathematical simulation of a spark ignition is also a difficult task because of the enormous numerical problems, due to the stiffness and high dimensionality of the problem (each chemical species introduces an additional conservation equation). Recently Thiele et al. (2002) have conducted detailed two dimensional numerical modeling of spark ignition of hydrogen-air mixtures. Their model considered heat conduction from the gas phase to the electrodes, detailed chemistry and molecular transport as well as the coupling of the gas dynamics to the properties of the electrical discharge through heating by the electrical current. They also performed spark ignition experiments using a highly reproducible ignition system. Shapes of early flame kernels were monitored by 2-D laser-induced fluorescence PLIF imaging of OH radicals produced during the ignition and the combustion process (Fig.2). In addition, for a central position within flame kernel, temperatures were measured using CARS. Results from experiments and simulations suggest the birth of a self sustaining flame propagation for process times between 50 to 70 μs after arc breakdown.

References and Sources

R. Maly, M. Vogel. (1978) *Initiation and propagation of the flame fronts in lean CH-air mixtures by three modes of the ignition spark.* Published in the Proceedings of the Combustion Institute, Vol. 17, pp. 821-831.

M.Thiele, J.Warnatz, A.Dreizler, S.Lindenmaier, R.Schiesl, U.Mass, A. Grant, P.Ewart, (2002), Spark Ignited Hydrogen/Air Mixtures: Two Dimensional Detailed Modeling and Laser Based Diagnostics, Combustion & Flame 128:74-87

3.1.5.4 Auto-ignition

Generally auto-ignition results from either the exothermic of chain branching character of the oxidation reactions that at certain conditions self-accelerate to reach high conversion and heat release rates. Auto-ignition limits can be established testing experimentally or theoretically a homogeneous mixture of volume V filling a vessel whose walls have a temperature T_w. Once the heat release rate in the volume due to reactions exceeds the heat lost to the walls or if the reaction rates in the vessel exceed the reaction quenching (termination) rates by the walls or in the gas a thermal or branched-chain (isothermal) auto-ignition occurs. Typically, as almost all combustion reactions are exothermic, chain auto-ignitions cause also self heating and are accelerated by both factors. Obviously auto-ignition limits are not only a feature of the mixture composition and parameters (pressure, temperature) but also of the vessel size, wall properties and internal flow conditions.

This is illustrated in Fig. 3-23 showing the auto-ignition limits often called also explosion limits for a stoichiometric mixture of hydrogen and oxygen (B. Lewis, 1987) providing the important parameters of the test vessel. We may note the logarithmic scale of pressure and linear scale of temperature showing that pressure effects on reaction rates are weaker than temperature effects as one would expect by the consideration of Arrhenius chemistry.

The first and second limits, although interesting from the fundamental point of view, correspond to very low pressure (up to about 0.3 bar) and are thus of little practical interest. The third limit follows the trend that one would expect from simple density considerations. As the pressure increases, the initial densities of the reactants increase and a lower temperature is necessary for the reactions to reach a critical reaction rate for explosion. For safety considerations explosions in large volumes where wall effects can be neglected at atmospheric conditions and for most

violently reacting, i.e. stoichiometric mixtures are considered. Thus, in typical safety manuals a temperature of 585°C is given as the auto-ignition temperature for hydrogen air systems.

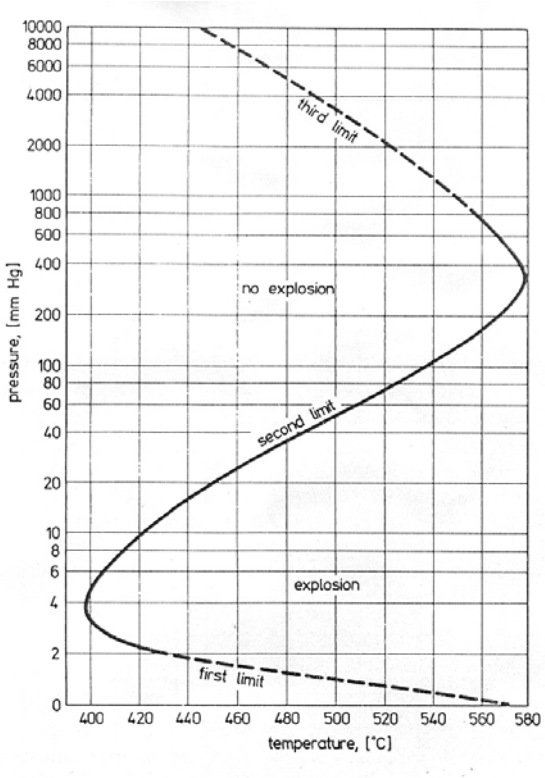

Fig. 3-23 Explosion limits of a stoichiometric hydrogen-oxygen mixture in a spherical HCl coated vessel of 7.4 cm diameter.

The initial reaction rate in auto-ignition is very small thus a certain time must pass before the reaction has reached a defined rate. This time interval is called ignition delay. Ignition delays are particularly important for operation of engines as they provide the engine speed limits where operation is possible due to auto-ignition (compression ignition engines) or where auto-ignition can be avoided when detrimental (knock in spark ignition engines).

Most accurate ignition delay measurements can be performed in shock tubes in wall reflected shocks where the heating of the mixture is practically instantaneous. A research issue is then prediction of the ignition delays using available kinetic data. The state of the art in this field is far from satisfactory as illustrated in Fig. 3-24 after Wang et al. (B. L. Wang, 2003) where a comparison of measured and calculated ignition delay times using different chemical reaction mechanism, available in the literature is provided.

In the low temperature range the measured ignition delay times are much shorter (even by orders of magnitude) than the theoretically predicted ones. Partially this is because in shock wave ignition mild and strong ignition regimes are possible. For the case of mild ignition multiple and random ignition kernels appear in the mixture. In the case of strong ignition typically reproducible direct transitions to detonation occur. Mild ignition is extremely sensitive to homogeneity of the mixture, impurities, wall properties of the shock tube and particularly to presence of even minute obstacles causing shock reflections, shock focusing and thus generating local hot spots. Thus, this form of ignition is very difficult to control particularly in natural conditions. If the volume of the mixture is large enough deflagration to detonation transition will eventually occur even after mild ignition causing convergence of effects of both types of ignition in accidental explosions.

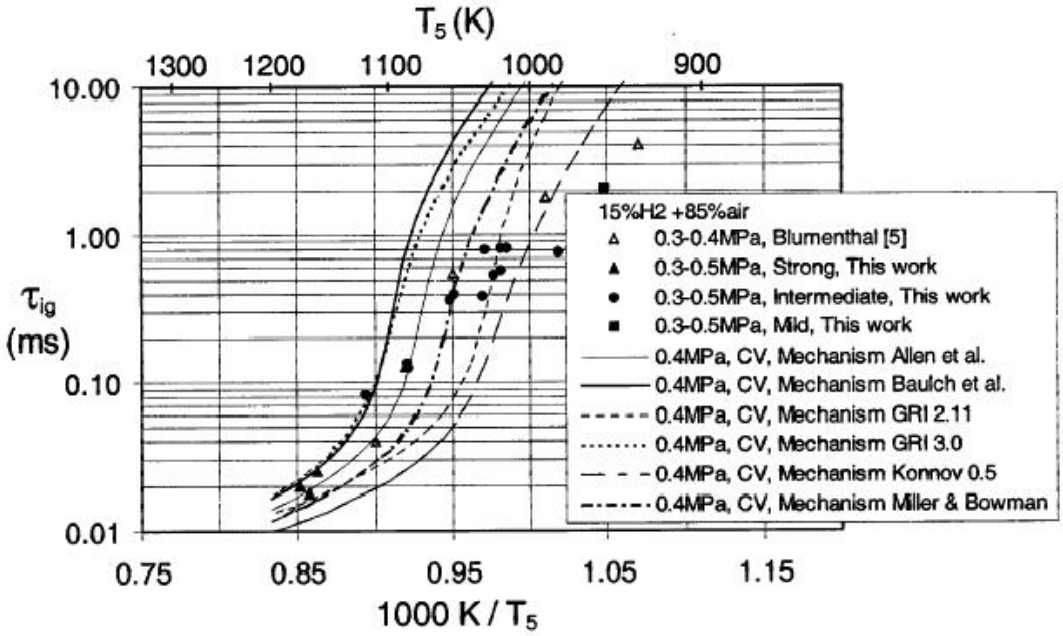

Fig. 3-24 Measured and calculated ignition delay times in a H2-air mixture.

An interesting case of shock wave induced ignition is the jet release auto-ignition that may happen when gas kept at high pressure is rapidly released from a volume into the atmosphere. The flow velocities in the jets reach supersonic levels due to further expansion after the release valve. Then shock waves will appear in the jets due to interaction with the surrounding gas, heating the nascent mixture to temperatures exceeding auto-ignition levels (Wolanski and Wojcicki, 1972). If obstacles are in the way of the jets the process is highly facilitated.

References & sources

Lewis, B. and von Elbe, G. (1987), *Combustion, Flames and Explosions of Gases*. (3rd Edition), Academic Press, New York.

Wang, B.L., Olivier, H. and Grőnig, H. (2003), Ignition of shock-heated H_2-air-stream mixtures. Combust. Flame, **133,** 93-106.

Wolanski, P and Wojcicki, S., (1972), *Investigation into the mechanism of the diffusion ignitron of a combustible gas flowing into an oxidizing atmosphere.* Proc. of the Combustion Institute, **14**, 1217-1223.

3.1.5.5 Mechanical Friction and Impact

Mechanical Rubbing

Brearley and Tolson (1995) measured power levels and contact loads required to ignite flammable gas mixtures by a 25 mm cube of stainless steel frictionally heated through rubbing against a stainless steel wheel at circumferential velocities of 5 and 20 m/s. In these tests a contact load of 750 N was required to ignite hydrogen. This equates to a dissipated power of approximately 2 kW and a power density of approximately 0.5 W/mm^2. No temperature recordings were made in the tests. It was noted that in most cases the ignition was caused by the hot spot close to the point of contact.

In Powell's (1984) review he summarises data from various experiments breaking them into two categories with rubbing speeds above and below 10 m/s. The Table is presented below and shows results from Group IIC gases (hydrogen etc).

Work at HSL (MECHEX Project) has shown that at low rubbing speeds, hydrogen was ignited at a temperature close to the auto-ignition temperature. The conditions were: power 0.7 kW and rubbing speed 0.7 m/s which caused ignition at 530°C. Ignition occurred from the hot surface with few sparks produced from the low speed conditions.

Impact

In his paper, Powell (1986) states how little energy is needed to ignite flammable gases and vapours with impact of light metals and their alloys, producing burning particles with temperatures in excess of 2000°C from light impacts (<1J) with material such as Cerium, Titanium Zirconium, Hafnium and their alloys. Impacts on smears of aluminium or magnesium on rusty steel are also equally incendive. There is therefore a high probability of igniting hydrogen under these conditions.

Powell reports on ignitions caused by impacts between very hard steels (>550 VPN). Energies of 250 to 1000 J are required to ignite methane-air, with slightly lower energies igniting IIA vapours. For steel with with VPN pf approximately 550, an energy of 180 J was sufficient to cause ignition. Ignition of hydrogen-air mixtures from impacts involving very hard steels are therefore very likely.

Mechanical sparks

There are a number of key properties of burning metal particles or sparks that are relevant to their ability to cause ignition of a flammable atmospheres. These include: size, material, velocity, temperature, number, combustion rate and time. There is a metal to metal contact pressure and relative velocity threshold for spark production during impact, rubbing or grinding. Above the threshold metal particles are lost from the weaker of the two materials. Generally, particles are only produced when the relative velocity between the two surfaces exceeds 1 m/s (Bernend and Ritter).

References & sources:

Bernend E. and Ritter K. Mechanically produced sparks. Section 2.4 of the Handbook of Explosion Protection, Edited by Henrikus Steen, Published by in Germany by Wiley VCH. HSE translation No 2000/20

Brearley and Tolson, (1995), The frictional ignition properties of (18/8) stainless steel. HSL internal report IR/L/IC/95/02

BS EN 1127-1:1997 Explosive atmosphere (1997) – Explosion prevention and protection Part 1. Basic concepts and methodology

ISO (2004), Basic considerations for the safety of hydrogen systems, Technical report ISO/TR 15916:2004(E)

Lees F. P., (1991), *Loss Prevention in the Process Industries*, Vol 3, Case History A77, pp A1/48, Butterworth Heinemann Ltd., Oxford.

NASA, (1997), Report NSS 1740.16. Safety Standard for Hydrogen and Hydrogen Systems

Powell F., (1984), Ignition of gases and vapours by hot surfaces and particles – a review, 9th International Symposium on the Prevention of Occupational Accidents and Diseases in the Chemical industry, Luzer, pp. 267-292.

Powell F. (1986), Can non-sparking tools and materials prevent gas explosions?, Gas-Wasser-Abwasser **66**, Jahrang Nr. 6

Snee T. J. and Griffiths J. F., (1989), Criteria for spontaneous ignition in exothermic, autocatalytic reactions: chain branching and self-heating in the oxidation of cyclohexane in closed vessels. Combustion and Flame, **75**, 381-95.

3.1.5.6 Ignition by Explosive

An explosive is a powerful ignition source and will readily ignite a flammable fuel/air mixture and even under the right conditions directly initiate a detonation in an unconfined mixture. No data has been found in the literature on the minimum amount of explosive required to ignite a fuel/air mixture, but there have been a number of experimental and theoretical studies to determine the minimum amount of explosive required to initiate an unconfined detonation by Bull et al (1978) and Bull (1979).

As might be predicted from the general behaviour with other ignition sources the mass of explosive required to initiate an unconfined detonation in a hydrogen/air mixture is very much less than that required for less reactive fuel/air mixtures such as propane or methane. Table 3-10 compares the minimum amount of tetryl required to initiate an unconfined detonation in the most detonable hydrogen/air mixture and other common fuel/air mixtures. For hydrogen and the other fuels listed in Table 3-10, apart from acetylene, the most detonable mixture lies within a stoichiometry range of between 1.1 and 1.3. For acetylene the value for the most detonable mixture is 2.05. For all fuels the minimum amount of explosive required increases rapidly as the mixture approaches the detonation limits. In the case of hydrogen it is predicted there is about a hundred-fold increase in the mass of tetryl required to initiate a detonation in near limit mixtures compared to the most detonable mixture (stoichiometry of about 1.1).

Table 3-10 Minimum mass of tetryl required to initiate unconfined detonation

Fuel	Mass tetryl (g)
Hydrogen	0.8
Methane	16,000
Propane	37
Ethylene	5.2
Acetylene	0.4

References & sources

Bull D.C., Elsworth J.E.and Hooper G., (1978), Acta Astronautica **5**, 997.

Bull D.C., (1979), Concentration limits to the initiation of unconfined detonation in fuel/air mixtures, Trans IChemE **57**, 219-227.

3.1.5.7 Ignition by Open Flame and Hot Surface

Open flames will in any circumstances ignite an explosive hydrogen / air mixture.

Ignition by Hot Surfaces

Ignition by a hot surface occurs as a result of local heating of the hydrogen-oxidant mixture to the point where a sufficently large volume reaches the autoignition temperature and the combustion reaction is initiated. For this to occur generally requires the surface to be at a temperature well above the autoignition temperature (see Powell, 1984), although the actual temperature depends on a number of factors in addition to the usual mixture concentration, ambient temperature etc. These additional factors determine the hot surface ignition behaviour of flammable gases and not just hydrogen, and include the size and shape of the hot surface, the degree of confinement around the surface, the strength of the convection currents across the surface (See Laurendau, 1982) and the material of the surface (Lewis von Elbe, 1987, page 380).

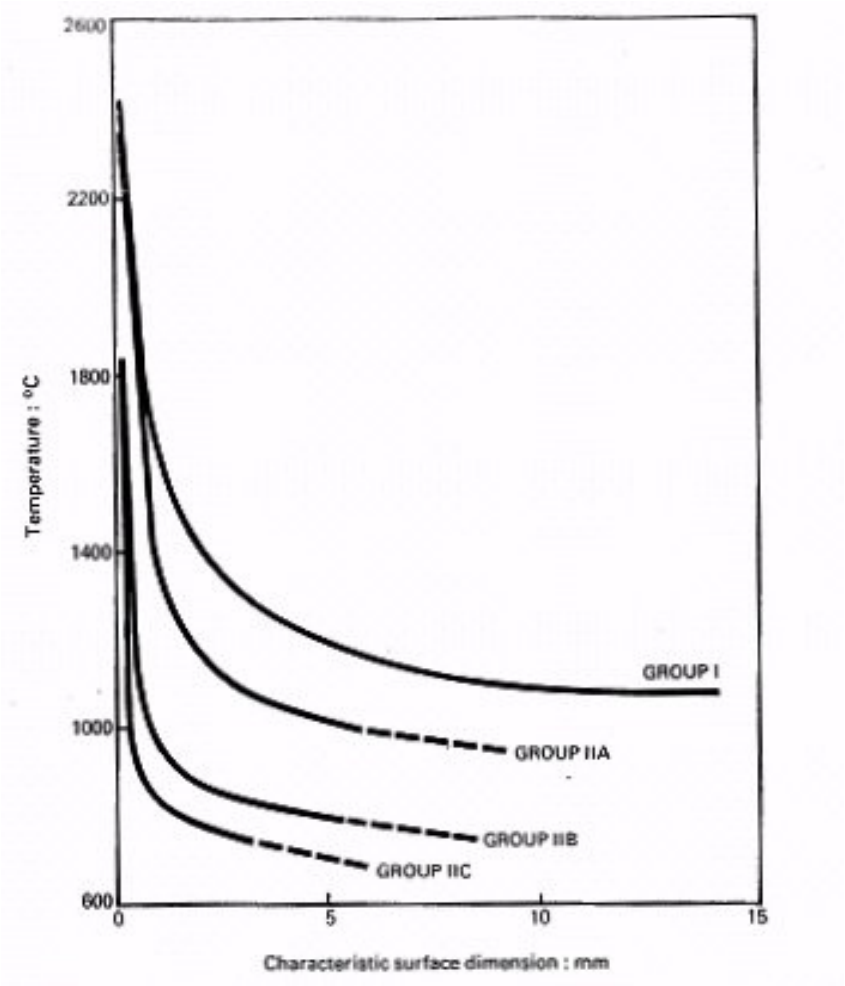

Figure 3-25 Size depenedence of hot surface ignition temperatures as a function of size (Hydrogen is represented by curve IIC).

For a particular hot surface, ignition is characterised by an ignition delay, which under ideal circumstances multiplied by the power for ignition gives a linear relationship between the product (energy) and ignition delay (Lewis von Elbe, 1987, page 365 & Carleton et al (2000)). The offset on the y-axis in this plot is the minimum power for ignition for that arrangement.

The temperatures required to cause ignition of mixtures of hydrogen with air and oxygen (see review in J W Buckle and S Chandra (1996) & Carleton et al 2000, Hawksworth et al 2005) range from 640°C to 930°C, the spread of temperatures being explained the size, geometry effects etc described in the first paragraph. While the temperatures quoted are above the auto ignition temperature, the increase is much less than seen for hydrocarbon-fuel air mixtures, as illustrated by the IIA curve in Figure 3-25. In terms of simple modelling of hot surface ignition, Laurendau (1982) presents a simple model in terms of a one step reaction chemical kinetics model.
Interestingly, the most easily ignited mixture of hydrogen wit air lies lean of stoichiometric (See Calcote and Gregory (1952)) while work using very small hotsurfaces (Carleton et al (2000) and Hawksworth et al (20004)) suggests that mixtures as low as 10 to 15% are the most easily ignited. For hydrogen-oxygen mixtures, the work of Buckle and Chandra indicates a fairly flat H2 concentration depenedence (slight positive slope with increasing hydrogen concentration) between roughly 20 and 90% hydrogen in oxygen.
Catalytic surfaces (e.g plantinium) have a dramatic effect on the ignition temperature required (Cho and Law 1986), ignitions reported at temperatures as low 70°C.

References & sources

Buckle J W and Chandra S (1996) “Hot Wire Ignition of Hydrogen-Oxygen Mixtures”, Int. Journal of Hydrogen Energy Vol. 21, No. 1, pp 39-44

Calcote, H F and Gregory C A Jr, Barnett C M and Gilmer R B (1952) Spark ignition - effect of molecular structure. Industrial and Engineering Chemistry, 44 (11), 2656-2662

Carleton F, Bothe H, Proust C & Hawksworth S (2000),“Prenormative research on the use of optics in potentially explosive atmospheres” European Commission BCR Information Project Report EUR 19617 EN

Cho P O and Law C K (1986) “Catalytic Ignition of Fuel/Oxygen Nitrogen Mixtures Over Plantinium”, Combustion and Flame 66, 159, 70

Laurendau N M (1982), “Thermal Ignition of methane-air mixtures by hot surfaces: A critical examination” Comb. and Flame, 46, pg 29-49

Lewis B & von Elbe G (1987), “Combustion, Flames and Explosions of Gases (Third Edition)”, Academic Press, 1987, ISBN 0-12-446751-2

Powell F (1984), “Ignition of Gases and Vapours by Hot Surfaces and Particles - A Review”, 9th International Symposium on the Prevention of Occupational Accidents and Diseases in the Chemical Industry, Luzer pg 267-292

3.1.5.8 Ignition of Liquid Hydrogen and Solid Oxygen Mixtures

Liquid hydrogen has properties which set it apart from the other cryogenic fuel of liquefied natural gas, in that its atmospheric boiling point is much lower than that of air. Pipe-work and vessels at liquid hydrogen temperatures of about 20 K will condense air from the atmosphere. It will also be cold enough to condense and freeze water and carbon dioxide from the air.

Work undertaken by Perlee et al (1964) indicated that liquid hydrogen can condense and freeze oxygen. The resultant solid oxygen in an excess of liquid hydrogen can be detonated by impact. They used a rifle and with a muzzle velocity of 600 m s^{-1}, detonation always occurred when the

bullet impacted the mixture. Detonation was indicated by the use of thin metal strip gauges which deflected permanently when a detonation occurred. The results indicated that the explosive yield of liquid hydrogen-solid oxygen mixtures was greater than those for equal weights of trinitrotoluene (TNT).

Table 3-11 Data from Yarwood & Castle (1961) except #International Critical Tables, McGraw Hill, (1933).

Material	Melting Point K	Boiling Point, K
Hydrogen	14	20
Helium	1	4
Oxygen	54	90
Nitrogen	63	77
Carbon Dioxide	sublimes	195#

Various experiments were carried out in which there was a large excess of liquid hydrogen. The specific gravity of liquid hydrogen is typically about 0.07, and that for the solid oxygen in the α state is about 1.426. The sonic velocities in the hydrogen and solid oxygen phases

References & sources

Perlee, H.E., Litchfield, E.L. and Zabetakis, M.G., (1964), Review of Fire and Explosion Hazards of Flight Vehicle Combustibles, Technical Report No. ASD TR 61-278 Supplement 3, AF Aero Propulsion Laboratory, Wright-Patterson Air Force Base, Ohio.

Yarwood, T.M., and Castle, F., (1961) Physical and Mathematical Tables, 2nd Edition, Macmillan & Co. Ltd.,

3.2 ACCIDENTAL CONSEQUENCES

Contributing author	Main contributions	Organisation	e.mail
Karl Verfondern	Chapter coordinator	FZJ	k.verfondern@fz-juelich.de
Stuart Miles	Heat radiation	BRE	
Thomas Jordan	Effect on people	FZK	
	Environmental impact	Risoe	

Contributing reviewer	Information reviewed	Organisation	e.mail
Mathieu Reimeringer	Pressure Waves and Pressure Loads	INERIS	Mathieu.Reimeringer@ineris.fr
Martijn van der Voort	Throw of debris and missiles	TNO	

3.2.1. Pressure Waves and Pressure Loads

3.2.1.1. Chemical Explosions

Essential to the consideration of accidental consequences is the estimation of hazards and hazard levels, e.g., overpressures, thermal radiation, the throw of debris or missiles, and the damage level or the vulnerability of the receiving objects. In chemical explosions which are usually exothermal oxidation reactions, a great portion of the combustion energy is carried by the developing blast wave uniformly distributed in all directions. Depending on the various types of combustion processes (slow deflagration or fast turbulent flame or detonation), the pressure history will be different. It is characterized by the peak overpressure and the pressure increase/decay rate. This effect is strongest at ground level (hemispherical) explosions where due to reflection the respective yield ratio can be twice as high as for a spherical explosion.

Deflagration and detonation differ in peak overpressure, in the duration of the impulse (time-integrated pressure), in the steepness of the wave front, and in the decrease of overpressure with propagation distance. Secondary blast wave parameters are the peak reflected pressure, peak dynamic (blast wind) pressure, shock front velocity, and blast wave length. The different pressure transients for the two combustion modes are shown in Fig. 3-26.

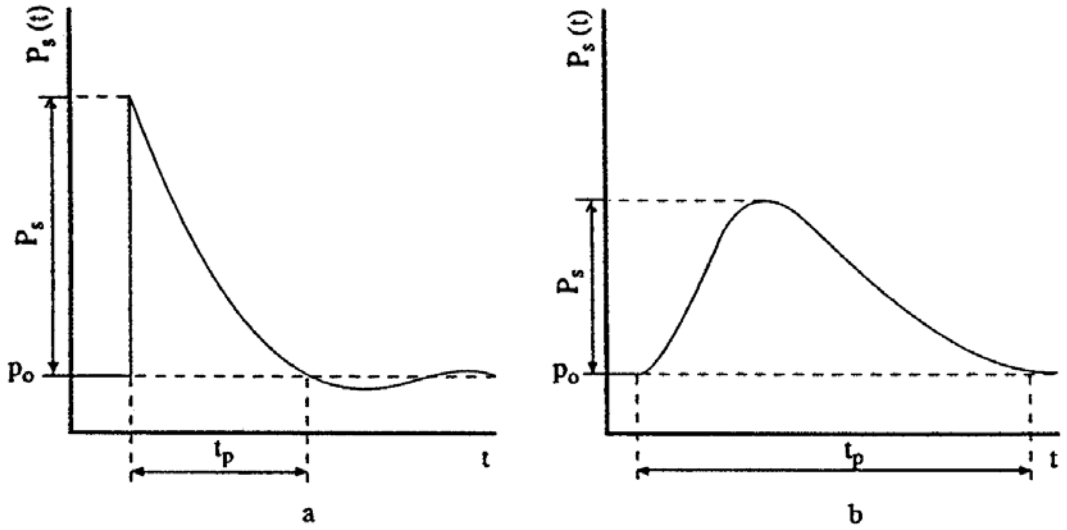

Fig. 3-26: Characteristic shape of pressure-time function for a detonation shock wave (left) and a deflagration pressure wave (right), from (TNO 1992)
(P_o: initial pressure; P_s: peak side-on overpressure; t_p: duration of positive phase)

Deflagration

In a deflagration with flame speeds of 1-10 m/s, the volume expansion of the gas acts like a piston displacing the unburnt gas. The deflagration pressure wave in a confined space is characterized by a slow increase of pressure and fluid velocity in the region preceding the flame front. Pressure buildup will take place even at low flame speeds and remain at the obtained level, since the gas cannot expand in a fixed volume. The pressure inside is independent of the location and mainly determined by the fraction of burnt gas. The static pressure loading in slow deflagration processes is described by the "adiabatic, isochoric, complete combustion (AICC)" pressure representing an upper bound in a confined space. For a given gas mixture at an initial temperature, the AICC pressure is a function of the initial pressure. A mitigation of the AICC pressure is given by incomplete combustion, venting, radiation/conduction heat losses, or the

addition of diluents. Therefore the maximum static pressure will be generally lower than the AICC pressure. On the other hand, initial turbulence increases the degree of combustion and thus the pressure. The peak pressure in a closed vessel for most hydrocarbon-air mixtures is in the order of 0.8 MPa, sufficient for many buildings to exceed their failure limits. For a hydrocarbon-oxygen mixture, it is even 1.6 MPa. An H_2-air mixture, initially at NTP, will reach a pressure of 0.815 MPa; its volume will increase by a factor of 6.89 (Baker 1983).

The pressure buildup depends on the flame propagation and the degree of confinement. Particularly hazardous configurations are those, which are heavily confined like tubes, pipes, or channels, where – if long enough – even in insensitive methane-air mixtures, high flame speeds and pressures can be reached. Venting can reduce the pressure.

Inside a spherical vessel, the pressure rise following the ignition of a flammable mixture is proportional to the cube of the burning velocity. In pipes with no obstacles, the transition distance increases with increasing diameter (example: 8 m for propane-air mixture in a 50 mm diameter pipe) (Moen 1993). Effective burning velocity must be as high as ~ 100 m/s to produce significant blast overpressures of 10 kPa. Comparing explosion tests in tubes and in spherical vessels, it was observed that pressures are generally lower in a spherical propagation of the gas mixture (unconfined) than in a planar propagation. The pressure behind the flame front is decaying away from the flame, since wave energy dissipates.

The combustion of a hydrogen-air mixture in an unconfined vapor cloud explosion (UVCE) typically liberates only a fraction of 0.1 - 10% of its thermal energy content, in most cases less than 1% (Lind 1975). Depending on the combustion mode (deflagration/detonation), the explosion is connected with a more or less destructive pressure shock wave. The overpressure to be expected in the deflagration of an unconfined hydrogen-air vapor cloud is in the order of 10 kPa.

Fast Deflagration

In the intermediate stage of a fast deflagration with the flame front still traveling at subsonic speed, a preceding shock wave is developing in the still unburnt mixture. The peak overpressure is lower, the pressure drop, however, takes place over a longer period of time. This means that the impulse, i.e., the integral of pressure over time, which is a measure for the load upon a structure, is about the same in both cases. The peak overpressure increases with increasing flame speed. Transient pressures can be locally higher than the AICC pressure. Inhomogeneities can result in local detonations decaying to deflagrations. When the shock wave leaves the cloud, it turns into an expanding decaying wave. In the long-distance range, the pressure wave for both deflagration and detonation exhibits about the same shape decaying with 1/r.

Local explosions like from jet flames result in locally high pressures and can also lead to high flame speeds in less confined areas and even trigger a detonation wave.

Detonation

In contrast to a deflagration, the detonation is a combustion mode with the flame traveling at supersonic speed in the order of 2000 m/s. The flame front proceeds by shock wave compression of the unburnt gas. It is characterized by a distinct pressure spike and a subsequent almost exponential decrease. The shock wave, which is at the same time the flame front, is followed by the reaction zone, in which a pressure discontinuity is observed where the pressure even drops to values lower than atmospheric pressure ("molecular collapse") due to the much denser oxidation product (water) upon hydrogen combustion. The essential parameters are peak overpressure and positive/negative phase of the specific impulse depending on the liberated

explosion energy. The combustion process is completed without an expansion of the gas cloud. Peak overpressures in the near field are typically in the range of 1.5-2 MPa. The pressure wave gradually decays and eventually turns into an acoustic wave.

In geometries which allow the transition from deflagration to detonation, pressures near the location where detonation takes place, may be much higher than the CJ (Chapman-Jouguet) pressure of a stabilized (and idealized) detonation wave, which is due to a pre-compression effect by the propagating shock wave (Van Wingerden 1999). In confined spaces, peak pressures can range between "normal" deflagration peak pressure and very high pressures following DDT. Worst case is considered the DDT on a reflected shock wave produced by a fast flame with an estimated peak pressure to be by a factor of 10 higher than the detonation pressure. The transfer of a detonation wave into adjacent mixtures is possible and has been observed for planar clouds, whereas in spherical clouds, fast deflagrations are more likely to occur.

An explosion in a vessel which is connected by a small opening to another vessel creates a peak overpressure and a pressure increase rate much higher than in a single vessel explosion, a phenomenon known as "pressure piling". A pressure of more than 3.5 MPa was measured in a two-chamber geometry for a stoichiometric hydrocarbon-air mixture, where 0.8 MPa were expected for the explosion in a single vessel. Unlike the length of the interconnecting tube, its diameter is pertinent for the peak overpressure.

Real Gas Cloud

In reality, a gas cloud shows the typically expected features of a non-premixed, inhomogeneous concentration distribution, air entrainment at the boundaries, and stratification if evolving from a pool of liquefied gas. Furthermore in case of an explosion, a real gas cloud is not an "ideal" explosion source due to a larger-than-infinitesimal volume and a lower energy density and energy deposition rate, thus leading to non-ideal blast waves. Deviations from the ideal situation are able to either enhance or to attenuate the pressure buildup. Non-stoichiometry as well as ignition at the cloud edge will certainly have a damping effect on the pressure buildup. The maximum blast impulse, which becomes larger with increasing shock duration, is not near the explosion center, but about 13-15 charge radii. A near-ground flat long-stretched cloud of heavy gases or vaporized cryogens may experience multi-point ignition connected with a sequence of pressure peaks, and more turbulence-generating terrain roughness or obstacles in the flow path, both effects of which lead to an enhancement of the pressure buildup.

Unlike a heavy gas cloud which would be of a pancake form, a hydrogen vapour cloud would soon cover an area, which is larger than that of a hemispherical cloud with the same explosive inventory. Only in case of just vaporized LH_2 after a large-scale spill, the cold gas cloud would travel and stretch near ground, until sufficient air has entrained from the outside to make the gas positively buoyant and develop soon to a vertically stretched cloud shape.

The flame spreading in a non-spherical cloud is spherically until it reaches the cloud edge at some point; then it continues in the direction, where still gas can be found. The pressure is decreasing immediately behind the flame front because of the upward expansion of the combustion products.

3.2.1.2. Physical Explosions

Shock wave blasts can also be produced from physical explosions, i.e., the sudden violent expansion of a fluid not connected with a chemical reaction. The strongest man-made physical explosion is surely the nuclear explosion of an atomic bomb. The resulting blast wave reaches overpressures of 170 kPa in the central zone (14 km radius for the example of a 20 Mt explosion in 5.5 km height) and gradually decaying to the outside with still 20 kPa at 60 km distance).

The most common physical explosion is a bursting or rocketing pressure vessel which may result from a fire-induced BLEVE (Boiling Liquid Expanding Vapor Cloud Explosion). The higher the liquid density, the more destructive is the BLEVE. If the liquid is flammable, a fireball will follow. Several pressure spikes are being created upon a BLEVE: from the flashing liquid, from the expanding vapor phase, and, if applicable, from the combustion. Missiles and projectiles may be emitted also from a physical explosion and may cause injuries, fatalities, or damage at considerable distances depending on the explosion energy liberated. Projectile hazard increases with average liquid temperature.

Another example of a physical explosion is the so-called rapid phase transition (RPT), a thermal vapor explosion resulting from the spontaneous phase change of a fluid getting in contact with a much hotter or colder liquid, e.g., a cryogen spilled onto water or the fluid-coolant interaction during a core melt accident in a light-water nuclear reactor. Prerequisites of such an explosive boiling are a temperature of the “hot” fluid above the boiling point of the “cold” fluid and a certain mixing of both fluids allowing a close and sufficiently long contact. Although the energy release is small compared with a chemical explosion, fragmentation and phase change of the “cold” fluid (vapor evolution) can occur at such a high rate that shock waves may be formed. For LNG onto a water surface, overpressures with damaging potential of up to 5 kPa were observed. RPT explosions with different materials (molten metal plus water) in the metal and chemical industries were even the cause for people killed by flying melt or the blast wave. Natural examples of RPT were the catastrophic explosions of the island volcanoes Krakatoa, Indonesia, in 1883 and Surtsey, Iceland, in 1963.

3.2.1.3. Experimental Work

Apart from the experience obtained by observations and lessons learned from explosion accidents, numerous experiments have been performed worldwide to investigate the transient behavior of overpressures following the explosive combustion of fuel-air mixtures. Tests were conducted under various conditions such as confined, partially confined, or unconfined, larger-scale or smaller-scale geometry, fuel type and constitution with the main goal of development of or comparison with simulation approaches. The most dangerous configurations were found to be, as expected, those with a major obstruction, even for less sensitive fuel gases such as methane. For DDT cases, travelling distance for the flame must be sufficiently long, which would be around 3 m for a stoichiometric hydrogen-air mixture. Only a few of those test series are mentioned in the following showing the broad range of activities.

Large-scale experiments were conducted by the Russian Kurchatov Institute using premixed hydrogen-air mixtures. The RUT facility with a confined volume of 480 m^3 was employed for a series of tests ranging from slow deflagration to detonation. H_2 concentration varied between 10 and 14%. During slow deflagration (no obstacles present), the overpressures measured increased with H_2 concentration, from around 0.1 MPa to 0.17-0.23 MPa. Insertion of obstacles (blockage ratio of 30 and 60 %) resulted in accelerated flames creating overpressures (1.1-1.6 MPa) for gas mixtures with 14 % H_2 concentration. There was even the observation of a detonation at a

H_2 concentration as low as 12.5 %. Examples of pressure transients are given in Fig. 3-27 (Breitung 1996).

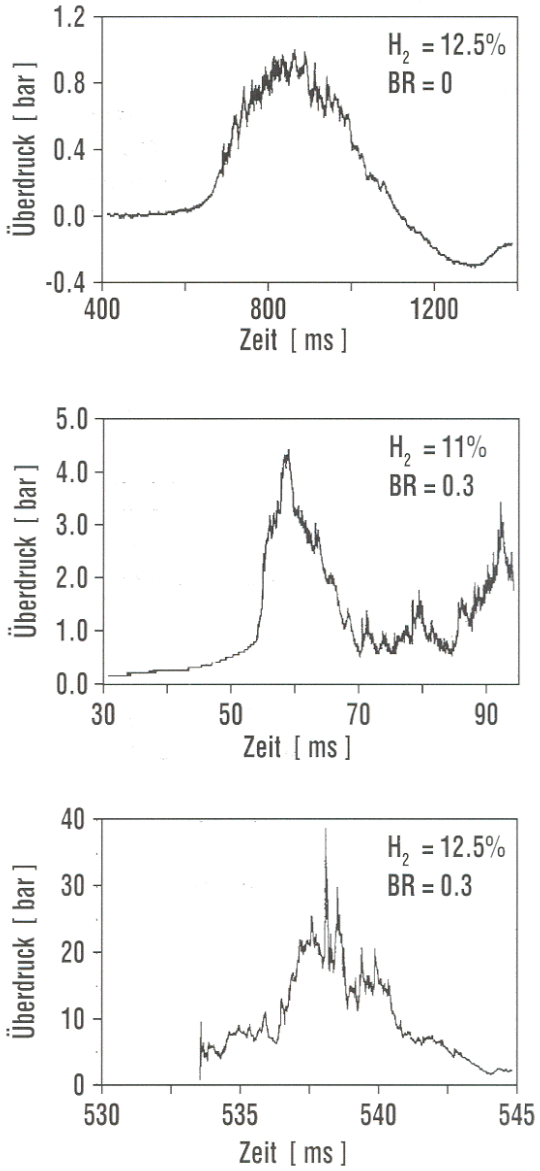

Fig. 3-27: Measured overpressure transients in RUT tests with different blockage ratios (BR) showing slow deflagration (top), fast deflagration (middle), detonation (bottom), from (Breitung 1996)

The Russian UTR facility, a tube with 66 mm diameter and a maximum length of 3 m was used for systematic studies on peak overpressures if the location of DDT is varied influencing the degree of precombustion. Peak pressures observed were well above the Chapman-Jouguet pressures for detonation of the undisturbed mixture.

Large-scale testing on DDT in hydrogen-air mixtures was conducted in the FLAME facility, a 30.5 m long, 2.44 m high, and 1.83 m wide rectangular channel with a closed ignition end and an open far end and venting/obstruction possibilities.

An explosion tube of 2.5 m diameter and 10 m length with one open end was used in Norway to study peak overpressures of ignited stoichiometric propane-air mixtures. The tests have shown the significant influence of the blockage ratio inside the tube on the flame speed and pressure increase, respectively, which can come close to the detonation range (GEXCON).

Smaller-scale detonation test tubes have been conducted at the Research Center Karlsruhe, the Technical University of Munich, the DLR in Stuttgart or the High-Temperature Combustion Facility, HTCF, at BNL employing different types of obstruction and differently diluted hydrogen-air mixtures to study flame acceleration and various DDT mechanisms.

Within the nuclear power plant safety program and the PNP gas cloud program, the German Fraunhofer Institute for Chemical Technology (FH-ICT) conducted various series of tests using mixtures of propane, ethylene, methane, and hydrogen with air to investigate detonation and DDT in spherical, hemispherical, and tube geometries. Unconfined hemisperically shaped H_2-air mixtures at volumes between 7.5 and 2100 m^3 were ignited measuring a maximum overpressure of 6.3 kPa which corresponds to a flame velocity of 84 m/s (Schneider 1978, Pfoertner 1983a, Pfoertner 1983b, Pfoertner 1985). Balloon tests were conducted with hemisperically shaped H_2-air mixtures with a volume of 50 m^3 and concentrations of 20 and 29.6 vol%, respectively. Ignition occurred at the center on the ground by means of an explosive to trigger detonation. Pressures were measured at various positions inside and outside the balloon. Visually measured flame speeds agreed well the theoretical values (see Fig. 3-28) (Breitung 1995).

The influence of partial confinement on the combustion behavior of H_2-air mixtures was examined in further ICT tests employing a 10 x 3 x 3 m^3 lane with parallel walls (Schneider 1984a, Schneider 1984b, Schneider 2005).

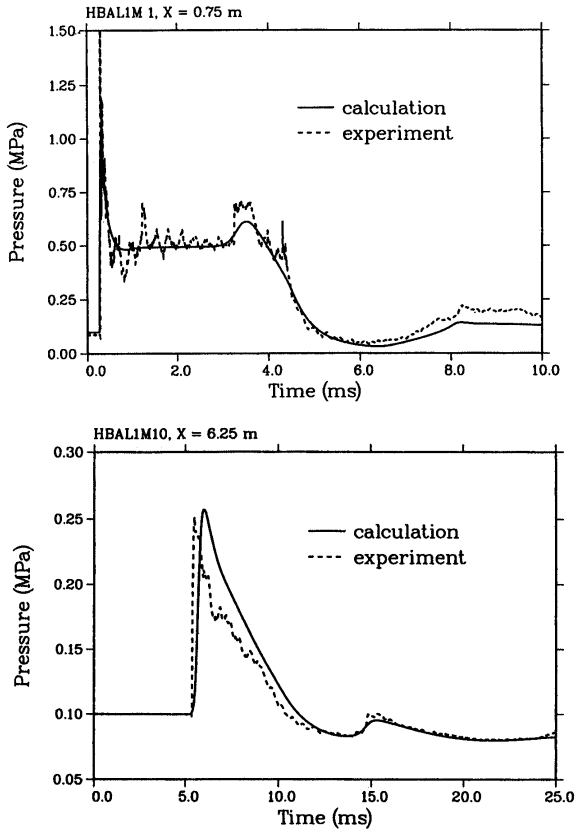

Fig. 3-28: Measured and calculated pressure transient inside (left) and outside (right) the balloon in an FH-ICT hemispherical balloon test with H_2-air detonation, from (Breitung 1995)

The extensive experimental research programs on gas explosions within the EU projects MERGE (Mercx 1994) and EMERGE (Mercx 1997) have shown that overpressures are mainly determined by fuel type, geometric scale as well as the arrangement and number of obstacles which are passed by the propagating flame.

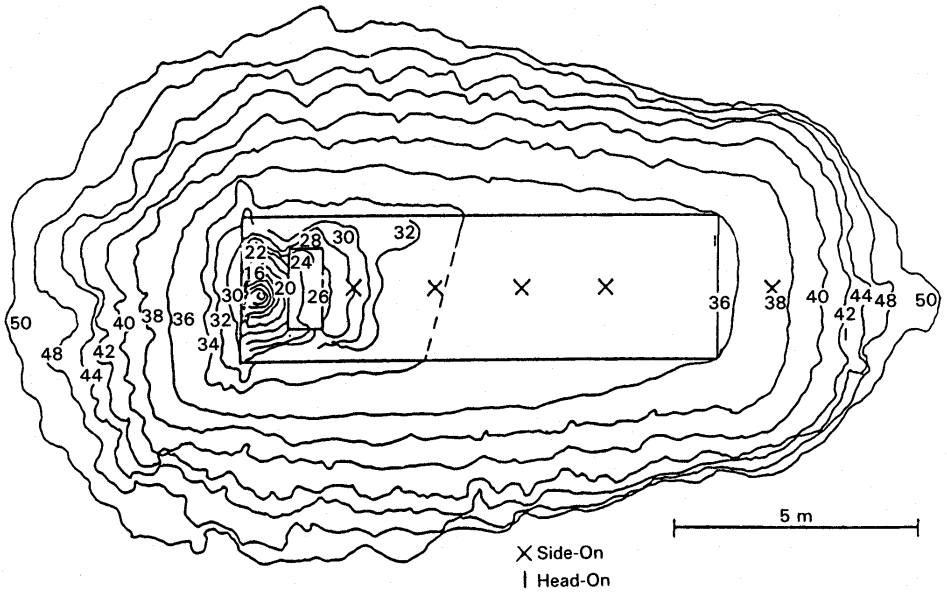

Fig. 3-29: Measured flame front profiles in an FH-ICT lane test with parallel walls (37 % H_2 air mixture), fan generated turbulence, and DDT near the wall (contour 34), from [Berman 1986]

Other unconfined explosion tests are known of the BASF company in Germany. In 1943 and 1948, explosion accidents occurred at BASF resulting from the bursting of liquid gas vessels, subsequent flash evaporation, and mixing of the fuel with ambient air and eventually ignition of the cloud. The cause of the bursting was a heating of the overfilled vessels by the radiation of the sun ,i.e., there was not enough vapor buffering inside of the tanks. The experimental simulation and modeling of these events has been performed in the 1970s by BASF and Fraunhofer ICT by use of differently sized vessels with volumes between 0.2 and 1.2 m^3 corresponding to a mass of up to 452 kg of liquid propylene. Pressures observed were in the range of 0.5-1.5 kPa for the smaller and 4-7 kPa for the larger vessels (Maurer 1975, Maurer 1977, Giesbrecht 1980, Giesbrecht 1981).

With respect to other physical explosions, tests were conducted in the 1970s and 1980s with the spillage of LNG into a pond of water (e.g., Coyote series, Burro series, Maplin Sands series) to measure among other parameters the strength of RPT pressure waves. After releasing LNG amounts of 40 m^3 onto water, observed RPT overpressures were as high as 5 kPa (Koopman 1982).

Gaz de France initiated an RPT research program in 1981 in Lorient with large-scale tests using LNG. The spillage of amounts between 1 and 9 m^3 onto water has shown that the occurrence and strength of RPT were strongly related to the volume of the mixing zone. Maximum explosion pressure recorded was equivalent to 4.15 kg of TNT. Research activities also included fundamental studies of the phenomena and computer code development. Due to the larger temperature difference, consequences of LH_2 spills onto water may be more severe.

3.2.1.4. Modeling of Pressure Waves

The explosion energy in case of a BLEVE can be assessed by the difference between final and initial state of the bursting vessel assuming isentropic expansion. This plus a certain portion of the bursting pressure energy contribute to the blast wave generation (CSChE 2004).

The propagation of a pressure wave in a compressible medium can be described by the Rankine-Hugoniot equations (or "jump conditions") based on the conservation equations for mass, momentum, and energy. From this relationship, it can be derived that the density ratio of air, if assumed to be an ideal gas, behind and in front of the shock front is limited to about 6. For air as a real gas, however, assuming to dissociate or ionize at high temperatures, this ratio can be significantly higher. A computer code, BLAST (Building Loads Analysis and Systems Thermodynamics), was developed based on the above equations as well as on empirical data from nuclear tests.

A first model description of the shock wave parameters for an explosion in air was given in 1870 by Rankine with shock front velocity, maximum dynamic pressure as functions of the peak static overpressure, speed of sound in air, and the atmospheric conditions. Later modelling efforts have used theoretical or empirical approaches to find agreement with experimental data (Pandey 2006). Fig. 3-30 shows a comparison of measured explosion pressures with different models. It was generally stated that agreement between theory and experiment is less good in the near-field compared to the medium and far-field because of the more complex flow pattern.

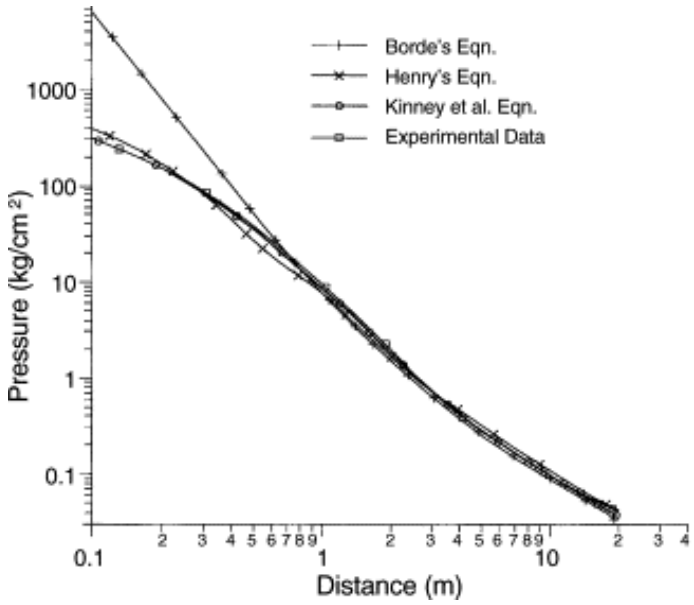

Fig. 3-30: Blast pressures vs. scaled distance for a detonation of 1 kg of TNT (Pandey 2006)

Accurate empirical and theoretical models are existing for detonation waves. According to the Chapman-Jouguet (CJ) theory from 1899 and 1905, respectively, detonation represents a linear discontinuity, transforming the reactants completely to products at an infinite reaction rate. Detonation velocity and pressure can be calculated from equilibrium chemistry as a function of the gas mixture only. Respective data for hydrogen at NTP in an unsupported detonation are

CJ velocity:	1968 m/s
CJ detonation pressure:	1.58 MPa

The CJ theory predicts the thermodynamic state immediately behind the detonation wave, but cannot describe the structure of the wave. Processes inside the detonation front are extremely complex involving multi-dimensional shock interactions in an intensive turbulent reacting medium. Still, the simple 1-dimensional CJ model prediction of velocity and overpressure is quite close to what is being observed, within a few per cent for velocity and 10-15 % difference for the pressure measurements (Tieszen 1993). CJ (and AICC) pressures of a fixed gas mixture increase linearly with the initial pressure at constant initial temperature, and are inversely proportional to the initial temperature at constant initial pressure. However, the CJ theory is not capable of determining the dynamic detonation parameters such as detonability limits, initial energy or critical tube diameter. No theory exists so far that provides estimates of these parameters. CJ parameters of a gas or gas mixtures can be calculated with the code STANJAN developed at the Stanford University.

In the ZND (Zel'dovich-von Neumann-Doering) theory, the detonation wave is described as a two-dimensional dome-shaped shock wave, where at its front both temperature and pressure rise. It is followed by a reaction zone whose thickness is determined by the reaction rate. Here the detonable substance reacts at high pressure and temperature until everything is transformed into product gases. The chemical reaction causes a rapid fall in pressure ("von Neumann spike"). The reaction zone remains unchanged (steady) when moving through the substance. A variable ranging between 0 and 1 describes the respective state and the progress of chemical reaction, respectively. Detonation velocities and pressures are less than for a plane shock front.

A very simple way of modeling blast effects is the TNT Equivalent method derived from the decay of shock waves from high-explosive or nuclear explosions in the atmosphere. It is an estimation of the mass of TNT per unit mass of fuel, whose detonation would result in the same blast wave at the same distance. One kg of TNT translates into energy of 4520 kg meaning that 1 Nm^3 of hydrogen gas corresponds to 2.22 kg of TNT. The weakness of the TNT Equivalent model, if applied to a VCE, is to ignore the pressure-time characteristic differences between a gas cloud and a detonative TNT explosion. It is deemed to overestimate near-field and underestimate far-field effects. Furthermore the model does not consider the influence of turbulence and confinement. The TNT model considers only the total amount of fuel involved and particularly does not take into account the yield factor in a VCE, which is generally only a small fraction, in most cases < 1 %.

The most common form of blast scaling law is that according to Hopkinson and Cranz (Baker 1983):

$$Z = R / E^{1/3} \quad \text{or} \quad Z = R / W^{1/3}$$

where Z is the scaled distance, E is the heat of combustion, W is the weight of the explosive, can be applied to predict blast wave properties of large-scale explosions based on the data of small-scale experiments (assuming same explosive, same geometry). The above relation appears to become inappropriate for $Z < 0.16$ $m/kg^{1/3}$.

Numerous explosion experiments have been evaluated to derive blast charts. Commonly known and accepted are the Baker-Strehlow blast curves for VCE in the open atmosphere or the TNO blast waves for hemispherical explosions. It is a good engineering tool finding its limits when real gas clouds rather than idealized are considered. An improvement towards a more realistic modeling was made with a new set of blast curves, called the Baker-Strehlow-Tang curves (Fig. 3-31), by considering a more precise blast pressure decay behavior. The result is a considerable reduction at long distances. The curves were validated in all combustion regimes (Tang 1999).

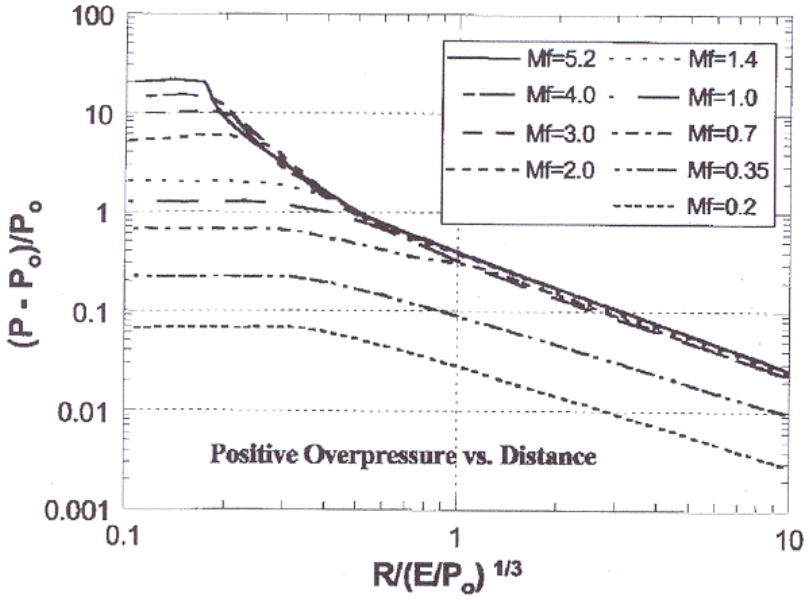

Fig. 3-31: Baker-Strehlow-Tang curves of overpressure vs. distance for various flame Mach numbers M_f, from [Tang 1999]

Models for BLEVE Blast prediction are also described in the CCPS guidelines (CCPS 1994) and the 'Yellow Book' (MVROM 2005). These references also describe models to predict the magnitude and duration of the fireball which often follows a BLEVE. Recently a new numerical method to calculate the blast effects originating from an exploding vessel of liquefied gas have been derived (Van den Berg 2004, Van den Berg 2005). Adequate blast calculation requires full knowledge of the blast source characteristics, i.e., the release and subsequent vaporization rate of the flashing liquid. As the conditions that allow explosive vaporization are not entirely clear and the vaporization rate of a flashing liquid is unknown, safe assumptions have been adopted as the starting point in the modelling. The blast effects from a BLEVE are numerically computed by imposing the vapour pressure of a flashing liquid as boundary condition for the gas dynamics of expansion. The modelling shows that the rupture of a pressure vessel containing a liquefied gas in free space only develops a blast of significant strength if the vessel near-instantaneously disintegrates.

The TNO Multi-Energy method is based on the Multi-Energy concept, which consists in the feature of gas deflagration that overpressure and blast develop only under appropriate boundary conditions, i.e., only where the flammable mixture is partially confined and/or obstructed (CCPS 1994, Mercx 1991, Mercx 2000). This assumption can be made provided that transition to detonation to DDT does not take place. For hydrogen, this requirement is not as easily fulfilled as it is for most hydrocarbons. Based on the Multi-Energy concept, a vapor cloud explosion is modeled as series of hemispherical model charges. Each model charge is characterized by a charge size and a charge strength. The charge size is related to the heat of combustion present in the source, while the charge strength is related to the explosion overpressure. Based on these characterizations, scaled blast parameters (peak overpressure, positive phase duration) as a function of scaled distance have been calculated with the TNO FCT Euler solver 'BLAST' (Fig. 3-32). (Mercx 2000).

The strength of the blast wave is expressed as a number between 1 and 10 representing categories of "insignificant" to "detonative". Calculation results suggest that damaging explosions can occur only, when flame acceleration takes place within a plant structure (Mercx

1991, Mercx 2000). The charge strength can be determined either by numerical calculation (CFD) or by using the experimentally based GAME correlation [Van den Berg 1996], a relation between the overpressure and details of obstacle configurations. The charge size is influenced by the Critical Separation Distance (CSD), the distance between two obstructed regions above which a vapor cloud explosion can be modeled as two separate sources of blast. Guidance on the CSD has been obtained in experimental research projects such as RIGOS (Van den Berg 2003). It has been found that the CSD between a 'donor' and an 'acceptor' increases with the explosion overpressure up to a maximum of half the donor dimension.

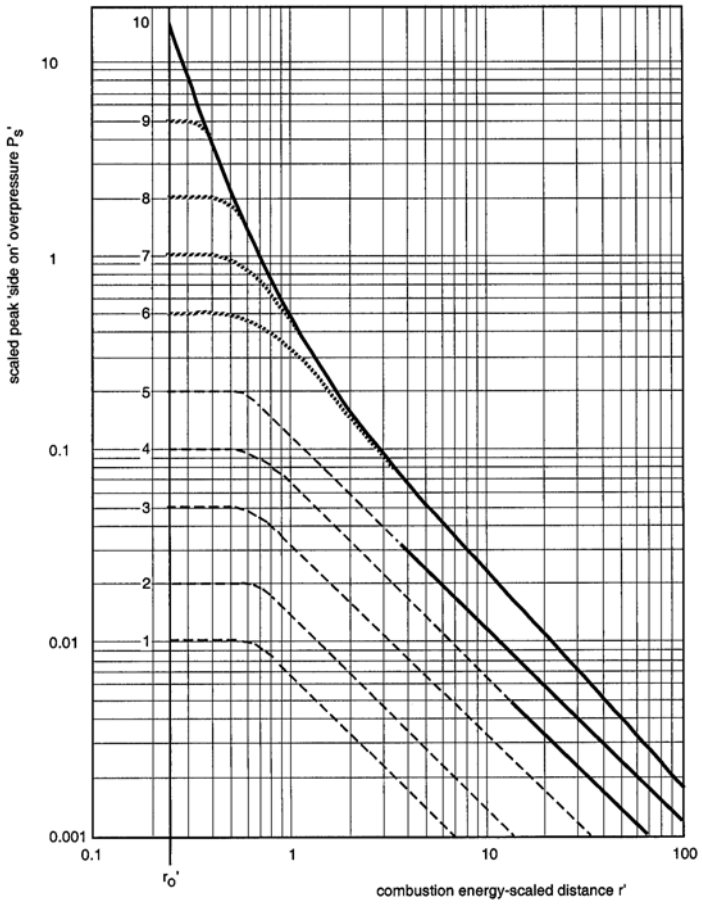

Fig. 3-32: Blast overpressure vs. scaled distance for different explosion strengths according to the Multi-Energy method, from [Mercx 2000]

The Research Center Karlsruhe has developed the calculation models DET1D and DET3D to determine the characteristic detonation parameters within the reaction zone and outside in the unburnt mixture. These models have been mainly applied to assess the load on a nuclear containment upon confined combustion of homogeneous mixtures of H_2, O_2, N_2, H_2O. Code validation was made against the Russian RUT experiments and FH-ICT balloon tests (see Figs. 3-2 and 3-3). Parameter calculations of a 3D detonation have shown that the 3D structure is not important for the pressure load and that a relatively coarse grid provides sufficient accuracy (Breitung 1995).

The state-of-the-art approach to modeling of combustion phenomena are 3D CFD codes, which need to be adapted to the spatial and temporal lengths characteristic for chemical reactions. Typical time steps for hydrodynamic flow calculations are in the order of 10^{-6} s and for the H_2-O_2 reaction mechanism 10^{-10} s (Breitung 1995). Many approaches are based on the assumption

of incompressible flows and are restricted to slow deflagrations or to pure detonations. For fast deflagrations with Mach numbers > 0.3, incompressibility can no longer be assumed, since pressure waves are not negligible.

Several methods of turbulence modelling have been developed. In the "Reynolds Averaged Navier Stokes" (RANS) equations, turbulence is modelled by means of a turbulence viscosity which can be calculated in a k-ε two-equations system. In contrast, the "Direct Numerical Simulation" (DNS) employs the direct and complete solution of the conservation equations taking into consideration all turbulent structures. Somewhere in between is the method "Large Eddy Simulation" (LES) where only the large turbulence structures are being dissolved by the calculation grid, whereas small turbulences are filtered away and covered a turbulence viscosity model approach.

Today's modeling and simulation show good agreement with a variety of fast combustion phenomena (Fischer 1996). It has the potential to provide accurate data for realistic scenarios depending on how accurately the respective submodels are working. For example, the above mentioned LES method for turbulent flows with high Reynolds numbers was successfully applied to the FH-ICT deflagration test with stoichiometric H_2-air mixture (Molkov 2005). The application of computer models, however, should be limited to cases or ranges, for which the codes were validated. Examples of CFD codes applied to combustion are AIXCO (RWTH, Germany), AUTOREAGAS (TNO & ANSYS Century Dynamics, The Netherlands), CFX (Harwell, UK), FLACS (CMI, Norway), FLUENT (Fluent, USA), GASFLOW (FZK, Germany), PHOENICS (CHAM, UK).

3.2.1.5. Throw of Debris and Missiles

No fully validated model exists in terms of predicting projectile hazards from bursting pressure vessels. However, this difficult physical problem may be divided in two parts:

- fragmentation process evaluation;
- projectiles trajectories;

The first part is probably the most complex one, and only numerical simulation seems to allow for prediction using appropriate material and fracture models as, e.g., shown in (Gurson 1977, Erdogan 1977, Mott 1943).

The second part couples beginning solicitation and ballistic considerations. Solutions as suggested in (Baum 1999, Baker 1983, UFIP 2002) are the most widely applied and easy-to-handle models. The software PROJEX using a method developed by INERIS may also be used and seems to give better results (INERIS 2004).

A global model based on statistical considerations is also being conceived in (Hauptmanns 2001).

Most modeling approaches deal with the effects of blast and fire. In many hydrogen explosion scenarios however, the throw of missiles or debris is also important and in some cases even dominant.

For hydrogen gas explosions this is typically the case for scenarios where some degree of confinement or enclosure is present. When in combination the combustion process changes from a deflagration to a detonation the throw of missiles or debris can be devastating. Examples are gas explosions inside industrial equipment, inside a garage or car park, or in a nuclear plant. These scenarios may lead to a major hazard of debris or missiles. Other types of explosions

involving hydrogen are BLEVE's and physical explosions. In these scenarios, it is typically a vessel rupture leading to the throw of missiles. Any risk assessment methodology for hydrogen should contain models for the throw of debris or missiles.

The Initial Conditions

In general the initial conditions for throw are defined by the distributions of the missile or debris mass, launch velocity, and launch direction. These conditions are determined by the failure process and the subsequent acceleration by the expanding gasses, or reaction products. This is accompanied by pressure relief as a result of the increasing vent area between the accelerating items.

The initial conditions for throw of missiles from vessels, as a result of physical explosions, BLEVE's and internal gas explosions can be determined with PGS02 (MVROM 2005), referred to as the 'Yellow Book', and the CCPS Guideline (CCPS 1994). In these references, the models of Baum (BLEVE's), Baker (physical explosions) and Gel'fand (physical explosions and internal gas explosions) are presented. For BLEVE's, the model of Baum predicts the initial velocity of missiles based on the amount of liberated energy. The model of Baker for physical explosions relates the initial velocity of missiles to a scaled overpressure, the vessel geometry, and the number of fragments. With the model of Gel'fand for internal gas explosions, the initial velocity is based on the scaled overpressure and a scaled energy release rate.

Numerical simulation in combination with appropriate material and fracture models, e.g., shown in (Gurson 1977, Erdogan 1977, Mott 1943) is another option.

The break-up process of buildings constructed from reinforced concrete or brick during an internal gas explosion is a more complicated phenomenon. In the case of a (weak) deflagration, the combustion continues during the break-up process and debris launch. The coupling between pressure build-up, venting, and break-up determines the part of the structure that will participate in the throw, and the distributions of debris launch velocity and launch direction.

When a hydrogen detonation takes place inside a building the combustion process is completed before the structure starts to break up. As a result, the structure is loaded with a quasi-static load of typically 0.8 MPa overpressure. This by far exceeds the structural strength of any typical industrial building. As a result, the structure will largely break up and accelerate. Hydrogen detonations in buildings can be compared with bare quantities of high explosives in ammunition magazines. A similar quasi-static load is obtained when a bare charge resulting in a loading density of 0.25 kg/m^3 of TNT is detonated. In Fig. 3-33, the result after the detonation of 2 kg of TNT in an 8 m^3 Kasun-building (Norwegian 'small quantities' ammunition storage building) is displayed (Langberg 2004).

Fig. 3-33: Kasun storage building with an internal volume of 8 m^3 (left). Result after detonation of 2 kg TNT (right). (Langberg 2004)

For detonations of bare explosives in ammunition magazines, relations for the distributions of debris mass, launch velocity, and launch direction have been derived within the Klotz Group (Van Doormaal 2006a, Van Doormaal 2006b). Those relations are based on debris pick-up data from a collection of large scale trials, and depend on loading density and wall thickness. The cumulative debris mass distribution was found to decay exponentially with debris mass. The characteristic length of debris decreases slowly with loading density. Fig. 3-34 shows this characteristic length for a large collection of trial data. Note that the effective loading density for hydrogen detonations of 0.25 kg/m^3 is situated at the low loading density regime of the trial database.

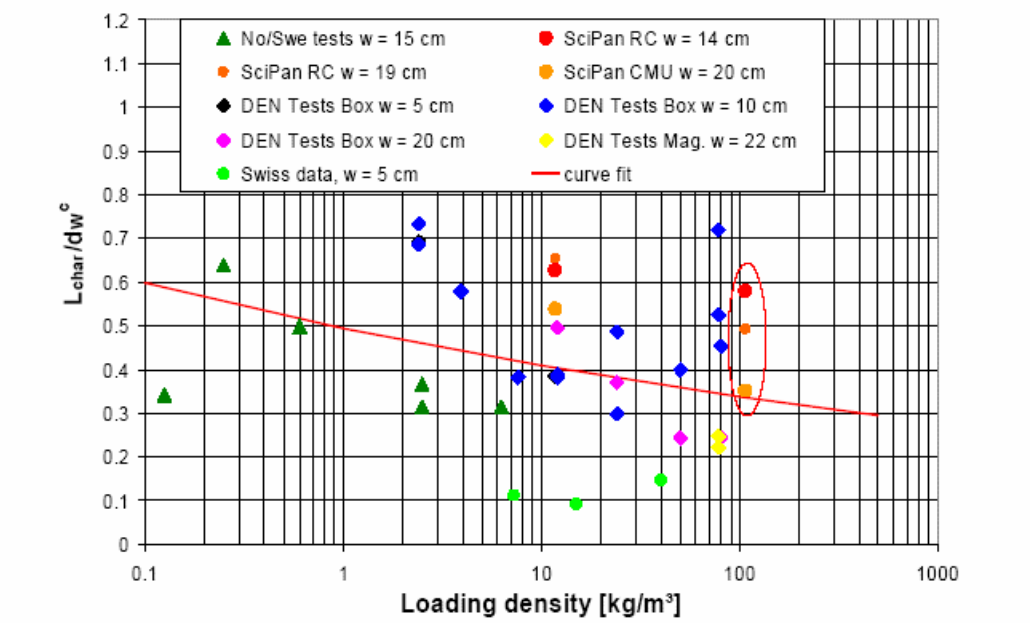

Fig. 3-34: Characteristic length versus loading density for the Klotz Group trial database (van Doormaal 2006a4)

The initial debris velocity decreases with debris mass around a typical velocity, the Debris Launch Velocity (DLV). This relation has been based on backward calculations. The launch angle distribution was found to be a rather sharp Gaussian distribution centered around a direction close to the wall normal directions. This directionality is illustrated in Fig. 3-35, where a frame is shown during the debris launch from a Kasun-building after detonation of 50 kg TNT. Note that this loading density exceeds the energy content of a hydrogen detonation by far.

Fig. 3-35: Development of the debris throw during a Kasun trial with 50 kg TNT illustrating the strong directionality of throw

The addition of the new Sci Pan 3 trial to the database was recently reported (Van der Voort 2006). The relations are currently being implemented in a software code, the KG-Engineering Tool.

The Throw of Debris and Missiles

The initial distributions are the required input for throw models. Throw models determine a collection of impact locations in the field. Together with the impact velocity and impact angle the consequences for the infrastructure and for human beings can be determined. Most existing throw models make use of a Monte Carlo technique. Predefined initial distributions of debris or missile mass, launch velocity and launch direction are sampled to obtain the initial conditions for a number of trajectory calculations. To obtain a proper representation of the debris or missile density in the field, the required number of Monte Carlo simulations needs to be very large. A global model based on statistical considerations is also being conceived in (Hauptmanns 2001).

Recently TNO has developed a universal throw model (Van der Voort 2006). The basis is the source function theorem, an underlying mathematical relation between the debris or missile density and the initial distributions. This model reduces the required number of trajectory calculations dramatically. Trajectory calculations have to be carried out with caution since the selected shape, orientation and drag coefficient of debris and missiles have a significant influence on throw distances.

In Fig. 3-36 an application to the Sci Pan 3 trial is shown together with experimental results (Van der Voort 2006). Compared to hydrogen detonations, this trial is situated at the other end of the loading density regime (> 100 kg/m^3), but illustrates the validity of the model in general. The calculations are in reasonable agreement with the experimental data. Differences can be recognized and understood as the model does not take into account:

- ricochet and roll (transport of missiles and debris after the first trajectory);
- coupled trajectories:
- break-up at impact.

In reality, these phenomena play a role, but are on the other hand not always important in the field of risk assessment.

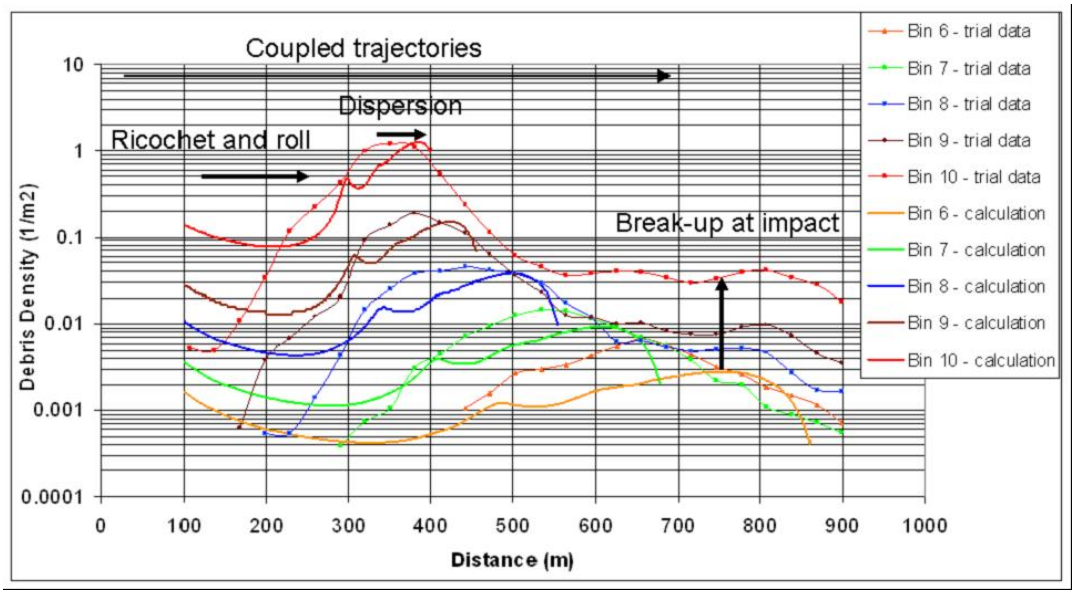

Fig. 3-36: Debris density calculated with the universal throw model together with experimental result. Sci pan 3 trial (Van der Voort 2006)

Solutions as suggested in [Baum 1999, Baker 1983, UFIP 2002] are widely applied and easy-to-handle models. The software PROJEX using a method developed by INERIS may also be used and seems to give better results [INERIS 2004].

Experimental data for the projectile hazards from bursting pressure vessels is displayed in Fig. 3-37. Data available are either from actual plant accidents on a large scale or from small-scale testing. The analysis shows among other findings that 80 % of all vessel ruptures resulting from fires lead to missiles, that non-fire ruptures have an increased number of fragments, that spherical vessels produce more fragments than cylindrical vessels, or that the end tubs of vessels travel further than other types of fragments. There is also the observed tendency of missiles to export fire [Leslie 1991].

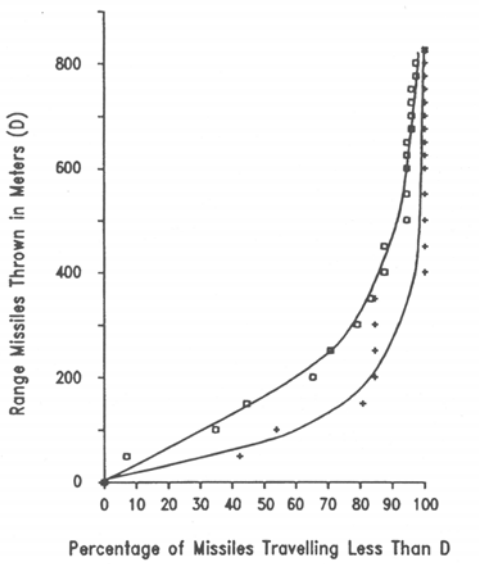

Fig. 3-37: Projectiles traveling after catastrophic pressure vessel failure
+: experimental data; □: case studies, from [Leslie 1991]

3.2.2. Interaction of Blast Wave with Structure and Structural Response

The effects from an explosion, which have an impact on structures, are pressure changes (blast wave) and air movement ("explosion wind") as well as thermal radiation and flying missiles. Only a third of the chemical explosion energy is involved in the generation of the detonation blast wave; the other two thirds are released much slower during the subsequent mixing and burning of the detonation products with the air [FEMA 2003]. In general, structural responses are highly dynamic, highly inelastic, and highly interactive. The mechanical effect of a blast wave is determined by the overpressure and the duration of the positive phase.

3.2.2.1. Interaction of Blast Wave with Structure

The blast parameters are dependent on the distance between structure and blast center. At close distances, the target is exposed to a high-intensity pressure load over a localized region; at greater distances, the load is reduced, but covers a larger surface area. The diagram in Fig. 3-38 describes the pressure load on a rectangular structure.

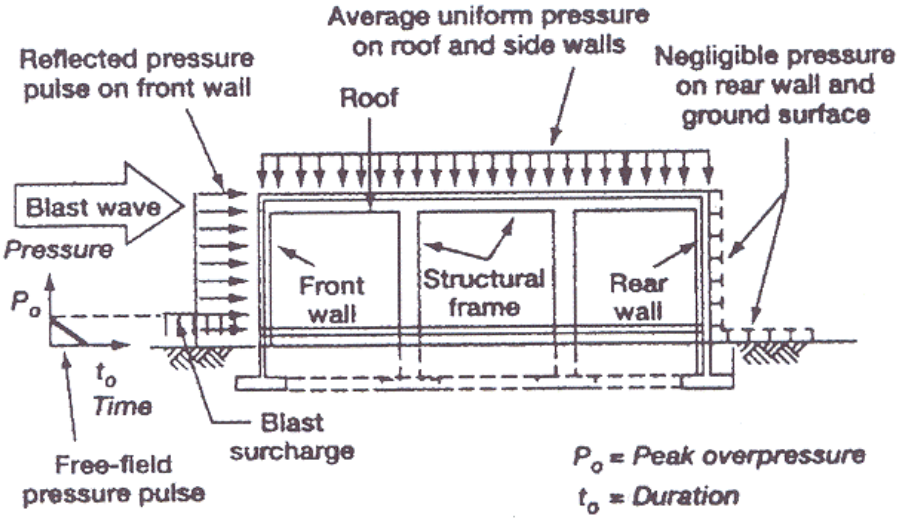

Fig. 3-38: Simplified blast loading diagram on a rectangular building [Benteftifa 1995]

The dynamic interaction of a blast wave with the structure depends on the pressure-time history, i.e., rise time and duration of positive phase and peak pressure or the impulse (which is the time integral of the pressure). Two phases are distinguished:

1. The initial "diffraction loading"
   Diffraction loading is given by forces resulting from direct and reflected pressures during the initial phase. Reflection of the pressure wave at the front side amplifies the incident peak pressurewith a normally reflected wave to represent an upper limit. Also density and temperature of the reflected wave are increased compared to the incident wave. The flow around the obstacle determines the further pressure development at the front and at the back side. The net horizontal loading is that on the front minus that on the back face. The reflection coefficient, i.e., the ratio between reflected and incident overpressure, is dependent on the blast wave type (pressure or shock wave), its intensity, and on the incident angle. For a pressure wave, this coefficient can have a value up to about 3 depending on the incident angle (the more usual case will have an oblique incidence). For a shock wave, it can be in the range of 2 to 8 and even higher for explosives (see Fig. 3-39). Dynamic loads of fast transient pressures are imposed, if the combustion energy is inhomogeneously distributed, and are specific to the structure geometry.

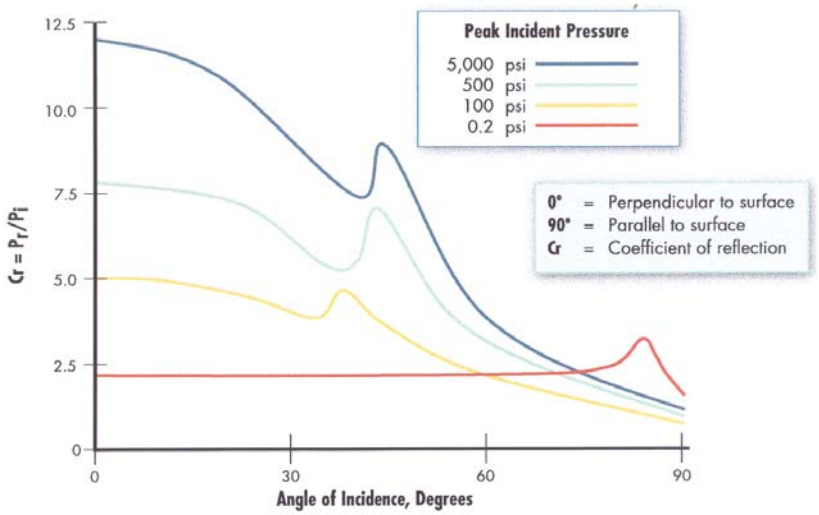

Fig. 3-39: Reflected pressure coefficient as a function of the incidence angle, from [FEMA 2003]; (100 psi = 2.26 MPa)

2. The "drag loading"
   After the diffraction phase is completed, the structure is subjected to a "stagnation pressure". The distance of the incident wave when interacting with the structure, causes major pressure differences developing from the edges of the structure. Resulting from this rarefaction wave, pressures decrease. During this so-called drag phase, strong transient winds (explosion wind) with flow velocities of several 100 m/s are effective. Drag forces will particularly have an impact on smaller structures such as pipe work. Load duration during vapor cloud explosions may be long enough to be comparable with the time required for the dynamic response time of the structure. In case of large structures, the rarefaction from the edges is insignificant.

Confined Areas

In a confined or partially obstructed area, an explosion will create a structure loading, where two phases can be distinguished, the reflected blast loading followed by the gas loading phase. When the pressure wave hits the (rigid) wall, gases are brought to a rest and the wave is reflected. At normal incidence, the reflected shock wave further compresses the burnt gases increasing the pressure by about a factor of 2.3. The mixture of reflected pressure waves and deflected air flows are the result of reverberation of the initial high-pressure, short-duration reflected wave with the amplitude decaying with each reflection until eventually pressure levels out at gas pressure loading. The latter phase lasts longer, the less venting is available. The more complex the structure, the more difficult is the prediction of the critical conditions for mechanical failure for a given load history.

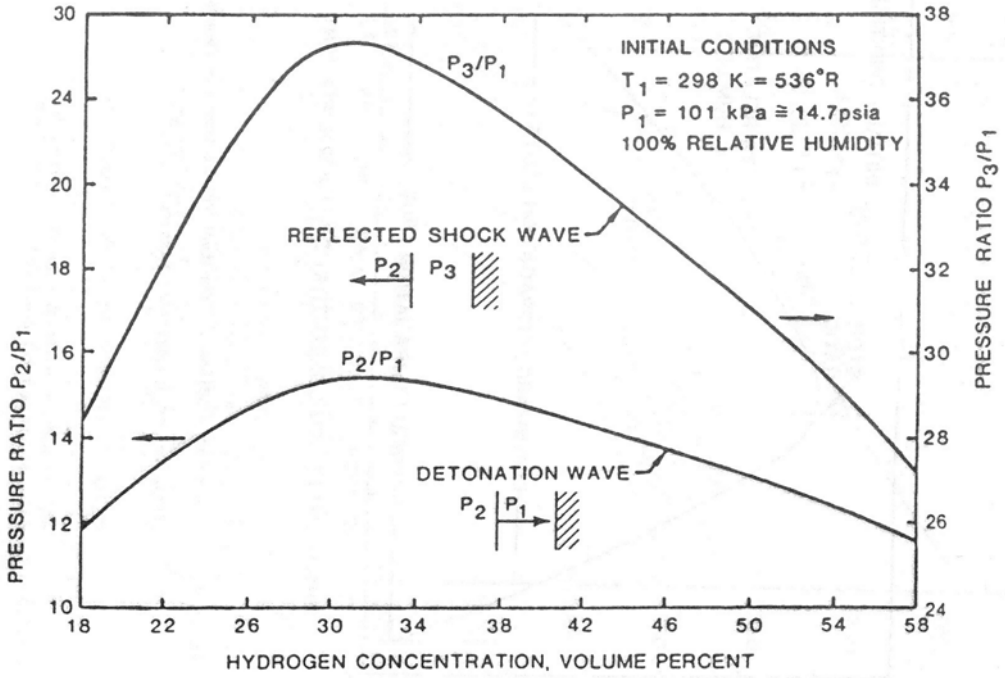

Fig. 3-40: Theoretical detonation pressure and normally reflected detonation pressure for hydrogen-air mixtures [IAEA 1990]

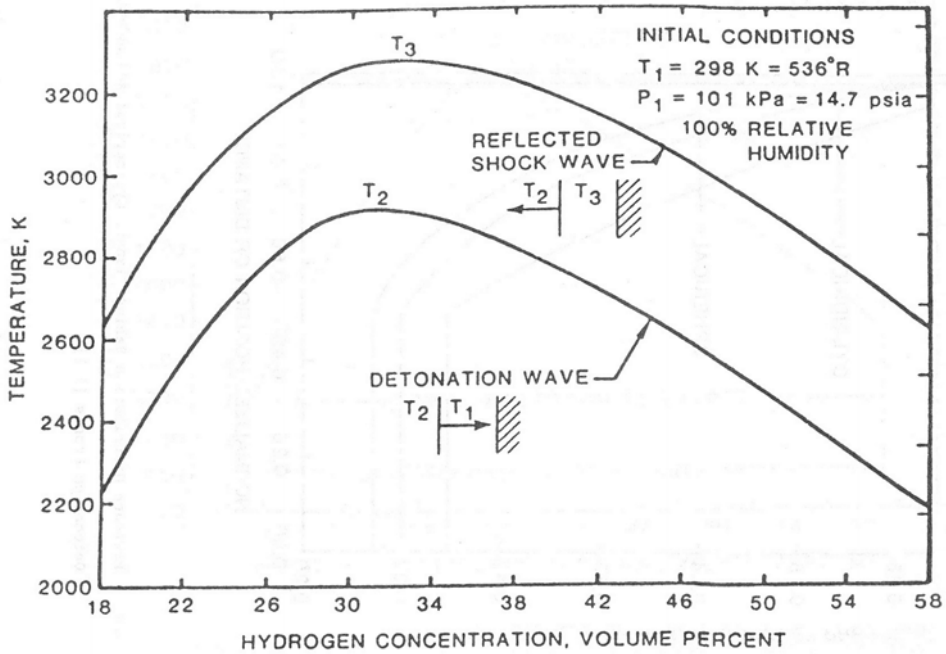

Fig. 3-41: Theoretical detonation temperature and normally reflected detonation temperature for hydrogen-air mixtures [IAEA 1990]

For a vented volume or a volume with weak surfaces, venting formula [NFPA 2002], [CEN 2004] may be a tool in order to predict the pressure applied. In case of a detonation, the loading may be divided in two parts [USACE 1990]: a shock pressure and a constant load.

3.2.2.2. Methods to Determine Structural Responses

Forces acting on a structure will lead to a deformation to an extend which depends on the material properties and structure composition. For a static or quasi-static load, i.e., a constant or slowly changing load like from a simple deflagration, it will be in equilibrium with the internal forces resulting in a deformation of the structure. For a dynamic load, i.e., a fast load transient, however, a "dynamic" contribution from inertia forces will add to the equilibrium, which can show positive or negative acceleration, i.e., mass and stiffness of the structure will play a major role. The load from a gas explosion is considered a dynamic load due to its short overpressure duration, which is typically in the range of 100 - 200 ms. Detonations tend to excite the high natural frequencies of a building, whereas deflagrations are more effective for the lower frequencies. It appears to be technically more difficult to design a building against both explosion modes rather than only one.

Methods used in order to determine structural response and resistance belong to three main categories:

- empirical methods that are widely used in risk assessment and that are mainly based on pressure peak values or P-I diagrams;
- analytical methods
- numerical methods that can be handled with the help of a CFD code coupled with a finite element method;

a) Empirical Methods

Methods Based on Pressure Peak Values

An empirical and very global approach of determining the strength of structures is to relate overpressures to the degree of observed damage. This very useful and easy handling method is widely used. The relationship between pressure and damage, which is derived from TNT explosions, cannot satisfactorily be transferred to vapor cloud explosions. The pressure decay from a TNT explosion is much faster than from a vapor cloud explosion. The high impulse and the suction effect due to the below-atmospheric pressure phase will certainly result in a different damage pattern. Thus damage criteria such as those derived by Schardin (see Fig. 3-42) from TNT explosions are not directly applicable [Giesbrecht 1988].

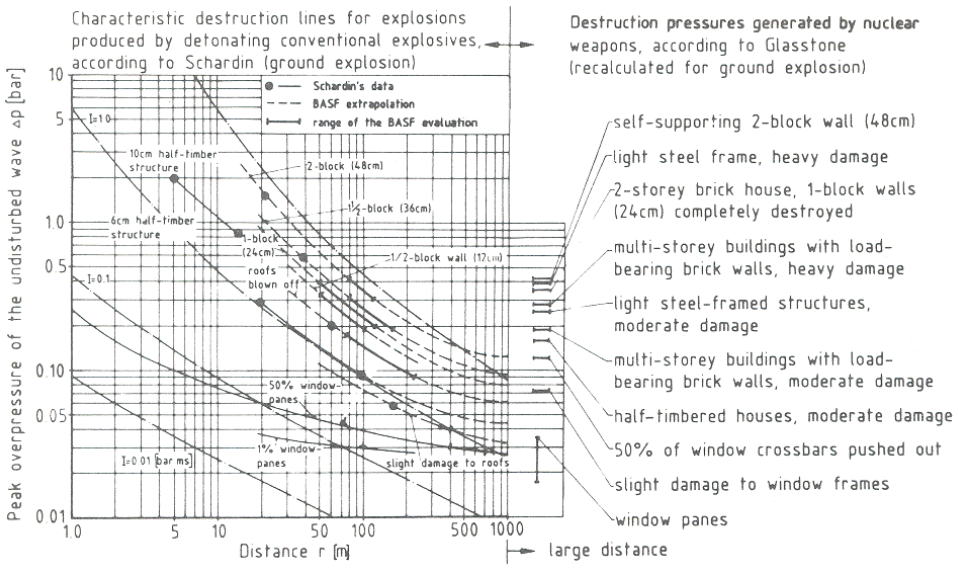

Fig. 3-42: Schardin destruction curves for detonation waves, from [Giesbrecht 1988]

Many pressure criteria were defined in the past related to various structures and specific components, however, varying over a large uncertainty range. A rough classification is given in Table 3-12.

Table 3-12: Damage classification, from [TNO 1992]

Zone	Damage level	Overpressure of incident blast wave [kPa]
A	Total destruction	> 83
B	Heavy damage	> 35
C	Moderate damage	> 17
D	Minor damage	> 3.5

A pressure peak for domino effect really useful for risk assessment may also be defined at a value of 20 kPa [MEDD 2004].

Methods based on P-I diagrams

Another global approach may couple pressure peak with impulse. The impulse, i.e., the pressure – negative and positive – integrated over time, is a measure for the explosion energy (Fig. 3-43), which also varies in time and space over the exposed structure surface. Damage to the structure resulting from a blast wave may be subdivided into direct effects and what is named "progressive collapse", a kind of secondary failure following the change of the load pattern on a structure due to the direct effects. Features of a P-I diagram are the asymptotes in P and I direction and the monotonic relation between P and I, which suggests a subdivision into three regimes: impulse-controlled, peak load-controlled, and an intermediate dynamic stage [Li 2002]. P-I diagrams are being widely used in damage assessments not only for structural damage, but also for predicting blast-induced human injuries. They are providing useful information on the vulnerability of targets.

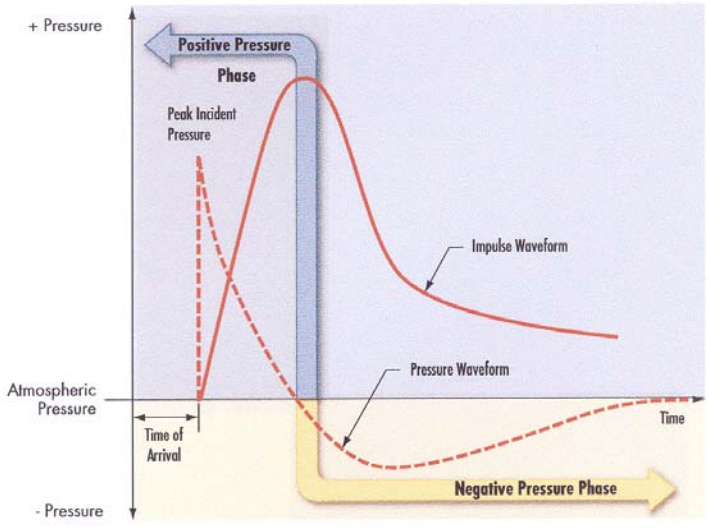

Fig. 3-43: Transient behavior of impulse, from [FEMA 2003]

Damage levels can also be visualized in pressure-impulse diagrams, where different regions can be defined by iso-lines. An example is given in Fig. 3-44 showing the experimental results for

the observed damage in per cent, after different types of houses were exposed to a certain explosion (pressure/impulse) load [TNO 1992]. Important for the damage effect of a short-term load (= shock wave) is only the impulse, whereas it is the maximum overpressure for that of the longer-term load (= pressure wave). The solid lines in the figure indicate the lower boundaries for light damages, for severe damages, and for collapsing structures of the houses investigated.

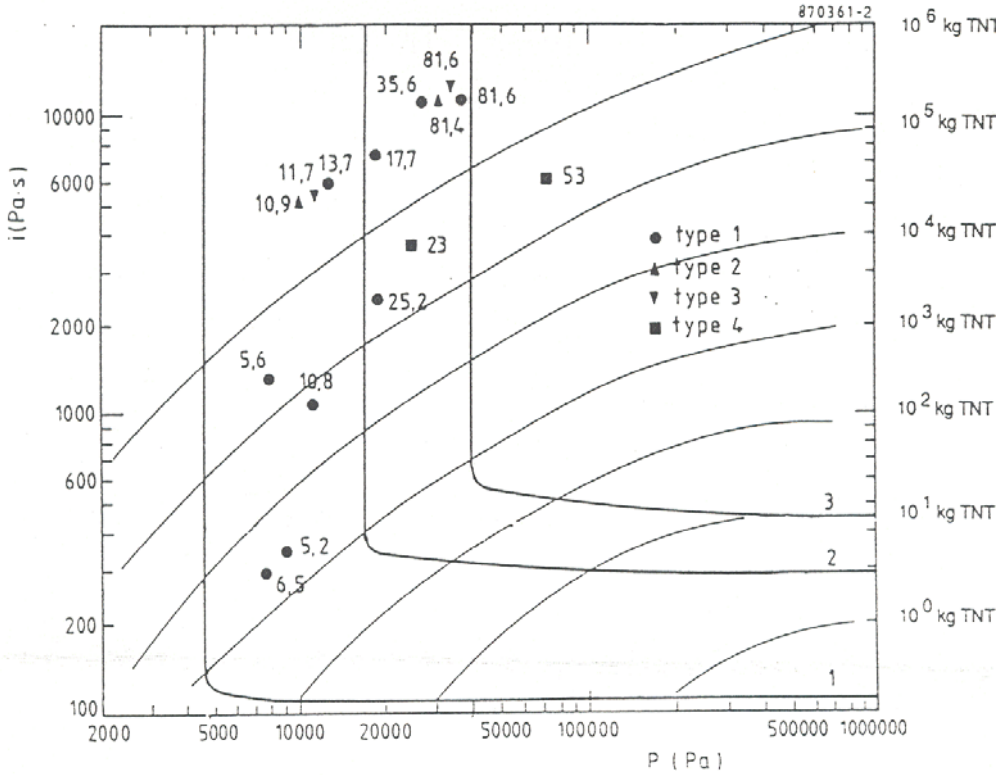

Fig. 3-44: Pressure-impulse diagram with experimental damage values for different types of houses, from [Mercx 1991]

The estimation of the level of damage is usually done taking either fixed-limits methods or the PROBIT method. In a fixed-limits method, the hazard level is compared to fixed limits like IDLH (Immediately Dangerous to Life or Health) values or pressure thresholds, as given in the literature. It is a simple method, but may lead to wrong conclusions in transient hazards. In such cases, the PROBIT method is the more appropriate one. First a hazard load, L, is estimated, which could be the overpressure in an explosion or the integrated thermal flux at a certain location. Then the PROBIT or probability unit, y, is given by $y = k_1 + k_2 * \ln L$, which can be related to a certain probability of death, injury, or damage. k_1 and k_2 are empirical parameters, which are specific to, e.g., toxic chemicals or fire and explosion effects and can taken also from the literature [CSChE 2004]. For the assessment of the probability to obtain a certain level of damage, so-called probit functions have been introduced and suitable damage criteria have been defined [TNO 1992].

Computer simulation techniques have been developed by SRI International, USA, for analyzing hydrogen explosions and the subsequent response of structures and humans. The thermodynamic code TIGER is used to calculate explosion pressures and expansion characteristics, which are input to the DYNA3D model to determine the impact on structures. A simplification of the blast load damage analysis has led to the development of the pressure-impulse (PI) methodology which is based on the observation that for a broad range of structures, the final damage state depends on peak pressure (P) and total impulse intensity (I) only. This

methodology allows for a quick and easy evaluation of accident scenarios by employing a continuously growing library of pressure-impulse load and damage curves that are based on either experimental data or computer simulations [Sanai 1996].

b) Analytical Methods

A structure can be schematically represented by a system of masses coupled with springs or dampers. For the static case, if linear-elastic or non-linear-elastic forces are acting, displacements of the masses become zero again, when the load disappears. In case of plastic or elasto-plastic behavior, displacement is zero or very small, until the maximum load is reached. Under a static load, the structure will then fail; under dynamic load, it may retain a residual displacement. In general, structures must be designed to react elastically under typical loads like wind. Plastic displacement must be limited to abnormal load conditions. The maximum displacement depends on load duration, t_D, and the natural frequency of the structure, T. For low t_D/T ratios, the displacement is smaller than for static loads. For large t_D/T ratios, the displacement can be larger than under static load conditions. Other important parameters are the static strength and the ductility. Load schemes are distinguished between a step function for a long-duration pressure wave and an impulse load for a short-impact shock wave.

Detonations tend to excite the high natural frequencies of a building, whereas deflagrations are more effective for the lower frequencies. It appears to be technically more difficult to design a building against both explosion modes rather than only one. However for hydrogen explosions experience proves that detonations or strong deflagrations must be preferred.

Several analytical procedures may be distinguished. They have to be coupled with structural engineering calculations. Still these methods are likely to lead to very conservative structural designs, and are rather suitable for hand calculations.

A comparison between detonations of explosives and blast waves resulting from nuclear weapon explosions, characterized by quasi-static pressure due to a longer impulse time shows that, assuming the same damage, the detonation pressure or the pressure resistance of an object is much higher than the resistance against a blast wave from nuclear tests [Pfoertner 1975]. The pressure resistance behavior of a building under detonative dynamic and quasi-static loading derived from numerous detonative explosion studies can be summarized in an empirical equation for the quasi-static reference overpressure of the building p_{st}:

$$p_{st} = 0.15 * p_r^{2/3},$$

where p_r is the perpendicularly reflected overpressure or the pressure resistance of the building subjected to a detonation. If the TNT equivalent, as derived from the damage of some of the severe accidents, is interpreted as the incident pressure wave in the order of 70 kPa, resulting from a deflagration, the respective quasi-static pressure would be with p_{st} = 22 kPa much smaller.

Dynamic Load Factor DLF

The analytical procedure is usually simplified by introducing a so-called dynamic load factor (DLF), which is defined as the ratio of maximum dynamic displacement over static displacement. It transforms a dynamic peak load into a static load with the same effect on the structure. The DLF is dependent on the dynamic load time and the natural frequencies of the structure. For long explosion times and in case of an idealized triangle-shaped shock wave load, the DLF approaches its boundary limit of 2 [MEDD 1994].

Single Degree-of-Freedom Model SDOF

In a simple method, a static working load is assumed to simulate the effects of blast loads onto structures. This conservative approach, however, cannot predict structure performance and seems to be not optimal for transient blast loads. An improvement of modeling is given with the quasi-static methods which specify a triangular pressure pulse and determine the dynamic structural capacity as a function of the material strengths of the structure. The structural response can be found by using the charts. Single degree-of-freedom (SDOF) models analyze critical components in terms of their structural resistance and predict the response of the structure which then determines the damage level [USACE 1990].

c) Numerical Methods

More information is obtained from multi-degree-of-freedom (MDOF) models, sophisticated CFD models with the possibility to consider flame propagation and pressure profiles also from local explosions. Dynamic finite-element analyses with tools such as ADINA, LS-DYNA, AUTODYN, ABAQUS Explicit may provide the best judgement on whether or not a structure is able to withstand a blast wave.

However, one must be very careful when using software which is still under development and which is still not fully validated to industrial applications. Numerical methods are also usually very sensitive to parameters and calculation grid changes.

3.2.3. Heat Radiation

There exists an extensive published literature on flame radiation from hydrocarbon flames and pool fires (see, for example, [De Ris 1979; Tien 1982; Mudan 1984; Faeth 1985; Viskanta 1987]). However, there is a limited number of studies on hydrogen flame radiation, particularly on large scale.

Thermal radiation is a primary mode of heat transfer. Radiation is the dominant mechanism of heat transfer in large fires involving hydrocarbons, producing intermediate unstable radicals (e.g., O, H, OH, N, etc.) and stable non-luminous gaseous combustion products (CO_2, CO, H_2O, NO_X, etc.) and soot particulates.

The contribution to the radiative transfer in flames can be regarded as due to luminous and non-luminous radiation. Non-luminous flame radiation originates from transitions in the molecular energy levels due to the absorption or emission of photons. Discrete absorption-emission lines of radiation are produced in the infrared spectrum as a result of transitions between quantised electronic states for monatomic gases. Energy released by the gaseous combustion products results from the transitions between the vibrational and rotational energy levels of the molecules of gas species, particularly CO_2, H_2O, CO, etc., producing non-luminous radiation concentrated in spectral lines. These gases do not scatter radiation significantly but they are strong selective absorbers and emitters of radiant energy.

In practical engineering systems, where pressure and geometric scales are large, pressure broadening of spectral lines cause them to overlap with each other, The resulting radiation is thus concentrated in gaseous absorption bands in infrared spectrum produced by various types of transitions between the molecular energy states, particularly the vibrational-rotational states. In luminous flames a continuum radiation in the visible and infrared is also emitted by the unburnt carbon particulates called soot that contribute greatly to the luminosity of the flames.

The actual quantity and distribution of combustion products and/or soot produced in fires depend on the type and configuration of fuel and local supply of oxygen. In contrast to hydrocarbon fuels, the hydrogen burns more cleanly in air, producing non-luminous, almost invisible, pale blue flame due to spectral water vapour bands.

In order to understand thermal radiation hazards from hydrogen flames, it is crucial to understand the relative assessment of the physical properties and combustion characteristics of hydrogen and hydrocarbon flames. Table 3-13 provides comparison of the physical properties of hydrogen with hydrocarbon methane.

Table 3-13: Physical properties of hydrogen and methane

	Hydrogen	**Methane**
Auto-ignition temperature	520°C	630°C
Heat of combustion (lower heating value)	119.9 MJ/kg	50.1 MJ/kg
(upper heating value)	141.9 MJ/kg	55.6 MJ/kg
Lower flammable limit (in air)	4.0 vol%	5.3 vol%
Upper flammable limit (in air)	75.0 vol%	15 vol%
Stoichiometric mixture (in air)	29.5 vol%	9.5 vol%
Density (@ 20°C, 100kPa)	0.08988 kg/m^3	0.71 kg/m^3
Diffusivity (@ 20°C, 100kPa)	0.61 cm^2/s	0.16 cm^2/s
Viscosity (@ 20°C, 100kPa)	8.814 µPa-s	11.023 µPa-s
Flame temperature (in air)	2045°C	1875°C
Minimum ignition energy (in air)	0.017 mJ	0.274 mJ

3.2.3.1. Flammability and Combustion Characteristics

Hydrogen has a much wider range of flammability in air (4% to 75% by volume) than methane (5% to 17% by volume), propane, or gasoline, and the minimum ignition energy (for a stoichiometric mixture) is about an order of magnitude lower (1/16th that of methane). In many accidental situations the lower flammable limit (LFL) is more important. The LFL for hydrogen is similar to that of methane, about twice that of propane, and four times that of gasoline. In addition, the minimum ignition energy for hydrogen at the LFL is also similar to that of methane.

Hydrogen-air mixture can burn either as a jet flame at a fixed point, with combustion taking place along the edges of the jet where it mixes with sufficient air. In a stationary mixture in the open with no confinement a flammable hydrogen mixture will undergo slow deflagration. Deflagration refers to a flame that relies on heat- and mass-transfer mechanisms to combust and move into areas of unburned fuel. If the flame speed is accelerated, perhaps due to extreme initial turbulence or turbulence induced by obstacles or confinement, the result is an explosion. In the extreme case the flame speed becomes supersonic and results in detonation. Once initiated, detonation is self-sustaining (no further turbulence or confinement is required) as long as the combusting mixture is within the detonable range.

The heat of combustion of hydrogen per unit weight is higher than any other material, but hydrogen has a relatively low heat of combustion per unit volume. Thus the combustion of a given volume of hydrogen will release less energy than the same volume of either natural gas or gasoline.

3.2.3.2. Radiation Characteristics

In contrast to other hydrocarbon fuels, a hydrogen flame radiates significantly less infrared (IR) radiation (heat) and virtually no visible radiation (light). As a result, hydrogen burns with a pale blue, almost invisible flame that is almost visually imperceptible in artificial light or daylight.

However, in contrast to hydrocarbon flames, hydrogen flame also emits some limited amount of radiation in the ultraviolet (UV) region around 180 to 300 nm, which is exploited by UV detectors to detect hydrogen flame. Most UV detectors are made immune to solar sensitivity by using a sensing device only sensitive to the UV radiation below the 360-nm range. The lower radiation from a hydrogen flame makes the flame itself hotter than a hydrocarbon flame, and objects engulfed by a hydrogen flame tend to heat faster. However, the lower radiation of heat from the flame means that less heat is radiated to objects or people outside the flame.

The consequence of the almost invisible hydrogen flame is that the human physical perception of the heat from a hydrogen fire does not occur until direct contact with the combustion gases. This problem is often resolved by throwing a dry fire extinguisher or dust into the air that will cause the flame to emit visible radiation.

3.2.3.3. Radiation Emissions from Intermediate Radicals and Atoms in Hydrogen Flames

The combustion chemistry of hydrogen flame gives rise to H, O and N atoms, and OH radicals, which emit specific peaks at specific wave lengths. The typical emission spectrum of the laser-induced plasma spectroscopy (LIPS) formed in hydrogen-air flame in the infrared region is shown in Fig. 3-45, and their wavelengths are listed in Table 3-14. LIPS is a promising method that enables spatially resolved elemental analysis of various chemical species based on their atomic emissions. The spectrometer was set to be centred at a wavelength of 720 nm so that atomic emissions of hydrogen H, nitrogen N, oxygen O, and tungsten W could be observed simultaneously. The continuum spectrum is also observed with the emission lines, which is mainly due to the recombination of ions with free electrons.

Table 3-14: Wavelength of each emission line [Itoh 2001]

Element	Wavelength [nm]
H	656.3
N	742.4, 744.3, 746.9, 818.5, 818.8, 821.6, 822.3, 824.2
O	777.2, 777.4, 777.5, 844.6

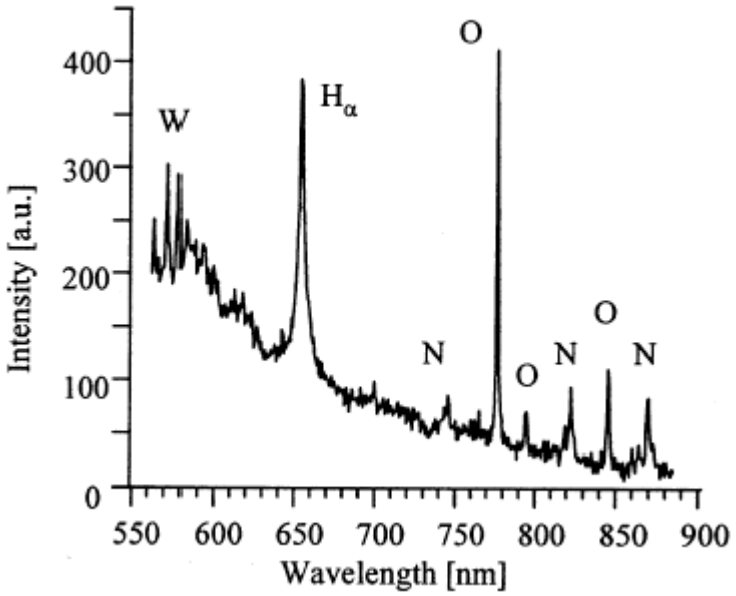

Fig. 3-45: A typical spectrum of laser induced plasma spectroscopy (LIPS) in a hydrogen-air flame
for wavelength range of 550-900 nm, from [Itoh 2001]

More recently, Choudhuri and Gollahalli [Choudhuri 2004] have used laser-induced fluorescence (LIFS) technique for measurements of H atom near 656 nm (2s → 3p) O atom near 845 nm (3s ^{3}S), and OH hydroxyl radical in the UV region near 315 nm.

The OH radical is one of the important intermediates in the combustion reaction mechanism, which is a reliable indicator of the flame zone, flow structure and flame temperature near stoichiometry. Here, the flame temperature was determined by measuring the rotational energy distribution of the OH radical at the excitation of (1,0) band of ($A^2\,\Sigma \leftarrow X^2\,\Pi$) system. Please note that it is not possible to avoid interference of the photolytic production of O atom at the wavelength of 845 nm with the adjacent NO excitation band (1,1) of ($A^2\,\Delta \leftarrow X^2\,\Pi$) system. Here the symbols s, p, d stand for the atomic orbitals and Σ, Π, Δ stand for the molecular orbitals. Maximum statistical uncertainties in measurements were estimated to be 20-30 K in the temperature range.

3.2.3.4. Radiation Emissions from Water Vapor Bands

The hydrogen-air flame emit infrared (heat) radiation mainly due to water vapour bands in the 1-6 μm wavelength region. The contribution of atoms and radicals to heat radiation in hydrogen flame is negligible. However, as mentioned earlier, OH radical effects the maximum temperature of the flame.

Figure 3-46 shows the comparison of the predicted and measured radial temperature distribution of H_2-air flame for different degrees of dilution by natural gas (NG), the dilution ranging between 0 and 100%. The measured values shown in Fig. 3-46(a) have been derived from OH fluorescence signals, and the predicted values shown in Fig. 3-46(b) have been computed using detailed chemical kinetics.

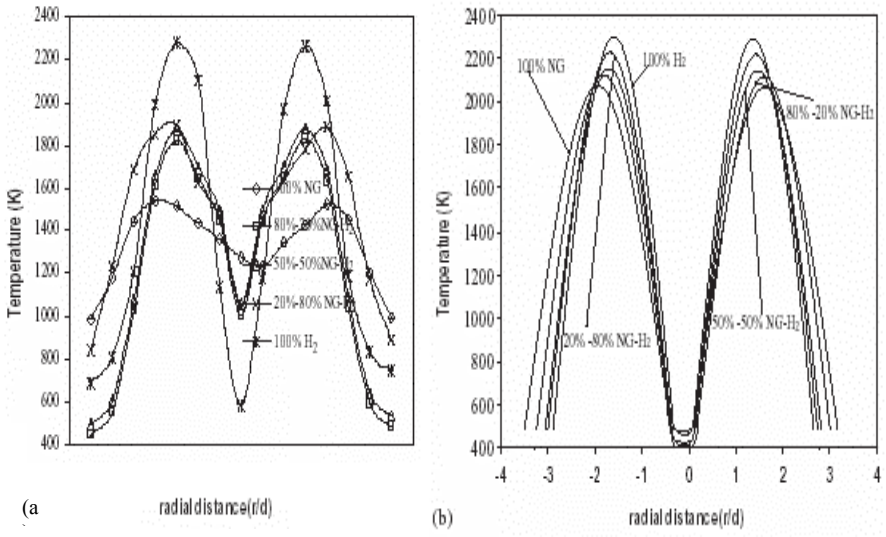

Fig. 3-46: Radial temperature distribution at the near-burner region, from [Choudhuri 2004] (a) spectrally derived from OH measurements (b) computed using detailed chemical kinetics

It can be seen from the figure that the peak temperature of the 100% hydrogen-air flame is 2320K and that of the 100% NG-air flame is 1600K. The lower peak temperature of the NG flame is attributed to the higher heat losses both in the form of banded non-luminous radiation from CO_2 and continuous luminous radiation from solid soot particulates, which are absent in the H_2-air flame. Both flames have heat losses from banded non-luminous radiation from H_2O. The computed stoichiometric temperature contours using the detailed chemical kinetics show a similar trend for the different mixture conditions. Compared to experimental results, predicted temperatures are higher and steeper in shape for all mixture conditions.

Liu et al [Liu 2004] have considered 6.3 μm, 2.7 μm, 1.87 μm, and 1.38 μm infrared bands of water vapor to calculate frequency distributions of radiative source terms. Due to different band intensity parameters and temperature for each band, the symmetrization of frequency distributions in each band is different. The symmetrization of frequency distributions for the radiative source term at 6.3 μm and 2.7 μm bands is better than at 1.87 μm and 1.38 μm bands.

3.2.3.5. Effect of Turbulence on Flame Radiation

Flame radiation intensities or fluxes are often computed from mean properties (e.g., mean emissivity, mean flame temperature). However, Cox [Cox 1977] has shown that neglecting turbulent fluctuations could cause significant error in flame radiation intensities, which is due to non-linear nature of radiation properties. Assuming a gray gas, the mean radiation intensity can be represented as:

$$\bar{I} = \frac{\sigma\phi\bar{\varepsilon}\bar{T}^4}{\pi}\left[1 + 6\left(\frac{\bar{A}}{\bar{T}^2}\right) + \left(\frac{\bar{B}}{\bar{\varepsilon}\bar{T}}\right) + \ldots\right]; A = T'^2, B = 4\varepsilon' T'$$

$$\bar{I} = \frac{\sigma\phi\bar{\varepsilon}\bar{T}^4}{\pi} \; when \left(\frac{\bar{A}}{\bar{T}^2}\right) > 0.4$$

where σ is the Stefan Boltzman constant, ϕ is the geometrical view factor, ε is the gray gas emissivity of flame, T is the flame temperature, and I is the flame intensity.

While this result suggests a strong effect of turbulence on radiation properties, the gray gas approximation is not very appropriate for turbulent flames. However, Faeth et al [Faeth 1985] have shown that the use of mean properties, in conjunction with existing narrow band models, provide an adequate framework for estimating flame radiation in both non-luminous and luminous flames. Fig. 3-47 shows the comparison of the predicted spectral radiation intensities by the mean and stochastic property methods with measurements, in the 1-6 μm wavelength range, for a turbulent hydrogen/air flame. The stochastic method is based on the assumption that the turbulent flow field consists of many eddies and that the properties of each eddy are uniform and statistically independent of one another. The figure shows that for hydrogen/air flames, effects of turbulent fluctuations are large, with as much as 2:1 difference between mean and stochastic property predictions. Faeth et al [Faeth 1985] have argued that this is because radiation properties of hydrogen/air diffusion flames vary rapidly near the stoichiometric condition.

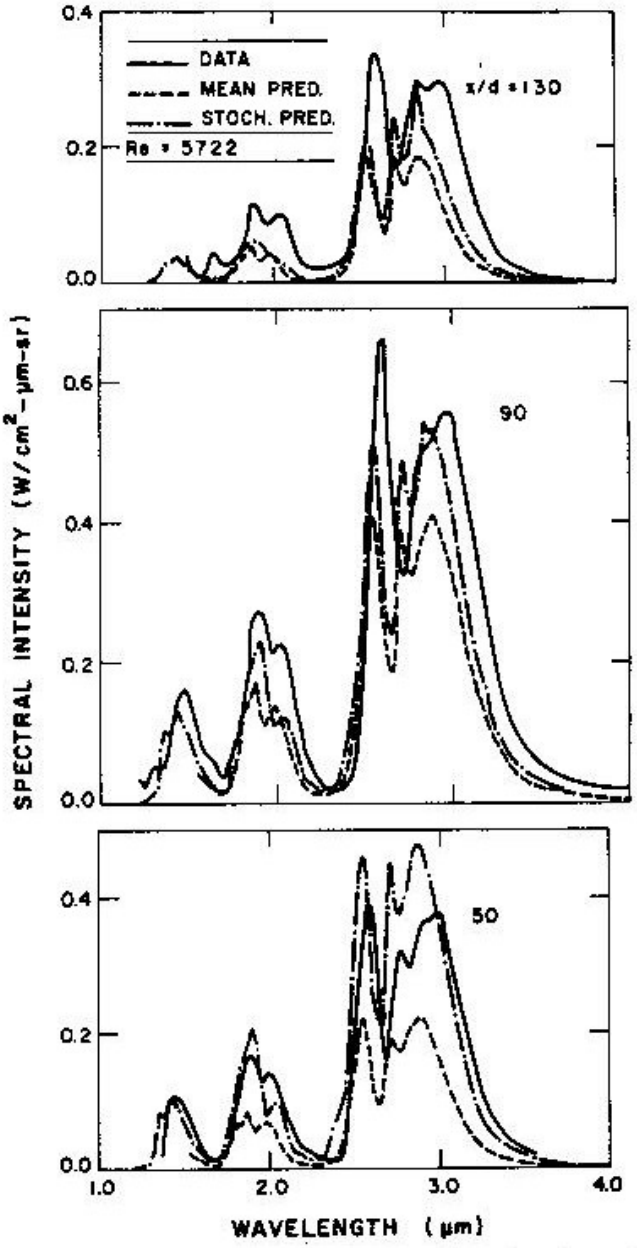

Fig. 3-47: Spectral radiation intensities of hydrogen/air diffusion flame at NTP

3.2.3.6. Radiation Transfer Calculation Methods

The theory of thermal radiation is very complex and an exact solution, even for reasonably simple situations, is generally impossible. The combustion products and soot, acting as participating media, add further complexity to the situation. Therefore, a wide range of calculation methods and mathematical models with varying levels of complexity and accuracy have been developed.

A number of radiation solution methods exist for solving the equation governing the transfer of thermal radiation [Siegel 1981]. The methods differ in complexity and accuracy of the calculation of view factors and economy of the solution algorithm. The most commonly used radiation solution methods and their key features are summarised below:

Zonal or View Factor Calculation Method

This popular method has been widely used by engineers to estimate the radiative transfer in the absence of detailed knowledge of participating media. The walls and interior of the enclosure are divided into zones of finite size. View factors are defined which are measures of the radiation exchange occurring between pairs of zones. This procedure results in n simultaneous equations for each of the n zones and leads to a system with a n^2 x n^2 matrix. This method is very accurate but its main drawback is that the view factor, for each geometry, must be worked in advance and for complex geometries the view factors are not available [Hottel 1958].

Statistical or Monte-Carlo Method

The purely statistical methods, such as the Monte-Carlo method, usually yield radiation heat transfer predictions as accurate as the exact method. There is no single Monte-Carlo method because there are many different statistical approaches.

The simplest Monte-Carlo method is based on simulating a finite number of photons (discretized energy bundles) histories through the use of a random number generator. For each photon, random numbers are generated and used to sample appropriate probability distributions for scattering angles and path lengths between collisions. As the number of photons initiated from each surface and/or volume element increases, this method is expected to converge to the exact solution of a problem. Thus, this statistical method is numerically precise provided the number of photons is large and the random number generator of the computer good enough.

Furthermore, in contrast to the zonal method, the Monte-Carlo method does also not suffer from the calculation of view factors in advance because the view factors are automatically calculated as the randomly chosen energy release bundles are tracked through the enclosure containing the fire. However, since the directions of photons are obtained from a random number generator of the computer used, the method is always subjected to statistical errors and lack of guaranteed convergence but this would improve as the next generation of computers (with more powerful random number generators) become more readily available [Howell 1964].

The Flux (or Multi-Flux) Method

The radiation intensity is a function of the location, the direction of propagation of radiation and of wavelength. Usually the angular dependence of the intensity complicates the problem since all possible directions must be taken into account. It is, therefore desirable to separate the angular (directional) dependence of the radiation intensity from its spatial dependence to simplify the governing radiation transfer equation (RTE). If it is assumed that the intensity is uniform on given intervals of the solid angle, then the RTE can be significantly simplified as the integro-differential RTE would be reduced to a series of coupled linear differential equations in terms of average radiation intensities or fluxes. This procedure yields the flux methods. By changing the number of solid angles over which radiative intensity is assumed constant, one can obtain different flux methods, such as two-flux for one-dimensional geometry, four-flux for two-dimensional geometry or six-flux methods for three-dimensional geometry. The accuracy of flux-methods will increase by increasing the number of fluxes. The six-flux methods have been reasonably successful for fire spread and smoke movement inside compartments [Kumar 1989; Kumar 1991]. They are not suitable for predicting flame spread over surfaces or flames projecting outside openings, where finer discretization of the solid angle than offered by the six-flux method would be necessary [Gosman 1973].

The Discrete Ordinate Method

The discrete-ordinate method [e.g., Chandrasekhar 1950, Lockwood 1978, Fiveland 1982] was originally suggested by [Chandrasekhar 1950] for astrophysical problems. It is derived by applying discrete-ordinate approximation to the RTE through discretising the entire solid angle ($\Omega = 4\pi$) using a finite number of ordinate directions and corresponding factors. A simpler version of the method is also called S_N-approximation because it is obtained by dividing the spherical space into N equal solid angles. More accurate S_N-approximations of the N discrete ordinates are obtained by using Gaussian or Lobatto quadratures and choosing N discrete values of the direction cosines ξ_n, η_n, μ_n such that they satisfy the identity $\xi_n^2 + \eta_n^2 + \mu_n^2 = 1$.The S_N-approximation has been used successfully for two-dimensional cylindrical and rectangular radiative transfer problems with combustion chamber applications, where reasonably accurate results were obtained in comparison to exact solutions [Fiveland 1982; Fiveland 1984]. However, the method suffers from the so called "ray effects", causing anomalies in the scalar flux distribution [Lathrop 1968; Lathrop1971]. The ray effects are particularly more pronounced when there are localised radiation sources in the medium (e.g., flame in an enclosure) and radiation is less important in comparison to absorption. Clearly, as scattering increases and radiation field becomes more isotropic, they become less noticeable. However, with increasing scattering and/or optical thickness, the convergence rate may become slow [Lewis 1984].

The Discrete Transfer Method

The discrete transfer method is a mixture of the Monte-Carlo, zone and flux methods [Lockwood 1981]. Similar to the zone method, the enclosure is divided into cells and equation is analytically integrated along rays in each cell, but the method is much faster and the calculation of the view factors is an inherent feature of the procedure. The only drawback of the method is that to obtain ray-insensitive solution the method may require more rays than affordable on economy grounds for practical problems [Cumber 2000].

3.2.3.7. Gas Property Models for Participating Media

The radiative properties (absorption and scattering coefficients) of the combustion products and enclosure wall emittance are required for the modelling. In an enclosure fire, the gas radiative properties vary considerably from the comparatively transparent entrained air close to the floor to the highly emissive, luminous flames of fire source, and the optically dense ceiling smoke layer. Various models are available to predict the gas radiative properties.

The participating media models (see, for example, [Tien 1982]) currently available for characterizing the flaming and smouldering fires and the resulting combustion products differ in their generality, sophistication, accuracy and computational cost. They are assessed in terms of their ability to predict radiative heat transfer from one-dimensional, idealised representations of the internal structure of buoyant and jet fires.

Exact results can be obtained by line-by-line calculations of spectral absorption-emission lines of molecular gases. However, such calculations are useful in the study of radiative transfer in the atmosphere but are not practical for most engineering applications, and are therefore not discussed here. Narrow-band and wide-band models constructed from the spectral lines, and on a simpler level, the gray gas representation of the molecular spectrum can be considered. The simplest treatment for the case of enclosure fire is to consider the gas to be a gray gas of prescribed constant absorption coefficient.

Narrow Band Model

A well known narrow band model is that proposed by Grosshandler and Modak [Grosshandler 1981], which is based on the statistical model by Goody [Goody 1964] for tri-atomic molecules with equal line strengths within each narrow band region, and with homogeneous effects accounted for through the Curtis-Godson approximation which employs suitable averages along a line-of-sight. For hydrogen flame, the five gas bands of the H_2O, the main combustion products in the infrared region (1-6m) are considered which are 1.14 μm, 1.38 μm, 1.87 μm, 2.7 μm and 6.3 μm. For flames involving mixtures of hydrogen and hydrocarbon (e.g., hydrogen flame diluted by CH_4), band overlap is also taken into account for multiple bands and mixture of CO_2, H_2O, CO and CH_4 gases, particularly for 4.3 μm of CO_2, 2.3 μm and 3.3 μm of CH_4, and 4.7 μm of CO.

Wide Band Model

Edward and Balakrishnan [Edwards 1973] developed a spectral version of exponential wide band model, which is based on the fact that the absorption and emission of radiation by a molecular gas is concentrated in between one and six vibrational bands. Within these bands, the spectral lines associated with rotational modes of energy storage are reordered in wave number space with exponentially decreasing line intensities moving from the band head. The band shape is then approximated by one of the three simple exponential functions, with radiative properties of each absorption band obtained from specified model parameters.

Grosshandler's Total Transmittance, Non-Homogeneous (TTNH) Model

The total transmittance, non-homogeneous (TTNH) model for CO_2 and H_2O mixture is based on total transmittance data for homogeneous systems, with effective pressure-path lengths and temperatures for non-homogeneous systems taken as gas concentrations weighted averages along a line-of-sight [Grosshandler 1980].

Mixed Gray Gas Model

The most popular mixed gray gas model for modeling combustion products (including soot) from fires is that proposed by Truelove [Truelove 1976], which is based on representing the banded spectra of CO_2 and H_2O as a mixture of clear and gray gases. The total emittance of the combined emissions of the CO_2 and H_2O vapors was obtained by Truelove by fitting the spectral data of the gases as gray gas mixture of one clear and three gray gases.

Banded Mixed Gray Gas Model

Truelove's mixed gray gas model, employing one clear and three gray gas representations, can be written in a banded form where, for a given model spectrum, the gray gas weightings are determined as the fractional amount of black body energy in the spectral regions where "gray gas absorption coefficients" exist [Modest 1991]. Recently, Cumber and Fairweather [Cumber 1999] have improved the method by incorporating CO and CH_4 emissions. Expressing total absorptivity and emissivity of a gas in terms of the weighted-sum of gray gases are useful, especially for the zonal method of analysis of radiative transfer.

3.2.4. Physiological Impact

3.2.4.1. Damage by Low Temperature Releases

Skin contact with liquid hydrogen or cold hydrogen gas may cause severe cold burns, comparable with those caused by boiling water. Unprotected skin may freeze onto surfaces cooled by the liquid, causing severe damage on removal.

Prolonged skin exposure to cold hydrogen may result in frostbite. A symptom is local pain which usually gives warning of freezing but sometimes no pain is felt or it is short-lived. Frozen tissues are painless and appear waxy, with a pale whitish or yellowish color. Thawing of the frozen tissue can cause intense pain. Shock may also occur.
The eyes are particularly susceptible – even small splashes of liquid hydrogen, or short exposures to cold vapor or gas, may cause instant freezing of eye tissues and permanent damage.
Transient exposure to very cold gas produces discomfort in breathing and can provoke an attack of asthma in susceptible people. Prolonged inhalation of cold vapor or gas may cause serious lung damage. Prolonged exposure of the entire body to cold can result in hypothermia.

3.2.4.2 Asphyxiation by hydrogen

Hydrogen is not poisonous, but as with any gas (except oxygen) a risk of asphyxiation exists mainly in confined areas as a result of oxygen depletion. Normal air contains around 20.8 % of oxygen, by volume. Besides the dilution by mixing with other gases, oxygen may be consumed in combustion of hydrogen or other burning gases and may be depleted via condensation on very cold surfaces like liquid hydrogen pools. Thus diluting the oxygen volumetric content below 19.5 % will cause effects on human beings.

Alarm levels are generally set at 19 % oxygen. This is less than 2 % below normal levels, so it is important that sensors are precise and stable in order to avoid false alarms. The different stages of asphyxiation at ground level are related to the remaining oxygen concentration as shown in the following Table 3-15.

Table 3-15: Asphyxia – Effect of O_2 concentration, from [NASA 1997], partially accomplished and synchronized with [DNV 2001] data

O_2 [vol %]	Effects and Symptoms
19-21	No discernible symptoms can be detected by the individual.
15-19	Reduction of physical and intellectual performance without the sufferer being aware. Early symptoms in persons with heart, lung, or circulatory problems may be induced.
12-15	Deeper respiration, faster pulse, poor coordination
10-12	Headaches, giddiness, poor judgement, slightly blue lips. Risk of death below 11 vol %, tolerance time 30 min
8-10	Nausea, vomiting, unconsciousness, pale face, fainting within a few minutes without prior warning, mental failure, tolerance time 5 min
6-8	Fainting occurs after approximately 3 min. Death in 8 min; 50 % death and 50 % recovery with treatment in 6 min, 100 % recovery with treatment in 4 to 5 min.
3-6	Coma in 40 s, respiration ceases, death or permanent brain damage, even if rescued
0-3	Death within 45 s

3.2.4.3 Pressure effects from explosions

Direct Blast Effects

These direct effects, also called primary effects, are caused by the dynamic pressure waves. Although the human body is able to adapt to slow pressure changes (diving, high altitudes, etc.) the dynamic changes in a blast front may cause severe damage. Those organs where large differences in densities are encountered, like the lung or the inner ear, are particularly vulnerable. Ear damage is not leading to death, but due to the ears' high sensitivity it is often

used as an indicator for an exposure. Lung damage is depending on a combination of peak overpressure P_s and on the pulse duration t_p (Fig. 3-48).

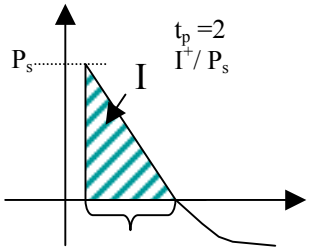

Fig. 3-48: Simplified relationship between positive impulse and time of the overpressure peak

Similar as for the structural effects threshold limits for ear and lung damage are displayed in pressure-impulse diagrams (Fig. 3-49).

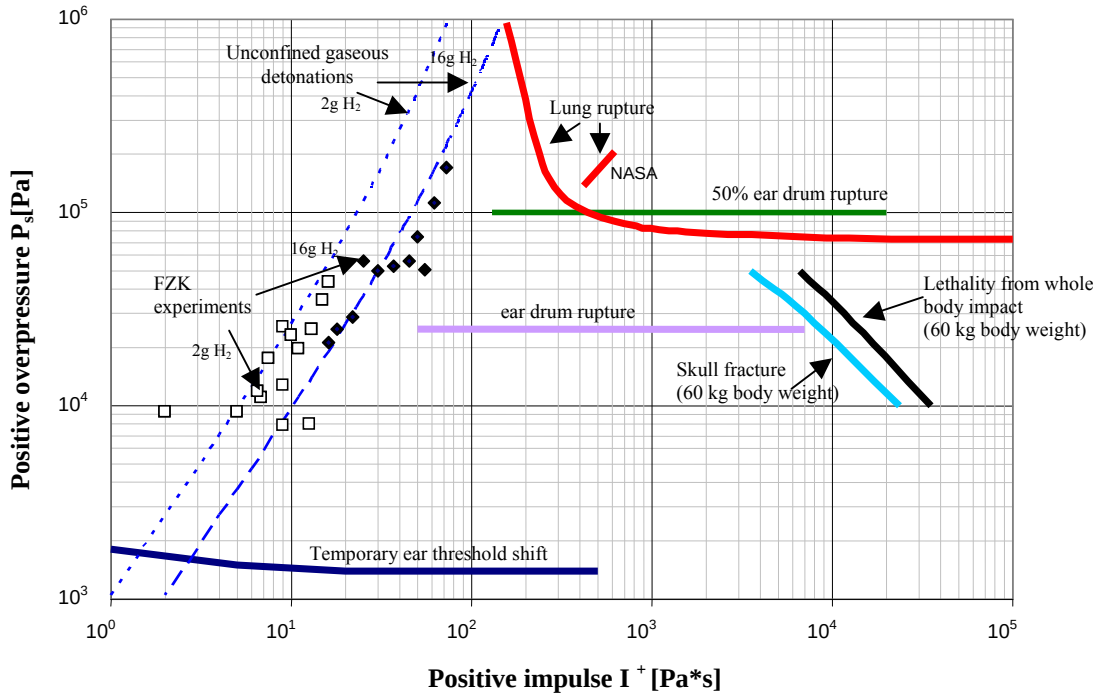

Fig. 3-49: Threshold data, from [Baker 1983, NASA 1997], and gaseous detonation data, from [Dorofeev 1995]

However, as impulse and pressure are correlated, the coordinates pressure and pulse duration provide a clearer and decoupled view. The transformed data are given in Figure 3-50.

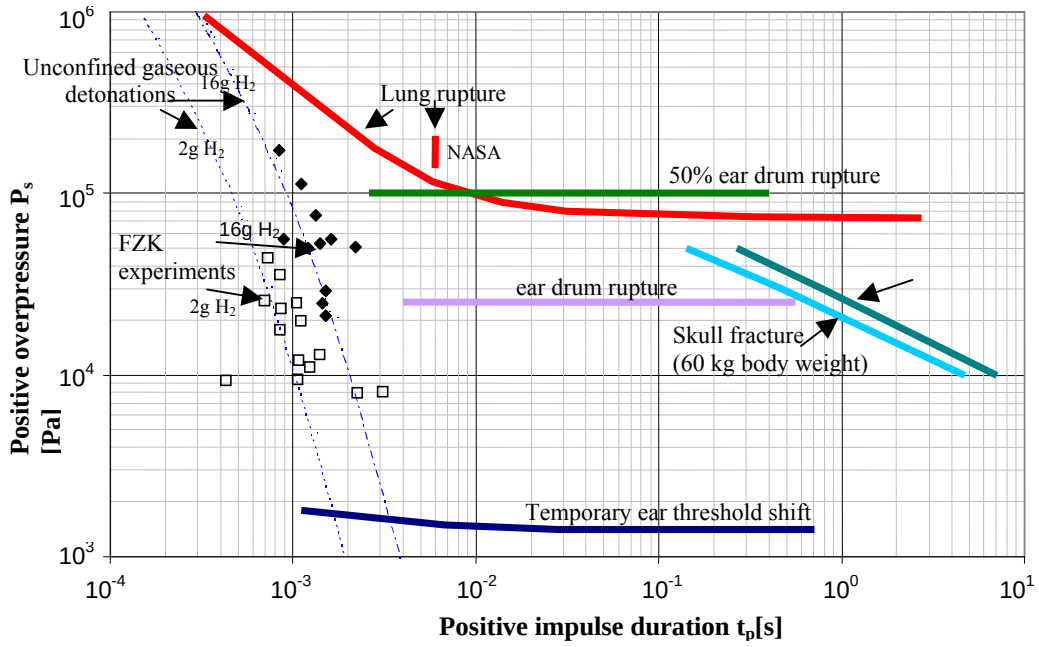

Fig. 3-50: Threshold data converted to pressure over impulse duration

Not only for the general mixing and detonation initiation but also for the physiological effects the spatial confinement is a very important factor. Generally one has to expect an increased immediate and late mortality in closed space blast scenarios compared to open-air explosions [Kluger 2003], [Kaiser 2002]. However, usually only little mortality is due to these primary effects compared to the more severe combination of indirect blast effects, like missiles, body translation and associated impact and heat effects.

Indirect Blast Effects

Indirect blast effects include secondary effects, these are generated by missiles (e.g. accelerated parts of the pressure vessel, parts of the building, glass, etc.) and tertiary effects linked to the body translation. Especially the impact, the deceleration when hitting a wall or any other a solid structure, can cause skull fractures with traumatic consequences, even death. With a simplified model the body displacement caused by the blast may be calculated and a lethality threshold may be attributed to the resulting velocities, see [Baker 1983]. See Figures 3-49 and 3-50 with the skull fracture as the representative indirect blast effect.

3.2.4.5 Thermal effects from fires

These effects are also called quaternary effects. Basically there are two phenomena linked with hydrogen fires which could harm human beings: elevated air temperature and heat radiation. Depending on the scenario only one of both or a suitable combination has to be considered.

Elevated Air Temperature Effect

Below 70°C no severe effect has to be expected. Between 70°C and 150°C the time to incapacitation may be 94 minutes and 6 minutes, respectively [TNO 1992]. Fig. 3-51 shows a plot of the empiric dependency.

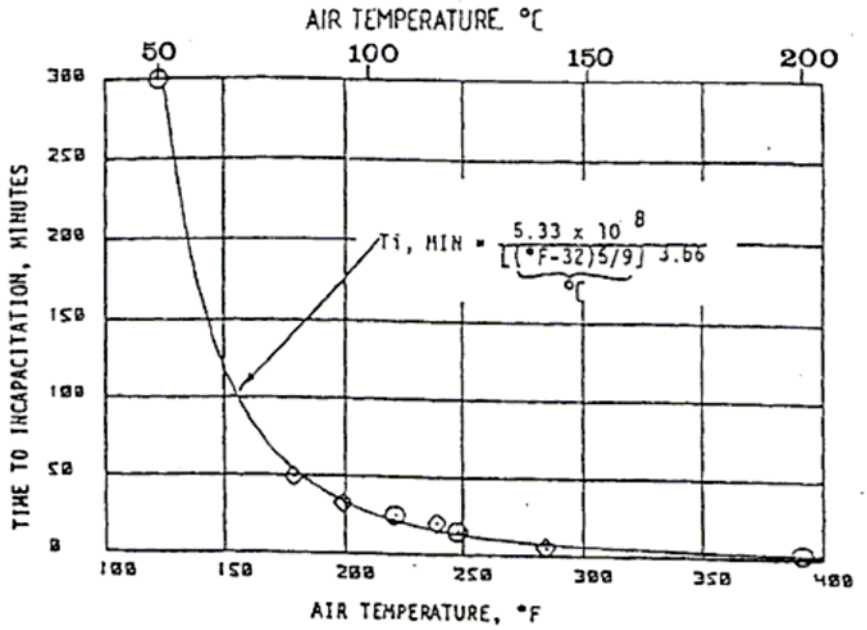

Fig. 3-51: Time to incapacitation as a function of the air temperature [TNO 1992]

Other physiological responses are summarized in the following Table 3-16.

Table 3-16: Elevated air temperature effects

Temperature [°C]	Effects and Symptoms
127	Difficult breathing
140	Tolerance time 5 min
149	Mouth breathing difficult, T limit for escape
160	Rapid, unbearable pain with dry skin
182	Irreversible injury in 30 s
203	Respiratory systems tolerance time less than 4 min with wet skin

Above 150°C, radiation effects become the dominant factor.

Heat Radiation Effect

Heat radiation may cause pain, first, second and third degree burns as well as fatal burns. The different burn types are characterized by the depth they reach in the skin. Similar as for the pressure effects a combination of the peak load, here radiation intensity, and the characteristic duration are the most important factors. Above 1.6 kW/m^2 negative effects on human beings have to be expected. The following Table 3-17 relates exposure times and pain thresholds.

Table 3-17: Threshold of pain, from [Kaiser 2002]

Exposure time [s]	Radiation Intensity [kW/m^2] (lightly clothed)
60	1.7
40	2.3
30	2.9
16	4.7
9	6.9
6	9.5
4	11.7
2	19.9

The fatality rate may be calculated by use of probit functions. Prominent probit functions are the Eisenberg functions and the TNO functions. The first is based on nuclear radiation, the second on the radiation of hydrocarbon fires. So, both are not directly applicable to hydrogen fires.

The following Table 3-18 based on the TNO probit function relates the exposure time and the radiation intensity for 100 % fatality:

Table 3-18: Maximum radiation exposure time [DNV 2001]

Exposure time leading to death	Radiation intensity [kW/m^2] (lightly clothed)	Radiation intensity [kW/m^2] (protectively clothed)
2 min … 10 min	2	4
1 min … 2 min	4	8
0.5 min … 1 min	10	13
< 0.5 min	16	25

Besides the infrared content hydrogen combustion produces UV radiation capable of sunburn-like effects. Hydrogen fires are difficult to see at daylight and due to the optical properties, the heat of smaller flames is felt late.

3.2.4.6 Personal Protective Equipment [ISO 2004]

Using the appropriate protective equipment can reduce the possible consequences of the above described hazards. The concerned personnel should be protected against exposure to cryogenic temperatures, high temperatures, thermal radiation from a hydrogen flame, and oxygen-deficient atmospheres.
Procedures that are established for operations involving hydrogen should describe the personal protective equipment (PPE) that is needed for the operations to be performed. Some general guidelines for PPE that should be considered beneficial in working with hydrogen are summarized below. These guidelines do not address PPE that should be considered when involved in other activities such as working on electrical circuits or performing a cleaning or decontamination operation.
Some specific recommendations for PPE are:

- Eye protection or better complete face shield should be worn when liquid hydrogen is handled,
- Properly insulated gloves should be worn when handling anything that comes in contact with liquid hydrogen or cold gaseous hydrogen. The gloves should fit loosely, remove easily, and not have large cuffs.
- Full-length trousers, preferably without cuffs, should be worn with the legs kept on the outside of boots or work shoes.
- Closed-toe shoes should be worn (open or porous shoes should not be worn).
- Clothing made of ordinary cotton or flame-retardant cotton should be worn. Avoid wearing clothing made of nylon or other synthetics, silk or wool because these materials can produce static electricity charges that can ignite flammable mixtures. Synthetics can melt and stick to the flesh, causing greater burn damage. Any clothing sprayed or splashed with hydrogen should be removed until they are completely free of hydrogen.
- Self-contained breathing equipment should be worn when working in a confined space that may have an oxygen-deficient atmosphere.
- Portable hydrogen- and fire-detection equipment should be used to warn of hydrogen leaks and fires.
- Alternatively it is often recommended to wave with a broom in front of oneself or to pluck some grass and throw it in the direction of the intended movement. If the broom or the grass comes in contact with the barely visible flame, the smoke indicates the flame position.
- Personnel should ground themselves before touching or using a tool on a hydrogen system.
- The use of spark-proof tools is often recommended; however, the energy required for ignition of a flammable hydrogen/air mixture is so small that even spark-proof tools can cause an ignition. Consequently, all tools should be used with caution to prevent slipping, glancing blows or dropping, all of which can cause sparks.
- Water sprays and wet clothes may reduce the thermal effects induced by hydrogen flames considerably.

The immediate treatment of persons which came in contact with liquid hydrogen or have been exposed to the very cold gases is to loosen any clothing that may restrict blood circulation and seek immediate hospital attention for all but the most superficial injuries. Do not apply direct heat to the affected parts, but if possible place in lukewarm water. Sterile dry dressings should be used to protect damaged tissues from infection or further injury, but they should not be allowed to restrict the blood circulation. Alcohol and cigarettes should not be given.

3.2.5. Effect on the Environment

One major claim for the introduction of hydrogen based technologies is the promising environmental benefits of such technologies. Hydrogen is considered a clean fuel capable to avoid the greenhouse effect caused by carbon dioxide releases using fossil fuels. A supporting argument is as follows: Hydrogen may be produced by water electrolysis and under usage it is oxidized back to water without producing any pollutants. However, this is to a certain extent an idealistic view as the major amount of hydrogen is currently produced based on fossil fuels, though in the future hydrogen to a much higher degree may be produced using sustainable energy sources as e.g. wind or water power. The environmentally friendly production of hydrogen depends therefore strongly on the technology applied. The usage of fossil fuels like natural gas conversion to produce hydrogen (see chapter 2.2) may result in an increase of greenhouse gas emissions and other pollutants compared with the present situation. More fossil fuels are needed to produce enough “hydrogen energy” for the customers. A solution to avoid such pollution could be technologies of carbon sequestration and other cleaning measures to

capture the pollutants to be considered for the specific fuel used, which also would favor central, large-scale hydrogen production and distribution facilities.

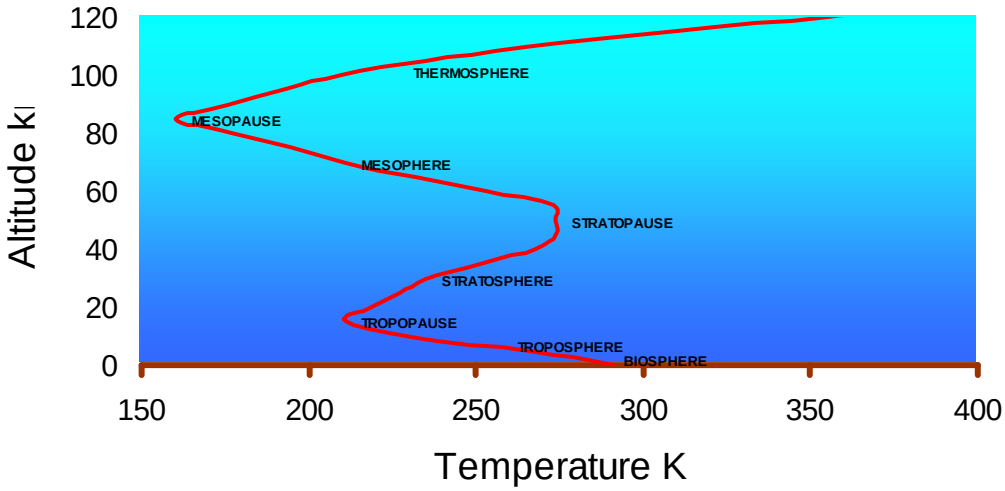

Fig. 3-52: Definition of the atmosphere based on the average temperature profile, from [Heicklen 1976]

Hydrogen is a permanent gas and any diffusive, targeted or accidental release will emit predominantly into the atmosphere. Presently, the major sources for hydrogen emissions are biomass burning, e.g., forest fires, emissions from the traffic using ICE's. It is also produced by photochemical atmospheric reactions of formaldehyde. It is resulting, e.g., from methane oxidation cycle in the atmosphere as shown in the following reaction equations where one photolysis path for formaldehyde (CH_2O) is generating hydrogen.

$$CH_4 + OH\cdot \xrightarrow{-H_2O} CH_3\cdot$$
$$CH_3\cdot \xrightarrow{+O_2,M} CH_3O_2\cdot$$
$$CH_3O_2\cdot \xrightarrow{+NO,-NO_2} CH_3O\cdot \xrightarrow{+O_2,-HO_2\cdot} CH_2O$$
$$CH_2O \xrightarrow{h\nu} CO + H_2$$

The hydrogen content of the atmosphere is compared to other atmospheric gases in Table 3-19 and is found to be on the trace gas level. The atmosphere is divided into different spheres as shown in Fig. 3-52 based on an average temperature profile, which is very important concerning the gas exchange between these spheres.

The hydrogen concentration profile with altitude is found constant at a level of about 0.5 ppm in the troposphere and stratosphere as shown in Table 3-20. Only in the very high atmosphere, there is an increase of hydrogen.

Hydrogen is the only gas capable to escape into space, but it is found that nearly 100 % of the hydrogen is degraded by the photochemical atmospheric processes or deposited back to the biosphere. The atmospheric degradation accounts for about 25 %, while the dry deposition is about 73 %[1] (Schultz 2004b). Therefore the biological processes to degrade hydrogen are very

[1] The current hydrogen releases are estimated as follows: 40 million tonnes/year from methane, VOC releases and their photochemical degradation, 16 million t/yr from biomass burning, 15 million t/yr from

important for its overall atmospheric balance. These processes are not well understood presently as, e.g., the capacity for hydrogen degradation is unknown. The biosphere could be acting as a large buffer keeping the atmospheric hydrogen concentration constant even though the releases are increased due to the activities from a hydrogen economy.

Table 3-19: Average relative composition of the troposphere at mid latitudes, [Heicklen 1976]

Gas	**Concentration** [ppm]
Nitrogen, N_2	780840
Oxygen, O_2	209460
Argon, Ar	9340
Carbon dioxide, CO_2	325
Sum of nobel gases (He, Ne, Kr, Xe)	24.6
Methane, CH_4	1.4
Hydrogen, H_2	0.5
Nitrous oxide, N_2O	0.25
Carbon monoxide, CO	0.08
Ozone, O_3	0.025
Nitroxides, NO+NO_2	0.006

Table 3-20: Average relative hydrogen concentration in different altitudes,[Heicklen 1976]

Altitude [km]	**Hydrogen [ppm]**
0	0.5
20	0.5
40	0.5
60	0.5
80	4.3
100	1.0

Recently some concerns on possible adverse environmental effects caused by large increased atmospheric hydrogen concentrations have been described in the literature. [Logan 1981; Schultz 2003; Tromp 2003; Prather 2003; Schultz 2004a; Wennberg 1998)]. In the following the present knowledge is presented.

Hydrogen is not a greenhouse gas, as it does not absorb electromagnetic radiation within the infrared spectrum. Therefore higher atmospheric hydrogen concentrations will not directly contribute to the climate forcing. The consumption of hydrogen will result in water regardless its usage in fuel cells, being burned under controlled or uncontrolled conditions like under accidental fires or explosions. The water will be released into the troposphere with its normally huge content of water. So the additional water will not raise considerably the overall content of water vapor in the troposphere. An adverse effect is identified when hydrogen is atmospherically degraded in the lower stratosphere, where the persistent ice (from the water) may have a cooling effect that again influences the temperature dependent ozone depletion mechanism.

This has a direct effect on the above mentioned possible cooling effect for the lower stratosphere, as it has been predicted through model calculations. It has been shown [Tromp

traffic and industries, and 6 million t/yr from soils and ocean. The sinks for hydrogen are: 19 million t/yr degraded by reaction with OH free radicals, and 56 million t/yr soil uptake. The numbers are uncertain and are estimated to be within ± 10 million t/yr for traffic and industry emissions and ± 15 million t/yr for soil deposition.

2003] that, e.g., a fourfold increase of atmospheric hydrogen will have considerable effects on the ozone depletion. For atmospheric photochemical degradation of hydrogen, the initiating and rate determining step is by an OH free radical reaction with hydrogen.

$$H_2 + OH\cdot \rightarrow H\cdot + H_2O$$
$$H\cdot + O_2 \xrightarrow{M} HO_2\cdot$$

For atmospheric photochemical degradation of carbon monoxide or other hydrocarbons, the initiating and rate determining step is by an OH free radical reaction with the CO or the hydrocarbon leading to stable products and other free radicals. The later (blue coloured equations) are reacting with other atmospheric components e.g. NO to give ozone and to regenerate OH free radicals in chemical and photolytic reaction steps. By that the atmosphere contains a stable OH concentration of about 10^6 molecules per cm^3 that is sufficient to remove pollutants.

$$CO + OH\cdot \xrightarrow{O_2} HO_2\cdot + CO_2$$

$$NO + HO_2\cdot \longrightarrow OH\cdot + NO_2$$
$$NO_2 \xrightarrow{h\nu} NO + O(^3P)$$
$$O(^3P) + O_2 \xrightarrow{M} O_3$$
$$O_3 \xrightarrow{h\nu} O_2 + O(^1S)$$
$$O(^1S) + H_2O \rightarrow 2OH\cdot$$

The emissions of hydrocarbons and nitrogen oxides lead to the generation of ozone. While this is a very important protection against short wave ultraviolet radiation in the stratosphere, ozone is to be considered a pollutant in the troposphere. It is part of the effects that lead to “forest dead” by acid rain as ozone destroys the protecting wax layer on leaves, and it has adverse health effects to people. In summertime, dangerous ozone levels can build up leading to restrictions for traffic, e.g., in Germany to mitigate high ozone levels. Therefore the establishment of the hydrogen economy will improve the air quality in the cities as the hydrocarbon and nitrogen oxide emissions are reduced. On the other hand nitrogen oxide is an important intermediate for the generation of the constant background concentration of OH free radicals. Model calculations have shown that the OH concentration is slightly decreasing when the nitrogen oxide concentration is substantially decreased. By that the oxidative capacity of the atmosphere is slightly reduced that would give a bit longer lifetime for e.g. the green house gas methane thus supporting the climate forcing effect [Schultz 2003]. On the other hand, the emission of carbon dioxide will be reduced avoiding climate forcing.

Nevertheless, less environmental pollution using hydrogen is only to be achieved using sustainable primary energy sources for hydrogen production. Using fossil fuels without carbon dioxide sequestration will result in total in even more pollutant emissions. Therefore the overall environmental benefits need to be assessed using live cycle assessments for the larger-scale production systems.

Conclusions

The environmental problems with hydrogen are connected with a strong increase of the emissions into the atmosphere. Most of the hydrogen is degraded in the biosphere. More precise knowledge on the mechanisms and capacities are needed to make better model calculations on the possible increase of hydrogen due to the new technologies based on hydrogen and fuel cells.

At the moment, a precaution may be to reduce the emissions as much as possible, which is not only related to the environment, but also to safety, as hydrogen fires and gas phase explosions are very prominent concerns for hydrogen applications. There may also be some economic benefits as production, distribution and storage of hydrogen need substantial amounts of energy making the hydrogen rather costly, but more detailed analyses are needed here. Therefore it would be a win-win situation to minimize leakages.

References and sources

Baek S.W., et.al., Effects of Addition of Solid Particles on Thermal Characteristics in Hydrogen-Air Flame, Combustion, Science and Technology, 174 (2002) 99-116.

Baker W.E., et.al., Explosion Hazards and Evaluation, Fundamental Studies in Engineering 5, Elsevier (1983).

Baum M.R., Failure of a Horizontal Pressure Vessel Containing a High Temperature Liquid : The Velocity of End-Cap and Rocket Missiles, J. Loss Prevention in the Process Industries 12 (1999) 137-145.

Barlow R.S., et.al, Effect of Damkohler Number on Superequilibrium OH Concentration in Turbulent Nonpremixed Jet Flames, Combustion, Science and Technology, 82 (1990) 235-251.

Barlow R.S., et.al., Nitric Oxides Formation in Dilute Hydrogen Jet Flames: Isolation of the Effects of Radiation and Turbulent-Chemistry Submodels, Combustion and Flame 117 (1999) 4-31.

Benteftifa C.A., Becht C., Improve Building Performance to Survive Vapor-Cloud Explosions, Hydrocarbon Processing (1995) 85-90.

Berman M., A Critical Review of Recent Large-Scale Experiments on Hydrogen-Air Detonations, Nucl. Sci. Eng. 93 (1986) 321-347.

Breitung W., Redlinger R., Containment Pressure Loads from Hydrogen Combustion in Unmitigated Severe Accidents, Nuc Tech 111 (1995) 395-419.

Breitung W., Kotchourko A., Numerische Simulation von turbulenten Wasserstoff-Verbrennungen bei schweren Kernreaktorunfaellen, Nachrichten-Forschungszentrum Karlsruhe, 28 (1996) No. 2-3 175-191.

CCPS, Guidelines for Evaluating the Characteristics of Vapour Cloud Explosions, Flash Fires and BLEVE's, Center for Chemical Process Safety, American Institute of Chemical Engineers, New York, USA (1994).

CEN, Gas Explosion Venting Protective Systems, PrEN 14494, European Committee for Standardization, Brussels, Belgium (2004).

Chandrasekhar, S., Radiative Transfer, Oxford University Press, Oxford, UK (1950).

Chelin P., Pina V., Investigative Method for Radiative Properties of Water Vapour in the 0.8m Region by Optical Diagnostic of H_2-Air Combustion, Combustion Science and Technology, 174 (2002) 215-229.

Choudhuri A.R., Gollahalli S.R., Intermediate Radical Concentrations in Hydrogen-Natural Gas Blended Fuel Jet Flames', Int. J. Hydrogen Energy, 29 (2004) 1291-1302.

Cox G., On Radiation Heat Transfer from Turbulent Flames, Combustion Science and Technology, 1 (1977) 75-78.

CSChE, Risk Assessment – Recommended Practices for Municipalities and Industry, Canadian Society for Chemical Engineering, Ottawa, Canada (2004).

Cumber P.S., Fairweather M., Evaluation of Participating Media Models for Fire Simulation, Proc. Sixth Int. Symp. on Fire Safety Science, (July 1999, Poitiers, France), Int. Ass. for Fire Safety Science, Boston, USA (1999) 337-348.

Cumber P.S., Ray Effect Mitigation in Jet Fire Radiation Modelling, Int. J. Heat Mass Transfer, 43 (2000) 935-943.

Cumber P.S., Fairweather M., Evaluation of Flame Emission Models Combined with the Discrete Transfer Method for Combustion System Simulation", Int. J. Heat and Mass Transfer, 48 (2005) 5221-5239.

Cumber P.S., Fairweather M., Ledin H.S., Application of Wide Band Radiation Models to Nonhomogeneous Combustion Systems, Int. J. Heat Mass Transfer, 41 (1998) 1573-1584.

De Ris J., Fire Radiation – A Review", Seventeenth Symp. (Int.) on Combustion, Combustion Institute, Pittsburgh, USA (1979) 1003.

DNV, Human Resistance against Thermal Effects, Explosion Effects, Toxic Effects, and Obscuration of Vision, DNV Technica, Scandpower A/S, Det Norske Veritas, Oslo, Norway (2001), (http://www.preventor.no/tol_lim.pdf).

Dorofeev S.B., Blast Effect of Confined and Unconfined Explosions, Proc. 20th Symp. on Shock Waves, Pasadena, USA (1995) 77-86.

Edwards D.K., Balakrishnan A., Thermal Radiation by Combustion Gases, Int. J. Heat Mass Transfer, 16 (1973) 25-40.

Edwards D.K., Molecular Gas Band Radiation, in: Irvine T.F., Hartnett J.P. (Eds.), Advances in Heat Transfer, Vol. 12, Academic Press, New York, USA (1976) 115 -193.

Erdogan F., Delale F., Owczarek J.A., Crack Propagation and Arrest in Pressurized Containers, J. Pressure Vessel Technology, 99 (1977) 90-99.

Faeth G.M., Jeng S.M., Gore J., Radiation from Fires, in: Law C.K., Yuen W.W., Miyasaka K. (Eds.), Heat Transfer in Fire and Combustion Systems, HTD, Vol. 45, ASME, New York, USA (1985) 137-151.

Felske J.D., Tien C.L., Wide Band Characterization of the Total Band Absorptance of Overlapping Infrared Gas Bands, Combustion Science and Technology, 11 (1975) 111-117.

FEMA, Explosive Blast, Chapter 4 in: Reference Manual to Mitigate Potential Terrorist Attacks Against Buildings, Report FEMA426, Federal Emergency Management Agency, Washington D.C., USA (2003).

Fischer M., Kratzel T., Pantow E., Turbulent Combustion and Detonation Processes in Hydrogen-Air Mixtures, Proc. 11th World Hydrogen Energy Conf., Stuttgart, Germany (1996) 2125-2136.

Fishburne E.S., Fergament H.S., The Dynamics and Radiant Intensity of Large Hydrogen Flames, 17th Int. Symp. on Combustion, The Combustion Institute, Pittsburgh, USA (1979) 1063-73.

Fiveland W.A., A Discrete Ordinate Method for Predicting Radiative Heat Transfer in Axisymmetric Enclosures", ASME Paper No. 82-HT-20 (1982).

Fiveland W.A., Discrete Ordinates Solutions of Radiation Transport Equation of Rectangular Enclosures", ASME Journal of Heat Transfer, 106 (1984) 699-706.

GEXCON, Gas Explosion Handbook, (http://www.gexcon.com/index.php?src=gas/handbook.html).

Giesbrecht H., et.al., Analyse der potentiellen Explosionswirkung von kurzzeitig in die Atmosphaere freigesetzten Brenngasmengen, Teil 1, Chemie-Ingenieur-Technik 52 (1980) No.2 114-122.

Giesbrecht H., et.al., Analyse der potentiellen Explosionswirkung von kurzzeitig in die Atmosphaere freigesetzten Brenngasmengen, Teil 2, Chemie-Ingenieur-Technik 53 (1981) No.1 1-10.

Giesbrecht H., Evaluation of Vapour Cloud Explosions by Damage Analysis, J. Haz. Mat. 17 (1988) 247-257.

Goody R.M., Atmospheric Radiation I: Theoretical Basis, Claredon Press, Oxford, UK (1964).

Gore J.P., Jeng S.M., Faith G.M., Spectral and Total Radiative Properties in Hydrogen/Air Diffusion Flames, J. Heat Transfer, 109 (1987) 165-171.

Gosman A.D., Lockwood F.C., Incorporation of a Flux Model for Radiation into a Finite-Difference Procedure for Furnace Calculations, 14th Int. Symp. on Combustion, The Combustion Institute, Pittsburgh, USA (1973) 661-671.

Gottuck D.T., White D.A., Liquid Fuel Fires, SFPE Handbook of Fire Protection Engineering, 3rd Edition, NFPA, Quincy, USA (2002) Section 2, Ch.15, 2-297 - 2-316.

Grosshandler W.L, Radiative Heat Transfer in Nonhomogeneous Gases: A Simplified Approach, Int. J. Heat Mass Transfer, 23 (1980) 1447-1459.

Grosshandler W.L., Modak A.T., Radiation from Nonhomogeneous Combustion Products, 18th Int. Symp. on Combustion, The Combustion Institute, Pittsburgh, USA (1981) 601-609.

Gurson A.L., Continuum Theory of Ductile Rupture by Void Nucleation and Growth, J. Eng. Mat. Technol., 123 (1977) 203-209.

Hauptmanns U., A Procedure for Analyzing the Flight of Missiles from Explosions of Cylindrical Vessels. J. Loss Prevention in the Process Industries, 14 (2001) 395-402.

Heicklen, J. Atmospheric Chemistry. Academic Press, London, UK (1976).

Hottel H.C., Cohen E.S., Radiant Heat Exchange in a Gas Filled Enclosure: Allowance for Non-Uniformity of Gas Temperature, AIChE Journal, 4 (1958) No 1.

Hottel H.C., Sarofim A.F., Radiative Heat Transfer, McGraw-Hill New York, USA (1967).

Howell J.R., Permutter M., Monte-Carlo Solution of Thermal Transfer through Radiant Media between Gray Walls, J. Heat Transfer, Trans ASME, 86 (1964) 116.

IAEA, Hydrogen in Water-Cooled Nuclear Power Reactors, International Atomic Energy Agency, Vienna, Austria, and Commission of the European Communities, Brussels, Belgium (1990).

Iibas M., The Effect of Thermal Radiation and Radiation Models on Hydrogen-Hydrocarbon Combustion Modelling, Int. J. Hydrogen Energy, 30 (2005) 1113-1126.

INERIS, Formalisation du Savoir et des Outils dans le Domaine des Risques Accidentels (DRA-35),Version Projet, Les éclatements de reservoirs, L'Institut National de l'Environnement Industriel et des Risques, Verneuil-en-Halatte, France (2004).

ISO, Basic Considerations for the Safety of Hydrogen Systems, Technical Report ISO/TR 15916:2004(E), International Organization of Standardization, Geneve, Switzerland (2004).

Itoh S., et.al., Spatially Resolved Elemental Analysis of a Hydrogen-Air Diffusion Flame by Laser-Induced Plasma Spectroscopy (LIPS), Microchemical Journal, 70 (2001) 143-152.

Kaiser W., et.al., Ermittlung und Berechnung von Stoerfallaublaufszenarien nach Massgabe der 3. Stoerfallverwaltungsvorschrift, Umweltbundesamt, Berlin, Germany (2002), (http://www.umweltbundesamt.de/anlagen/Leitfaden.pdf).

Kim S. H., et.al., The Effect of Flame Radiation on the Scaling of Nitrogen Oxide Emission in Turbulent Hydrogen Non-Premixed Flames, Proceedings of Combustion Institute, 29 (2002) 1951-1956.

Kluger, Y., Bomb Explosions in Acts of Terrorism, Israeli Medical Association, IMAJ 5 (2003) 235-240.

Koopman R.P., et.al., Analysis of BURRO Series 40 m^3 LNG Spill Experiments, J. Hazardous Materials, 6 (1982) 43-83.

Kumar S., Cox G., Radiation, Convection and Surface Roughness Effects in the Numerical Modelling of Enclosure Fires, Proc. 2nd Int. Symp. on Fire Safety Science, (June 1988, Tokyo, Japan), Hemisphere Publishers, Washington D.C., USA (1989) 851-860.

Kumar S., Gupta A.K., Cox G., Effect of Thermal Radiation on the Fluid Dynamics of Compartment Fires, Proc. 3rd Int. Symp. on Fire Safety Science, (July 1991, Edingburgh, UK), Elsevier Applied Science, London, UK (1991) 345-354.

Kusharin A.Y., et.al., Initiation of Premixed Flames in H_2-Air-H_2O Mixtures, Experimental Thermal and Fluid Sciences, 21 (2000) 2-8.

Langberg H., Christensen S.O., Skudal S., Test Program with Small Concrete "Kasun" Houses, Forsvarsbygg, FoU Rapport Nr. 24/2004, Kristiansand, Norway (2004).

Lathrop K.D., Ray Effects in Discrete Ordinates Equations, Nucl. Sci. Eng., 32 (1968) 357; ibid, 45 (1971) 255.

Leslie I.R.M., Birk A.M., State of the Art Review of Pressure Liquefied Gas Container Failure Modes and Associated Projectile Hazards. J. Hazardous Materials, 28 (1991) 329-365.

Lewis E.E., Miller Jr. W.F., Computational Methods of Neutron Transport, Wiley, New York, USA (1984).

Li Q.M., Meng H., Pressure-Impulse Diagram for Blast Loads Based on Dimensional Analysis and Single-Degree-of-Freedom Model, J. Eng. Mechanics, 128 (2002) 87-92.

Lind C.D., What Causes Unconfined Vapor Cloud Explosions, Loss Prevention, 9 (1975) 101-105.

Liu L.H., et.al., Fluctuating Characteristics of Radiative Source Term in Hydrogen Turbulent Jet Diffusion Flame", J. Quantitative Spectroscopy & Radiative Transfer, 87 (2004) 193-201.

Lockwood F.C., Shah N.G., Heat Transfer, Vol. 2, Hemisphere Publishing Corporation, Washington D.C., USA (1978) 33-40.

Lockwood F.C., Shah N.G., A New Radiation Solution Method for Incorporation in General Combustion Prediction Procedures, 18th Int. Symp. on Combustion, The Combustion Institute, Pittsburgh, USA (1981) 1405-1414.

Logan J.A., Tropospheric Chemistry: A Global Perspective, J. Geophysical Research, 86 (1981) 7210-7254.

Ludwig C.B., et.al., Handbook of Radiation from Combustion Gases, Report NASA SP-3080, Washington D.C., USA (1973).

Maurer B., et.al., Modellversuche zur Flash-Entspannung, atmosphaerischer Vermischung und Deflagration von Fluessiggasen nach deren Freisetzung bei Behaelterzerknall, Int. Sem. ELCALAP, Berlin, Germany (1975).

Maurer B., et.al., Modelling of Vapour Cloud Dispersion and Deflagration after Bursting of Tanks Filled with Liquified Gas, 2nd Int. Symp. on Loss Prevention and Safety Promotion in the Process Industries (1977).

MEDD, Guide de Sécurité pour la Conception de Salles de Contrôle Résistant à l'Explosion dans les Raffineries de Pétrole et sur les Sites Pétrochimiques, Ministère de l'Ecologie et du Développement Durable, Paris, France (1994).

MEDD, Durable Relatif aux Valeurs de Référence de Seuils d'Effets des Phénomènes Accidentels des Installations Classées, Arrêté du 22 Octobre 2004 du Ministère de l'Ecologie et du Développement Durable, Paris, France (2004).

Mercx W.P.M., Weerheijm J., Verhagen T.L.A., Some Considerations on the Damage Criteria and Safety Distances for Industrial Explosions, HAZARDS XI – New Directions in Process Safety, UMIST, Manchester, UK, April 16-18, 1991.

Mercx W.P.M. (Ed.), Modelling and Experimental Research into Gas Explosions, Overall Final Report of the Project MERGE, CEC Contract STEP-CT-0111 (SSMA), European Commission, Directorate General XII, Brussels, Belgium (1994).

Mercx W.P.M. (Ed.), Extended Modelling and Experimental Research into Gas Explosions, Final Summary Report of the Project EMERGE, CEC Contract EV5VCT930274, European Commission, Directorate General XII, Brussels, Belgium (1997).

Mercx W.P.M., et.al., Developments in Vapour Cloud Explosion Blast Modeling, J. Hazardous Materials, 71 (2000) 301-319.

Modest M. F., The Weighted-Sum-of-Gray-Gases Model for Arbitrary Solution Methods in Radiative Transfer, J. Heat Transfer, 113 (1991) 650-656.

Moen I.O., Transition to Detonation in Fuel-Air Explosive Clouds, J. Hazardous Materials, 33 (1993) 159-192.

Molkov V.V., Makarov D.V., Schneider H., Hydrogen Air Deflagrations in Open Atmosphere: Large Eddy Simulation Analysis of Experimental Data, Int. Conf. on Hydrogen Safety (ICHS), Pisa, Italy (2005).

Mott N.F., Fragmentation of H.E. Shells, A Theoretical Formula for the Distribution of Weight of Fragments, A.O.R.G. Memorandum, Army Operational Research Group, Richmond, UK (1943).

Mudan K.S., Thermal Radiation Hazards from Hydrocarbon Pool Fires, Prog. Energy Combus. Sci., 10 (1984) 59-80.

MVROM, Methods for the calculations of physical effects. Publicatiereeks Gevaarlijke Stoffen 2 (PGS 02)., Ministerie van Volkshuisvesting, Ruimtelijke Ordening en Milieubeheer, Den Haag, The Netherlands (2005).

NASA, Safety Standard for Hydrogen and Hydrogen Systems NSS 1740.16, National Aeronautics and Space Administration, Washington D.C., USA (1997).

NFPA 68, National Fire Codes, Guide for Venting of Deflagrations, National Fire Protection Association, Quincy, USA (2002).

Pandey A.K., et.al., Non-Linear Response of Reinforced Concrete Containment Structure under Blast Loading, Nucl. Eng. Des., 236 (2006) 993-1002.

Pfoertner H., Gas Cloud Explosions and Resulting Blast Effects, Int. Seminar on Extreme Load Conditions and Limit Analysis Procedures for Structural Reactor Safeguards and Containment Structures, Berlin, Germany (1975).

Pfoertner H., et.al., Flame Acceleration and Pressure Build Up in Free and Partially Confined Hydrogen Air Clouds. 9th ICDERS, Poitiers, France (1983a).

Pfoertner H., Schneider H., Ballonversuche zur Untersuchung der Deflagration von Wasserstoff Luft Gemischen (Abschlussbericht). PNP-Sicherheitssofortprogramm: “Prozessgasfreisetzung - Explosion in der Gasfabrik und Auswirkungen von Druckwellen auf das Containment”, ICT Internal Report, Fraunhofer Institut für Chemische Technologie, Pfinztal, Germany (1983b).

Pfoertner H., The Effects of Gas Explosions in Free and Partially Confined Fuel/Air Mixtures, Propellants, Explosives, Pyrotechnics, 10 (1985) No.5 151-155.

Prather M. J., An Environmental Experiment with H_2?, Science, 302 (2003) 581-582.

Sanai M., Computer Simulation of Explosion of a Hydrogen Storage Tank, Proc. 11th World Hydrogen Energy Conf., Stuttgart, Germany (1996) 2149-2158.

Schneider H., Pfoertner H., Flammen- und Druckwellenausbreitung bei der Deflagration von Wasserstoff Luft Gemischen. PNP-Sicherheitssofortprogramm: "Prozessgasfreisetzung - Explosion in der Gasfabrik und Auswirkungen von Druckwellen auf das Containment", Jahrestagung des Fraunhofer Instituts für Treib- und Explosivstoffe, Karlsruhe, Germany (1978).

Schneider H., Pfoertner H., Explosion von Wasserstoff Luft Gemischen unter teilverdaemmten Bedingungen und unter dem Einfluss einer turbulenten Stroemung, PNP-Sicherheitssofortprogramm: "Prozessgasfreisetzung - Explosion in der Gasfabrik und Auswirkungen von Druckwellen auf das Containment", ICT Internal Report, Fraunhofer Institut für Chemische Technologie, Pfinztal, Germany (1984a).

Schneider H., Pfoertner, H., Versuche zur Freistrahlzuendung partiell verdaemmter Wasserstoff Luft Gemische im Hinblick auf die Skalierbarkeit des Uebergangs Deflagration Detonation, Final Report for Firma Interatom, Bergisch-Gladbach, ICT Internal Report, Fraunhofer Institut für Chemische Technologie, Pfinztal, Germany (1984b).

Schneider H., Large Scale Experiments: Deflagration and Deflagration to Detonation Transition within a Partial Confinement Similar to a Lane, Int. Conf. on Hydrogen Safety (ICHS), Pisa, Italy (2005).

Shah N.G., Radiation Heat Transfer, PhD Thesis, Imperial College, London, UK (1979).

Schultz M.G., Air pollution and Climate-Forcing Impacts of a Global Hydrogen Economy, Science, 302 (2003) 624-627.

Schultz, M.G., et al., Ozone and Climate Impacts of a Global Hydrogen Economy, Poster at the Quadrennial Ozone Symposium 2004, Kos, Greece (2004a).

Schultz M.G., Markert F., Pilegaard K., Hydrogen and the Environment, Larsen H., Feidenhans'l R., Pedersen L. S. (Ed.), Hydrogen and its Competitors (3), 58-62, 2004. Risø Energy Report, Roskilde, Risø National Laboratory (2004b).

Siegel R., Howell H.R., Thermal Radiation Heat Transfer, McGraw-Hill, New York, USA (1981).

Sparrow E.M., Cess R.D., Radiation Heat Transfer; McGraw-Hill, New York, USA (1978).

Tang M.J., Baker Q.A., A New Set of Blast Curves from Vapor Cloud Explosion, Process Safety Progress, 18 (1999) No. 3, 235-240.

Tien C.L., in: Handbook of Heat Transfer Fundamentals, McGraw-Hill, New York, USA (1985).

Tien C.L., Lee S.C., Flame Radiation, Progress in Energy and Combustion Science, 8 (1982) 41-59.

Tieszen S.R., Effect of Initial Conditions on Combustion Generated Loads, Nucl. Eng. Des., 140 (1993) 81-94.

TNO Green Book, Methods for the Determination of Possible Damage to People and Objects Resulting from Releases of Hazardous Materials, Report CPR 16E, Voorburg, The Netherlands (1992).

Tromp T.K., et al., Potential Environmental Impact of a Hydrogen Economy on the Stratosphere, Science, 300 (2003) 1740-1742.

Truelove J.S., A Mixed Gray Gas Model for Flame Radiation, Report AERE-R8494, UKAEA Harwell, UK (1976).

UFIP, Guide Méthodologique UFIP pour la Réalisation des Études de Dangers en Raffineries, Stockages et Dépôts de Produits Liquides et Liquéfiés, L'Universite de Formation Inter-professionnelle, Saint Laurent du Var, France (2002).

USACE, Structures to Resist Accidental Explosions, TM5-1300, US Army Corps of Engineers, Hyattsville, USA (1990).

Van den Berg A.C., Eggen J.B.M., GAME-Guidance for the Application of the Multi-Energy Method, 2nd Int. Specialist Meeting on Fuel Air Explosions, held at Bergen, Norway, June 27-28, 1996.

Van den Berg A.C., Versloot N.H.A., The Multi-Energy Critical Separation Distance, J. Loss Prevention in the Process Industries, 16 (2003) 111-120.

Van den Berg A.C., et.al., Expansion-Controlled Evaporation: A Safe Approach to BLEVE Blast, J. Loss Prevention in the Process Industries, 17 (2004) 397-405.

Van den Berg A.C., et.al., BLEVE Blast by Expansion-Controlled Evaporation, Process Safety Progress, 25 (2005) No. 1.

Van der Voort M.M., et.al., Analysis of the Sci Pan 3 Debris Throw Data Using the Klotz Group Approach, Presented at the 32th Explosives Safety Seminar, held at Philadelphia, August 22-24, 2006, Department of Defense Explosives Safety Board (2006).

Van Doormaal J.C.A.M., et.al., Design of KG-Engineering Tool for Debris Throw Prediction. TNO Report TNO-DV2 2005 C112, Rijswijk, The Netherlands (2006a).

Van Doormaal J.C.A.M., Weerheijm J., Klotz Group Engineering Tool for Debris Launch Prediction, Presented at the 32th Explosives Safety Seminar, held at Philadelphia, August 22-24, 2006, Department of Defense Explosives Safety Board (2006b).

Van Wingerden K., Detonations in Pipes and in the Open, CMR Internal Report, Christian Michelsen Research, Bergen, Norway (1999).

Viskanta R., Menguc M.P., Radiation Transfer in Combustion Systems", Prog. Energy Combus. Sci., 13 (1987) 97-160.

Wennberg P. O., et al., Hydrogen Radicals, Nitrogen Radicals, and the Production of O3 in the Upper Troposphere, Science, 279 (1998) 49-53.

3.3 MATERIAL CONSIDERATIONS WHEN WORKING WITH HYDROGEN

Contributing author	Main contributions	Organisation	e.mail
Azkarate Peña Iñaki	All	INASMET	*IAzkara@inasmet.es*
Hervé Barthelemy	All	Air Liquide	*Herve.BARTHELEMY @AirLiquide.com*
Karl Verfondern	All	FZJ	

Contributing reviewer	Information reviewed	Organisation	e.mail
Chris Moen	All	Sandia National Laboratories	*cmoen@sandia.gov*
Brian Somerday	All	Sandia National Laboratories	*bpsomer@sandia.gov*
Christopher San Marchi	All	Sandia National Laboratories	*cwsanma@sandia.gov*

3.3.1 Influence of Hydrogen on Materials

All materials deform under load. The stress which a structural material is able to withstand is conditioned by its ductility. Ductility is the ability to deform permanently prior to fracture, and it is measured in terms of percentage elongation at fracture.

Most materials behave linearly under low loads. A material is elastic if, after being elongated under stress, it returns to its original shape as soon as the stress is removed. Elastic deformation is recoverable and involves both a change of shape and a change of volume.

At a certain strain, when the load exceeds the yield load called 'yield stress', the stress strain behaviour becomes non-linear. It departs from linearity meaning that the material will retain a permanent elongation. Behaviour is not reversible, i.e. permanent changes in shape occur, but the volume remains constant. A further increase of the strain eventually reaches the ultimate load called 'ultimate tensile stress' beyond which the stress decreases finally leading to rupture.

Ductile materials can accommodate local stress concentrations, they can be greatly bent and reshaped without breaking, i.e. in a ductile material, the molecular bonds gradually break and re-form. In contrast, brittle materials have only a small amount of elongation at fracture, i.e. in a brittle material, all the molecular bonds break suddenly at a certain stress level. The strength of ductile material is approximately the same in tension and compression, whereas that of brittle material is much higher in compression than it is in tension. Brittle materials do not show significant permanent elongation. They fail suddenly and catastrophically when they are exposed to their tensile stress.

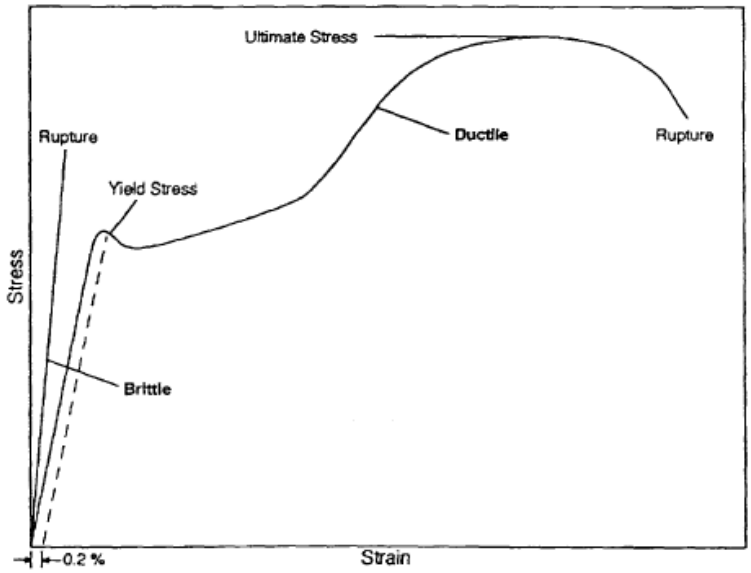

Figure 3-53: Ductile and brittle behaviour (K. Verfondern, 1999 and M. Mohitpuro, C.L. Pierce, P. Graham, 1990)

Hydrogen can have two main effects on materials:

1°- At low temperature for example when it is stored in liquid form it can have an indirect effect called "*cold embrittlement*". This effect is not specific to hydrogen and can occur with all the cryogenic gases if the operating temperature is below the ductile-brittle transition temperature.

Cryogenic temperatures can affect structural materials. With decreasing temperature, there is a decrease in toughness that is very slight in face centred cubic materials, but can be very marked in body centre cubic ones such as ferritic steels. This phenomenon shall be considered for liquid hydrogen storages and associated equipment used at low temperature.

Metals that work successfully at low temperatures include aluminium and its alloys, copper and its alloys, nickel and some of its alloys, as well as stable austenitic stainless steels.

2°- Hydrogen can have a direct effect on the material by degrading its mechanical properties; this effect is called "*hydrogen embrittlement*" and is specific to the action of hydrogen and some other hydrogenated gases.

3.3.1.1 Hydrogen Embrittlement

The effect of hydrogen on material behaviour, on its physical properties, is a fact. Hydrogen may degrade the mechanical behaviour of metallic materials and lead them to failure.

Hydrogen embrittlement affects the three basic systems of any industry that uses hydrogen:

- Production;
- Transport/Storage;
- Use.

In fact, the presence of hydrogen atoms in a solid metal dissolved in the metal grid and accumulated in disturbed lattice regions results in the reduction of its ductility by decreasing the energy of cohesion and consequently in the increase of its probability of brittle fracture.

When tensile stresses are applied to a hydrogen embrittled component, it may fail prematurely in a unexpected and sometimes catastrophic way. An externally applied load is not required as the tensile stresses may be due to residual stresses in the material. The threshold stresses to cause cracking are commonly below the yield stress of the material. Thus, catastrophic failure can occur without significant deformation or obvious deterioration of the component.

This form of cracking, which typically changes from transgranular[2] to intergranular[3] with increasing yield strength and other processing variables and which is maximum around room temperature, is normally referred to as '*Hydrogen Embrittlement Cracking*' (HEC).

This phenomenon is different from the so called "*hydrogen attack*" that can lead to failure of steels at temperature above 473 K, being the result of the reaction of hydrogen with the carbon of the steel forming voids in the metals . In this case the solution is to use low alloy steels with addition of Cr, Mo or other elements able to fix the carbon; the Nelson curves give the pressure and temperature regions at which the different steels can safely be used; but again because it is relevant only at temperature higher than 473 K, this is normally not a concern for most of the hydrogen storage systems.

The reasons that cause the embrittlement of materials are still debated in the scientific community. Hydrogen embrittlement detection seems to be one of the most difficult aspects of the problem. However, it is known that strain, geometry, the medium and also material influence to which extent metal is degraded by hydrogen.

[2] A transgranular fracture progresses across the grains.
[3] An intergranular fracture follows the grain boundaries.

Purity of hydrogen is important. Some impurities can be used for putting off or avoiding the cracking phenomena due to hydrogen, because hydrogen permeability in metals can be diminished by reaction of the surface of the metal to inhibitors.

Phenomena

Embrittlement involves the ingress of hydrogen into a component, an event that can seriously reduce the ductility and load-bearing capacity, and causes cracking and catastrophic brittle failures at stresses below the yield stress of susceptible materials.

It is understood that hydrogen can cause embrittlement when present in a metal or alloy in its atomic form and not as a molecule. Dissolved hydrogen atoms in metals tend to concentrate in defects of the crystal structure (dislocations, grain boundaries …), imposing a barrier to the movement of dislocations, effectively impeding the plastic flow of the material. As a result, the ductility of the metal decreases and the material becomes brittle.

Furthermore, the concentration of hydrogen at grain boundaries, possibly in molecular form, and the potential of formation of hydrates after the reaction of hydrogen with the metal, are additional mechanisms that may lead to embrittlement.

Atomic hydrogen may enter the metal via several mechanisms: via dissolution during welding, while the metal melts locally dissolving hydrogen from water or other contaminants; via electrochemical processes, such as surface treating (electroplating, acid pickling….) or aqueous corrosion, where molecular hydrogen dissociates into atoms that diffuse into the metal; or via chemisorption, resulting from van der Waals forces between a metal surface and hydrogen molecules also resulting in the dissociation of the hydrogen molecules into atoms.

Mechanisms

Several mechanisms have been proposed which might explain at least partially the degradation of metal by hydrogen embrittlement and which might act simultaneously:

- The formation of hydrides can lead to new hydrogen-related phases which may be brittle and also may have a lower density than the pure metal leading to internal stress.
- The hydrogen distribution in a metal under stress is highly non-uniform which can lead to locally increased hydrogen-enhanced plasticity causing local microscopic deformation and eventually a failure.
- The lattice decohesion effect is presumed to cause embrittlement by a decrease in the atomic bonding strength in the presence of hydrogen. A fracture occurs when the stress exceeds the cohesive stress.
- Molecular hydrogen precipitation forming high pressures and compound formation are other mechanisms identified.

The above ideas help understand the observations that whether or not a metal is susceptible to embrittlement by hydrogen or a hydrogen compound, depends on the metal and also its metallurgical history which affect the migration behaviour of hydrogen within the metal.

The embrittlement is strongly connected with locally high hydrogen concentrations which can be caused by stress-enhanced diffusion rates to lattice defects and reaction sites to initiate cracks. Cracks grow when hydrogen concentrations reach a critical level; crack growth stops when the crack has grown through the H2-enriched region or when the stress factor has decreased sufficiently.

Sources of hydrogen and Embrittlement categories

Sources of hydrogen causing embrittlement have been encountered in the fabrication of steel, in processing parts, in welding, in storage or containment of hydrogen gas, and related to hydrogen as a contaminant in the environment that is often a by-product of general corrosion.

Hydrogen entry, the obvious pre-requisite of embrittlement, can be facilitated in a number of ways summarized below:

- By some manufacturing operations such as welding, electroplating, pickling…

  If a material subject to such operations is susceptible to hydrogen embrittlement then, a final baking heat treatment to force out any hydrogen is employed.

- As a by-product of a corrosion reaction such as in circumstances when the hydrogen production reaction results from a cathodic reaction since some of the hydrogen produced may enter the metal in atomic form rather than evolving as a gas into the surrounding environment.

  In this situation, cracking failures can often be thought of as a type of stress corrosion cracking. If the presence of hydrogen sulphide causes entry of hydrogen into the component, the cracking phenomenon is often termed '*Sulphide Stress Cracking*' (SSC).

- The use of cathodic protection for corrosion protection if the process is not properly controlled.

These ways lead to the definition of three different categories of the phenomena:

- Environmental Hydrogen Embrittlement

  Occurs when the material is being subjected to a hydrogen atmosphere, e.g., storage tanks. Absorbed and/or adsorbed hydrogen modifies the mechanical response of the material without necessarily forming a second phase. The effect strongly depends on the stress imposed on the metal. It also maximizes at around room temperature.

- Internal Reversible Hydrogen Embrittlement

  Takes place when hydrogen enters the metal during its processing. It is a phenomenon that may lead to the structural failure of material that never has been exposed to hydrogen before. Internal cracks are initiated showing a discontinuous growth. Not more than 0.1 - 10 ppm hydrogen in the average are involved. The effect is observed in the temperature range between 173 and 373 K and is most severe near room temperature.

- Hydrogen Reaction Embrittlement

  It is a phenomenon in which the hydrogen chemically reacts with a constituent of the metal to form a new microstructural element or phase such as a hydride or to generate gas bubbles -'blistering'-. These reactions usually occur at higher temperatures. They result in the formation of blisters or expansions from which cracks may start to weaken the metal.

Thus, this phenomenon leads to the formation of internal hydrogen blisters or blister-like cracks at internal delaminations or at sites of non-metallic inclusions in low strength materials. These internal cracks may propagate by a process called '*Hydrogen-Induced Cracking*' (HIC) or hydrogen blistering.

This embrittlement category is also responsible for failures in hydrogen-related process plants, a phenomenon known as '*Hydrogen attack'*. Hydrogen attack has been reported in plain carbon steel, low alloy steels and even some stainless steels operating above 473 K. It is one of the major causes of problems in refineries, where hydrogen and hydrocarbon streams are handled under conditions of up to 20 MPa and 773 K. In this context, failure is the result of the formation of intermetallic phases from the host metal and hydrogen dissolved in the metallic matrix via chemisorption and electrochemical reactions, changing the properties of the material, degrading its mechanical properties and forming methane gas that accumulates in the grain boundaries of metallic components leading to failure caused by void growth and assisted by creep.

The case of hydride formation presents a different nature and that of titanium alloys is a typical one. The microstructure of these alloys consists usually of two phases (α and β) with different hydrogen solubilities and diffusivities. Hydrogen enters the alloy via grain boundaries or other easy paths as β phase forming hydrides that precipitate in the α phase. The mechanism of embrittlement is related in these alloys to this localized hydride precipitation.

Materials

Material suitability for hydrogen service should be evaluated carefully before it is used. A material should not be used unless data are available to prove that it is suitable for the planned service conditions. In case of any doubt the material can be subjected to hydrogen embrittlement susceptibility testing (e.g. ISO 11114-4).

According to the information included in the *ISO/TR 15916:2004 Basic considerations for the safety of hydrogen systems /Technical Report* most of the metallic materials present a certain degree of sensitivity to hydrogen embrittlement. However, there are some that can be used without any specific precautions as for example brass and most of the copper alloys or aluminium and its alloys. On the other hand, nickel and high nickel alloys or titanium and its alloys are known to be sensitive to hydrogen embrittlement. For steels the sensitivity may depend on several factors as the exact chemical composition, heat or mechanical treatment, microstructure, impurities and strength. Concerning non-metallic materials, ISO/TR 15916:2004 also provides information as far as the suitability of some selected materials.

Fortunately many materials can be safely used under controlled conditions (e.g. limited stress , absence of stress raisers such as surface defects….).

3.3.2 Knowledge gaps and recent progress

The main knowledge gaps on this matter are concentrated on the reasons that cause the embrittlement of materials. As it was said in the previous subchapter, these reasons are still debated in the scientific community. Currently this phenomenon is not completely understood and hydrogen embrittlement detection, in particular, seems to be one of the most difficult aspects of the problem. Now, a materials test equipment has been developed in Japan within the WE-NET (World Energy NETwork) project to investigate the environmental hydrogen

embrittlement under particular conditions (high pressure hydrogen up to 10MPa, and temperatures between 20-1500K).

Sources used

Dechema A. *Study for the Generation, Inter-Continental Transport, and Use of Hydrogen as a Source of Clean Energy on the Basis of Large-Scale and Cheap Hydro-Electricity*. Final Report on Contract Nº. EN3S-0024-D(B), Deutsche Gesellschaft für Chemisches Apparatewesen. Frankfurt, 1987.

Abm Glossary. *Hydrogen Embrittlement*. Abm Glossary, Corrosion Doctors. Published on the website:

(http://www.corrosion-doctors.org/Forms/embrittlement.htm)

American National Standard. API 941, *Steels for Hydrogen Service at Elevated Temperatures and Pressures in Petroleum Refineries and Petrochemical Plants*. American National Standard ANSI/API, Publ. 941-1990.

Hüsing B., Reib T.. *Perspectives and Limitations of Biological Hydrogen Production* (11th World Hydrogen Energy Conf., Stuttgart, FR6, 1996), T.N. VERIZOGLU,., et al., Hydrogen Energy Progress XI, International Association for Hydrogen Energy. 1996.

Corrosion source. *Hydrogen Embrittlement – Handbook*. Corrosion source. Published on the website: (http://www.corrosionsource.com/handbook/testing/he.htm)

E.Tzimas, C. Filiou, S.D. Peteves, J.B. Veyret. *Hydrogen Storage: State – Of – The – Art and Future Perspective', 2003*. European Commission - Directorate General Joint Research Centre (DG JRC) -Institute for Energy. Petten-The Netherlands, 2003.

(http://www.jrc.nl/publ/P2003-181=EUR20995EN.pdf)

Escuela Superior Técnica de Ingenieros Industriales UPM - Grupo de apoyo: Laboratorio Energético del Hidrógeno. *Confinamiento del hidrógeno*. Fundación Iberdrola - Energía Sostenible.net. Published on the website:

(http://www.energiasostenible.net/materiales_hidrogeno.htm)

Escuela Superior Técnica de Ingenieros Industriales UPM - Grupo de apoyo: Laboratorio Energético del Hidrógeno. *Materiales en la tecnología del hidrógeno*. Fundación Iberdrola - Energía Sostenible.net. Published on the website:

(http://www.energiasostenible.net/materiales_hidrogeno.htm)

F.J. Edeskuty, W.F. Stewart. *Safety in Handling of Cryogenic Fluids*. The International Cryogenics Monograph Series, Plenum Press. New York, 1996.

Faculty of Architecture- The University of Sidney Australia. *5 Material Behaviour and Sections DESC 1004 Building principles*. Faculty of Architecture- The University of Sidney Australia. Published on the website:

(http://www.arch.usyd.edu.au/~mike/Struct01/BPNotesWebFiles/BP0029to37.pdf)

H. Barthélémy. *Compatibility of metallic materials with hydrogen – Review of the present knowledge*. 16th World Hydrogen Energy Conference. Lyon, France, 13-16 June 2006.

ISO/TR 15916:2004 *Basic considerations for the safety of hydrogen systems* /Technical Report. First edition 2004-02-15

K. Kussmaul, P. Deimel, *Materialverhalten in H2-Hochdrucksystemen*, VDI Berichte Nº. 1201, VDI-Verlag, Düsseldorf, 1995.

K. Verfondern. *Hydrogen as an energy carrier and its production by nuclear power (IAEA-TECDOC-1085)*. International Atomic Energy Agency -IAEA-. Vienna, May 1999.

(http://www.iaea.or.at/inis/aws/htgr/fulltext/30027279.pdf)

M. Mohitporu, C.L. Pierce, P. Graham. *Design Basis Developer for H2 Pipeline*. Published in Oil & Gas Journal. 28 May,1990.

M.R. Louthan, M.J. Morgan. Some *Technology Gaps in the Detection and Prediction of Hydrogen-Induced Degradation of Metals and Alloys*. J. Nondestructive Evaluation 15, 1996.

Metallurgical Consultants. *Hydrogen Embrittlement.* Metallurgical Consultants - Engineering Consulting. Published on the website:

(http://www.materialsengineer.com/CA-hydrogen.htm)

National High Magnetic Field Laboratory, University of Florida. *Section3 – Physical / Health Hazards and Protection*. National High Magnetic Field Laboratory, Operated by Florida State University, University of Florida, Los Alamos National Laboratory. Published on the website:

(http://www.magnet.fsu.edu/users/safety/cryogenics/cryogenics3.html)

P. Hoffmann, (Ed.) *Hydrogen & Fuel Cells Letter.*13 January 1998.

Plating Systems and Technologies. *Hydrogen Embrittlement.* Plating Systems and Technologies. Published on the website: (http://www.mechanicalplating.com/hydrogen.htm)

Princeton Plasma Physics Laboratory. *Chapter 3 – Cryogenic Safety*. Published on the website:

(http://www.pppl.gov/eshis/ESHD_MANUAL/Old_ESHD_sections/occh3.pdf)

Spallation Neutron Source. *Cryogenic Safety.* Spallation Neutron Source, January 2004. Published on the website:

(https://www.sns.gov/projectinfo/operations/training/lectures/Good%20information/Cryo_Safety.pdf)

University of Glasgow. *Safety & Environmental Protection Services -Health and Safety Note-Liquid Nitrogen*. University of Glasgow, July 2001. Published on the website:

(http://www.gla.ac.uk/services/seps/01-024.html)

V. Calder. *Ask a Scientist- Chemistry Archive-Hydrogen Holders*. Laboratory of Chicago – Newton BBS, Department of Energy – United States of America. Published on the website:

(http://www.newton.dep.anl.gov/askasci/chem00/chem00094.htm)

5.Topic 2:Yielding. Published on the website:
(https://www3.imperial.ac.uk/pls/portallive/docs/1/10151.PDF)

References

A. Dechema. *Study for the Generation, Inter-Continental Transport, and Use of Hydrogen as a Source of Clean Energy on the Basis of Large-Scale and Cheap Hydro-Electricity.* Final Report on Contract Nº. EN3S-0024-D(B), Deutsche Gesellschaft für Chemisches Apparatewesen. Frankfurt, 1987.

B. Hüsing, T. Reib. *Perspectives and Limitations of Biological Hydrogen Production* (11th World Hydrogen Energy Conf., Stuttgart, FR6, 1996), T.N. VERIZOGLU,., et al., Hydrogen Energy Progress XI, International Association for Hydrogen Energy. 1996.

E.Tzimas, C. Filiou, S.D. Peteves, J.B. Veyret. *Hydrogen Storage: State – Of – The – Art and Future Perspective', 2003*. European Commission - Directorate General Joint Research Centre (DG JRC) -Institute for Energy. Petten-The Netherlands, 2003.

(http://www.jrc.nl/publ/P2003-181=EUR20995EN.pdf)

F.J. Edeskuty, W.F. Stewart. *Safety in Handling of Cryogenic Fluids*. The International Cryogenics Monograph Series, Plenum Press. New York, 1996.

H. Barthélémy. *Behavior of steel in the presence of pressurized hydrogen – Recommendation for the construction of pressurized equipment*. Third meeting on inspection in the Chemical Industry organized by the Chemical Industry Union, Marseille, France, 22-23 November 1990.

H. Barthélémy. *How to Select Steel for Compressed and Liquefied Hydrogen Equipment", "Instrumentation of Steels with hydrogen in petroleum industry pressure vessel service"*. Proceeding of the Industrial Conference held in Paris, 29-30 March 1989).

H. Barthélémy. *Learning from gas cylinders incidents – A general overview.* 14TH Symposium EIGA : Packaged gases : past, present and future. Strasbourg, France, January 2004.

H. Barthélémy. *Periodic inspection of compressed gas cylinders and transport vessels by using acoustic emission testing. ASTM STP 1077*

H. Barthélémy, G. Chateau. *Hydrogen embrittlement of low alloyed ferritic steels by hydrogen and hydrogen sulfide under high pressure. Hydrogen and Materials*. Beijing, 9-13 May 1988.

H. Barthélémy, G. Chateau. *Hydrogen gas embrittlement of some austenitic stainless steels, Hydrogen and Materials.* Beijing, 9-13 May 1988.

I. Azkarate. *Corrosión bajo factores mecánicos asistida por hidrógeno de aleaciones de titanio*. Tesis Doctoral. Instituto Químico de Sarriá. Via Augusta 390. 08017 Barcelona. 11 de Junio de 1992.

I. Azkarate, E. Erauzkin, A. Pelayo, A.Mª Irisarri. *Fragilización por hidrógeno de tubos de acero API5 LX-52 y X-60*. Madrid. Rev. Metalurgia. 24 (5), 331-336. 1988.

K. Kussmaul, P. Deimel, *Materialverhalten in H2-Hochdrucksystemen*, VDI Berichte Nº. 1201, VDI-Verlag, Düsseldorf, 1995.

M. Mohitporu, C.L. Pierce, P. Graham. *Design Basis Developer for H2 Pipeline*. Published in Oil & Gas Journal. 28 May,1990.

M.P. Foulc (CEA Le Ripault), P. Mazabraud (CEA Le Ripault), C. Farys (CEA Valduc), L. Coudreuse (Industeel Groupe Arcelor), CEA Commissariat A L'Energie Atomique Le Ripault. *State of the Art "Durability & Integrity"- CEA contribution (Work Package 3. Task 3.1)*. Naturalhy Project (Contract Number: FP6-502661). 24 November 2004.

M.R. Louthan, M.J. Morgan. *Some Technology Gaps in the Detection and Prediction of Hydrogen-Induced Degradation of Metals and Alloys*. J. Nondestructive Evaluation 15, 1996.

P. Hoffmann, (Ed.) *Hydrogen & Fuel Cells Letter.*13 January 1998.

V. Calder. *Ask a Scientist- Chemistry Archive-Hydrogen Holders*. Laboratory of Chicago – Newton BBS, Department of Energy – United States of America. Published on the website:

(http://www.newton.dep.anl.gov/askasci/chem00/chem00094.htm)

Acknowledgement

Many thanks to Sandia National Laboratories and especially to Mr. Moen and Drs. Somerday and San Marchi for their contribution to this chapter.